A WEARABLE KNEE JOINT MONITORING SYSTEM

DEVELOPMENT OF A LOW-COST AND EASY-TO-USE WEARABLE KNEE JOINT MONITORING SYSTEM

By
ABU ILIUS FAISAL

B. SC. ISLAMIC UNIVERSITY OF TECHNOLOGY, 2009

A Thesis Submitted to the Department of Electrical & Computer Engineering
and
School of Graduate Studies in Partial Fulfilment of the Requirements for the Degree of
Master of Applied Science

McMaster University
Hamilton, Ontario

Master of Applied Science (2020)
(Electrical and Computer Engineering)

TITLE:	Development of a Low-Cost and Easy-to-Use Wearable Knee Joint Monitoring System
AUTHOR:	Abu Ilius Faisal, B. Sc. (Electrical and Electronic Engineering) Islamic University of Technology, Gazipur, Bangladesh
SUPERVISOR:	Dr. M. Jamal Deen, Distinguished University Professor
NUMBER OF PAGES:	xix, 116

Abstract

The loss of mobility among the elderly has become a significant health and socio-economic concern worldwide. Poor mobility due to gradual deterioration of the musculoskeletal system causes older adults to be more vulnerable to serious health risks such as joint injuries, bone fractures and traumatic brain injury. The costs associated with the treatment and management of these injuries are a huge financial/social burden on the government, society and family. Knee is one of the key joints that bear most of the body weight, so its proper function is essential for good mobility. Further, Continuous monitoring of the knee joint can potentially provide important quantitative information related to knee health and mobility that can be utilized for health assessment and early diagnoses of mobility-related problems.

In this research work, we developed an easy-to-use, low-cost, multi-sensor-based wearable device to monitor and assess the knee joint and proposed an analysis system to characterize and classify an individual's knee joint features with respect to the baseline characteristics of his/her peer group. The system is composed of a set of different miniaturized sensors (inertial motion, temperature, pressure and galvanic skin response) to obtain linear acceleration, angular velocity, skin temperature, muscle pressure and sweat rate of a knee joint during different daily activities. A database is constructed from 70 healthy adults in the age range from 18 to 86 years using the combination of all signals from our knee joint monitoring system.

In order to extract relevant features from the datasets, we employed computationally efficient methods such as complementary filter and wavelet packet decomposition. Minimum redundancy maximum relevance algorithm and principal component analysis were used to select key features and reduce the dimension of the feature vectors. The obtained features were classified using the support vector machine, forming two distinct clusters in the baseline knee joint characteristics corresponding to gender, age, body mass

index and knee/leg health condition. Thus, this simple, easy-to-use, cost-effective, non-invasive and unobtrusive knee monitoring system can be used for real-time evaluation and early diagnoses of joint disorders, fall detection, mobility monitoring and rehabilitation.

Acknowledgements

I would like to express my utmost gratitude to those people who, by there assistance and valuable advice helped me to prepare and complete this thesis.

First and foremost, I am deeply indebted to my supervisor Dr. M. Jamal Deen for giving me this exciting and challenging project to work on, and also for his consistent support, invaluable guidance and countless technical advice during the entire course of my graduate studies and research work. It has been a great honor and privilege to be a student of such a renowned Professor, researcher and teacher. The way he guided and mentored me throughout my research was very encouraging and motivational for me, even during the difficult times of my research. In addition, I truly appreciate the opportunities Dr. Deen gave me to collaborate with some top medical doctors and researchers whose cooperation and insightful advice helped me a lot.

I would like to express my profound appreciation and acknowledgments to Dr. Tapas Mondal from Department of Pediatrics, McMaster University and Dr. David Cowan from Department of Medicine, St. Joseph's Healthcare Hamilton for their active collaboration and support in the participant recruitment and data collection process, for the helpful discussions, and for the valuable assistance offered during my research. Their clinical experience and knowledge in health-related research have greatly helped me. I am also indebted to all the participants who are involved in this research. Without them, my work would not have been possible.

My special thanks to Sumit Majumder for his continuous cooperation and creative suggestions from the very beginning of my research. Together, we built a strong health research team under the supervision of Dr. Deen. I would also like to thank Dr. O. Marinov and Dr. Arif Ul Alam for their cordial support and valuable assistance during my research.

I was privileged to have some top-notch researchers as my lab-mate in Dr. Deen's team. They were a source of inspiration for me. I would like to genuinely thank my lab-mates,

Wei Jiang, Yamn Chalich, Ryan Scott, Hythm Afifi, Dr. Si Pan, Dr. Ahmed Elsharabasy and Mahdi Naghshvarianjahromi for the numerous discussions and technical remarks on my research. I am also very much thankful to Dr. Chih-Hung (James) Chen for chairing my thesis examination, Dr. Tapas Mondal for being a member of my examining committee and to both of them for their advice on my research and for taking the time to review my thesis.

Last but not the least, I am grateful for the support and help that I have received from my friends Md. Nour Hossain, Md. Shariful Islam Chowdhury, Md. Shafiul Alam, Md Roqibul Hasan and Hosnee Mobarak. I sincerely thank my parents for their unconditional support and encouragement over all these years, and my dear wife, Nahid Sultana for her endless love and for always being there for me and putting me first. This thesis is dedicated to them.

Table of Contents

Abstract ..... **iii**
Acknowledgements ..... **v**
Table of Contents ..... **vii**
Lists of Figures ..... **x**
List of Tables ..... **xiii**
List of Appendices ..... **xiv**
List of Abbreviations ..... **xv**
List of Symbols ..... **xvii**
Declaration of Academic Achievement ..... **xix**
Chapter 1 Introduction **1**
1.1. Overview of Human Body Joint monitoring 1
1.1.1. Key Joints for Mobility 2
1.1.2. Key Parameters for Joint Monitoring 4
1.2. Importance of Knee Joints 6
1.3. Research motivation 7
1.4. Research contributions 10
1.5. Thesis organization 12
Chapter 2 Literature Review **14**
2.1. Traditional Methods of Joint Monitoring 15
2.2. State-of-the-Art Sensors and Technologies 16
2.2.1. Optical Sensors 16
2.2.2. Imaging and Video-based Tracking System 20
2.2.3. Textile-based Sensors 22
2.2.4. Inertial Measurement Unit Sensors 24
2.2.5. Other Sensors and Techniques 29
2.3. Sensor Fusion 30

2.4. Research Challenges 32
Chapter 3 Knee Monitoring System Design and Methodologies 35
3.1. Sensors 35
3.1.1. Inertial Measurement Unit Sensors 36
3.1.2. Temperature Sensor 37
3.1.3. Pressure Sensor 38
3.1.4. Galvanic Skin Response Sensor 39
3.2. Knee Monitoring System 40
3.2.1. Integration of External Sensors with IMU Board 40
3.2.2. Implementation of Multi-Sensors-based System 41
3.3. Data Acquisition System and Protocol 42
3.4. Conclusions 48
Chapter 4 Signal Processing and Data Analysis 49
4.1. Preprocessing 49
4.2. Estimation of Knee Joint and Gait Parameters 50
4.2.1. Knee Angle 50
4.2.2. Stride Length and Minimum Foot Clearance 53
4.2.3. Gait Speed and Cadence 56
4.2.4. Temperature, Pressure and Skin Conductance 56
4.3. Measurement Validation 58
4.3.1. Knee Angle 58
4.3.2. Stride Length, Gait Speed and Cadence 60
4.3.3. Minimum Foot Clearance 62
4.4. Feature Extraction 63
4.5. Conclusions 66
Chapter 5 Characterization and Classification of Knee Data 67
5.1. Feature Selection and Dimensionality Reduction 68
5.2. Characteristics of Key Extracted Features and Parameters 69
5.2.1. Angles and Gait Parameters 70

5.2.2. Energy Features 73
5.2.3. Other Physiological Parameters 75
5.3. Classification and Cross-Validation of Knee Data 77
5.3.1. Gender 78
5.3.2. Age 79
5.3.3. BMI 81
5.3.4. Knee and Leg Health 83
5.4. Conclusions 85
Chapter 6 Conclusions and Future Work 86
6.1. Conclusions 86
6.2. Future Work 88
References 92
Appendix A Supporting Information for Chapter 1 104
Movements of key human body joints 104
Normative values of different body joint range of motion (ROM) 105
Appendix B Supporting Information for Chapter 3 106
MetaWear CPro IMU board pin assignments and their functions 106
Letter of Information/Consent 108
Data Collection/Case Report 113
Screenshots of Data Collection from Two IMU Boards Using MetaBase Android application 114
Screenshots of Data Collection from Temperature, Pressure and GSR Sensors Using MetaWear Android application 115
Appendix C Copyright permissions 116

Lists of Figures

Figure 1-1. (a) A Synovial Joint; (b) Types of Synovial Joints. 3
Figure 1-2. The knee joint in the human body. 6
Figure 2-1. Universal goniometer**.** 15
Figure 2-2. (a) Optical fiber configuration and working principle; (b) Construction and operation method of the fiber-optic curvature sensor with a "teeth-like" sensitive zone; (c) Flexible OFS-based joint monitoring system configuration. 18
Figure 2-3. Components and working principle of optical-based goniometer system. The system was composed of five components: (1) a semiconductor laser as light source, (2) a Si p-i-n photodiode as photo detector, (3,4) two linear polarizers as polarizing and analyzing filters, and (5) a single-mode optical fiber as stress-induced birefringence polarization controller (SIBPC). 19
Figure 2-4. (a) Sensing setup of optical-based goniometer system for human elbow joint measurement; (b) Operation method of the system. 20
Figure 2-5. Block diagram of imaging-based human skeletal tracking. 21
Figure 2-6. (a) Sensing setup of optical-based goniometer system for human elbow joint measurement; (b) Operation method of the system. 22
Figure 2-7. Schematic design of conductive wire sensor-based wearable joint monitoring device. 23
Figure 2-8. IMU sensors' orientation and position for knee angle measurement. 25
Figure 2-9. Process flow of joint angle measurement with IMU devices. 28
Figure 2-10. A simplified block diagram of sensor fusion methods. 31
Figure 3-1. MetaWear CPro IMU board. 37
Figure 3-2. Temperature sensor (135-104LAG-J01 Discrete Thermistor). 38
Figure 3-3. Pressure sensor (FSR® 402 Short). 38
Figure 3-4. (a) GSR Sensors Schematics; (b) GSR Electrodes. 39
Figure 3-5. Integration of external sensors with MetaWear CPro IMU board. 40

Figure 3-6. Multi-sensor-based smart wearable wireless knee joint monitoring system. . 42
Figure 3-7. Walkway for the walking exercise. 44
Figure 3-8. Block diagram (process flow) of the knee joint health analyzer. 47
Figure 4-1. IMU signal preprocessing flowchart. 50
Figure 4-2. Knee angle from IMU sensors. 51
Figure 4-3. Sensor fusion to calculate knee angle 51
Figure 4-4. Complementary filter. 52
Figure 4-5. Stride length and minimum foot clearance in one gait cycle. 54
Figure 4-6. Minimum foot clearance (MFC) detection from vertical displacement. 54
Figure 4-7. Force vs. resistance (FSR® 402 Short). 57
Figure 4-8. Reflective Markers attached on the subject's right lower limb (thigh, knee and shank) for knee angle measurement validation. 58
Figure 4-9. Knee joint angle of a walking test on treadmill. 60
Figure 4-10. Comparison and estimation errors (in cm) of the stride length calculation. 61
Figure 4-11. MFC measurement validation using video-based motion analysis system. . 62
Figure 4-12. Wavelet packet decomposition tree up to 3rd level 63
Figure 4-13. Original and four components of the mediolateral signal decomposed at 2nd level with wavelet packet decomposition. 65
Figure 5-1. Comparison of magnitude of knee, thigh and shank angle changes for the three age groups. 71
Figure 5-2. Comparison of magnitude of different gait-related features among the three age groups. 72
Figure 5-3. Comparison of rotational energy among different age groups. 74
Figure 5-4. Comparison of acceleration energy among different age groups. 74
Figure 5-5. Comparison of thigh anterior compartment muscle pressure between different subject groups. 76
Figure 5-6. Classification results: (a) two distinct gender groups (excluding outliers – data fallen on the wrong side of the boundary); (b) One instance of cross-validation showing one subject is falsely classified. 79

Figure 5-7. Classification results: (a) two distinct age groups (excluding outliers – data fallen on the wrong side of the boundary); (b) One instance of cross-validation showing one subject is falsely classified. 80
Figure 5-8. Classification results: (a) two distinct BMI groups (excluding outliers – data fallen on the wrong side of the boundary); (b) One instance of cross-validation showing one subject is falsely classified. 82
Figure 5-9. Classification results: (a) two distinct groups with (undiagnosed) and without joint issue (excluding outliers); (b) One instance of cross-validation showing one subject is falsely classified. 84

Appendix Figures

Figure A-1: Different types of human body joints' movements. 104
Figure B-2: MetaWear CPro IMU Board Pin Assignments. 106

List of Tables

Table 1-1: Types of Synovial Joints. 2
Table 3-1: Technical specifications of MetaWear CPro IMU board. 37
Table 3-2: Technical specifications of temperature sensor (135-104LAG-J01 Discrete Thermistor). 38
Table 3-3: Technical specifications of Pressure sensor (FSR® 402 Short). 39
Table 3-4: Summary of the subjects' characteristics. 43
Table 3-5: List of different joint monitoring systems, and their advantages and limitations. 46
Table 4-1: Descriptive scale for values of the concordance correlation coefficient. 59
Table 4-2: Concordance correlation coefficient ρ_C for walking test. 60
Table 4-3: MFC comparison. 62
Table 4-4: Extracted features. 65
Table 5-1: Knee, thigh and shank angles during walking. 71
Table 5-2: Stride length, cadence and MFC of walking. 72
Table 5-3: Rotational energy. 73
Table 5-4: Acceleration energy. 74
Table 5-5: Thigh anterior compartment muscle pressure while walking. 76
Table 5-6: Confusion matrix for gender-specific classifier. 78
Table 5-7: Confusion matrix for age-specific classifier. 80
Table 5-8: Confusion matrix for BMI-specific classifier. 82
Table 5-9: Confusion matrix for knee and leg health-based classifier. 84
Table A-1: Active range of motion (ROM) (°) for human joints by gender and age [19]. 105
Table B-2: MetaWear CPro Board Pin Functions. 107

List of Appendices

Appendix A Supporting Information for Chapter 1 104
Appendix B Supporting Information for Chapter 3.....106
Appendix C Copyright permissions 116

List of Abbreviations

2D	Two-dimensional
3D	Three-dimensional
ADC	Analog-to-digital converter
API	Application programming interface
BMI	Body mass index
DC	Determination coefficient
DCT	Discrete cosine transform
DWT	Discrete wavelet transform
EKF	Extended Kalman Filter
EMG	Electromyography
FPR	False positive rate
FSR	Force sensitive resistor
GBD	Global disability burden
GPIO	General-purpose input/output
GSR	Galvanic skin response
HPF	High-pass filter
ICF	Information-weighted consensus filter
IMU	Inertial measurement unit
IoT	Internet of things
KOA	Knee osteoarthritis
LPF	Low-pass filter
MEMS	Micro-electro-mechanical systems
MFC	Minimum foot clearance
mRMR	Minimum redundancy maximum relevance
NDVR	Normal data variation rate
NTC	Negative temperature coefficient
OFS	Optical fiber sensor
PCA	Principal component analysis
REB	Research Ethics Board
RMSE	Root mean square error
ROM	Range of motion
SNR	Signal-to-noise ratio

SVM	Support vector machine
TPR	True positive rate
UKF	Unscented Kalman Filter
VAG	Vibroarthrography
WPD	Wavelet packet decomposition

List of Symbols

θ_{acc}	Angle from accelerometer (°)
$\overrightarrow{a_{st}}$	Acceleration vector in stationary position (ms^{-2})
$\vec{a}$	Acceleration vector during walking (ms^{-2})
$\theta_{T_{acc}}$	Thigh angle from accelerometer (°)
$\theta_{S_{acc}}$	Shank angle from accelerometer (°)
$\theta_{st_{acc}}$	Knee angle from accelerometer in stationary position (°)
$\overrightarrow{a_{T_{st}}}$	Acceleration vector (thigh) in stationary position (ms^{-2})
$\overrightarrow{a_{S_{st}}}$	Acceleration vector (shank) in stationary position (ms^{-2})
$\theta_{K_{acc}}$	Knee angle from accelerometer during walking (°)
$\theta_{K_{gyr}}$	Knee angle from gyroscope during walking (°)
j_1	Joint axes for IMU_1
j_2	Joint axes for IMU_2
g_1	Gyroscope value from IMU_1 (°/s)
g_2	Gyroscope value from IMU_2 (°/s)
θ_K	Knee angle from complementary filter (°)
α	Complementary filter constant
τ	Time constant (s)
T_S	Sampling time (s)
θ_S	Shank angle (°)
v	Velocity (ms^{-1})
ω	Angular velocity (rad/s)
r	Radius (m)
v_{hor}	Horizontal component of linear velocity (ms^{-1})
v_{ver}	Vertical component of linear velocity (ms^{-1})
$v_{hor,s}$	Horizontal component of linear velocity in sagittal plane (ms^{-1})
$v_{hor,t}$	Horizontal component of linear velocity in transverse plane (ms^{-1})
v_{gait}	Horizontal gait velocity (ms^{-1})
t	Time (s)
$t_{one\ cycle}$	End time of one cycle (s)

v_{ver}	Vertical velocity (ms^{-1})
s_{ver}	Vertical displacement (m)
D_{total}	Total walking distance (m)
t_{start}	Start time (s)
t_{stop}	Stop time (s)
N	Total number of gait cycles
R	Resistance (Ω)
R_B	Bias resistor (Ω)
T	Temperature (°C)
R_0	Resistance at 25 °C (Ω)
T_0	Room temperature (°C)
β	Thermistor constant
G_{skin}	Skin conductance (S)
R_{GSR}	Skin resistance (Ω)
ρ_C	Concordance correlation coefficient
ρ	Pearson correlation coefficient
C_b	Bias correction factor
D	Measured distance for walking exercise (m)
E	Energy of a signal
S	Decomposed signal components
X_i	i-th feature
m	Total features
f^{mRMR}	Feature importance
Y	Response variable
S	Selected features
X_S	features out of the feature set S
$I(.,.)$	Function denotes mutual information
Ω	Sample spaces
$p(x, y)$	Combined probability density
$\max_{X_i \in S} f^{mRMR}(X_i)$	Feature importance score
C	Covariance matrix
Dim	Matrix dimension

Declaration of Academic Achievement

This thesis was written by Abu Ilius Faisal under the supervision of Dr. M. Jamal Deen, Distinguished University Professor of McMaster University. The research was carried out in collaboration with the Department of Pediatrics, McMaster University and the Department of Medicine, St. Joseph's Healthcare Hamilton.

- Chapter 1: I described the importance and motivation of the research, and summarized the research results.
- Chapter 2: I conducted the literature review and addressed the research challenges.
- Chapter 3: I designed and developed a prototype of the wearable knee monitoring system, described the protocol and data acquisition process.
- Chapter 4: I applied different signal processing and data analysis techniques to interpret the collected data and conducted measurement validation.
- Chapter 5: I applied different statistical and machine learning algorithms to characterize and classify the knee data.
- Chapter 6: I summarized the system and discussed future research possibilities.

Chapter 1
Introduction*

1.1. Overview of Human Body Joint monitoring

The human body is a well-developed mechanical structure. The skeleton of the human body is made up of 206 different shaped bones, which serves as a framework of the body, and the joints are the locations where bones meet each other. Joints hold the bones together and give the skeleton stability and mobility [1]. As we grow older, joints begin to deteriorate due to wear and tear as well as disease states. As a consequence, joint motion becomes more restricted, flexibility decreases as well as joints become painful, inflamed and arthritic. These kinds of joint problems, also known as musculoskeletal disorders, have become a serious threat to healthy aging. Musculoskeletal disorders are one of the major causes of mobility loss [2] as well as reduced productivity [3] among older adults, and the highest contributor to global disability [4]. Persons with these disorders have significant morbidity and higher mortality rates than their age- and gender-matched peers [5]. The cost for direct treatment and healthcare services for the musculoskeletal disorders and mobility-related problems is becoming a major social and financial burden on government, society and family. Also, costs due to lost productivity (the indirect economic loss to society) outweigh the direct costs by a factor of five [6]. Responding to this increasing socio-economic burden demands a multilevel, integrated response, including primary prevention, early detection and effective intervention for persons at risk with common musculoskeletal health issues. Therefore, unobtrusive and continuous joint monitoring during the normal daily activities of an individual is becoming essential to assess a person's mobility and

* Part of this work will be submitted for consideration for publication as: A. I. Faisal, S. Majumder, R. Scott, T. Mondal, D. Cowan, and M. J. Deen, A Simple, Low-Cost Multi-Sensor-based Smart Wearable Knee Joint Monitoring System, March 2020. (in preparation)

musculoskeletal health status as well as for accurate diagnosis of different musculoskeletal and mobility-related disorders.

1.1.1. Key Joints for Mobility

Three types of joints are present in the human body: Fibrous (immovable), Cartilaginous (semi-movable) and Synovial (freely movable) joints [7]. Among them, synovial joints (Figure 1-1(a)) are the key joints of our body to provide mobility by allowing load-bearing, low-friction, wear-resistant smooth movement between articulating bone surfaces [8]. We have six groups of synovial joints in our body. These are categorized by the apposing bone surface at joints and the types of movement they permit: pivot, hinge, saddle, plane, condyloid and ball-and-socket joints [8]. These are presented in Table 1-1 and illustrated in Figure 1-1(b). All synovial joints of the human body are bound by a complicated system of ligaments, muscles, tendons and cartilage [9]. There are protective membranes and synovial fluid which lubricate those joints to facilitate smooth movements and load-bearing [10]. Throughout our life and for every functional activity, these joints are critical and several bear our weight and are key to our movements. With aging, synovial fluid production is reduced, the cartilage wears, and the articulating bones come into direct contact, causing musculoskeletal damage such as irregular articular surface and loss in bone density [10]. Pain, stiffness, deformation, inflammation and swelling in the joints are the signs of this musculoskeletal damage [11].

Table 1-1: Types of Synovial Joints.

Joint Type	Joint Movement	Examples
Pivot	Rotation of one bone around another	Top of the neck
Hinge	Flexion/Extension	Elbow/Knee/Ankle
Saddle	Flexion/Extension/Adduction/Abduction/Circumduction	Thumb
Plane	Gliding movements	Inter-carpal/Tarsal bones
Condyloid	Flexion/Extension/Adduction/Abduction/Circumduction	Wrist
Ball-and-socket	Flexion/Extension/Adduction/Abduction/Rotation	Shoulder/Hip

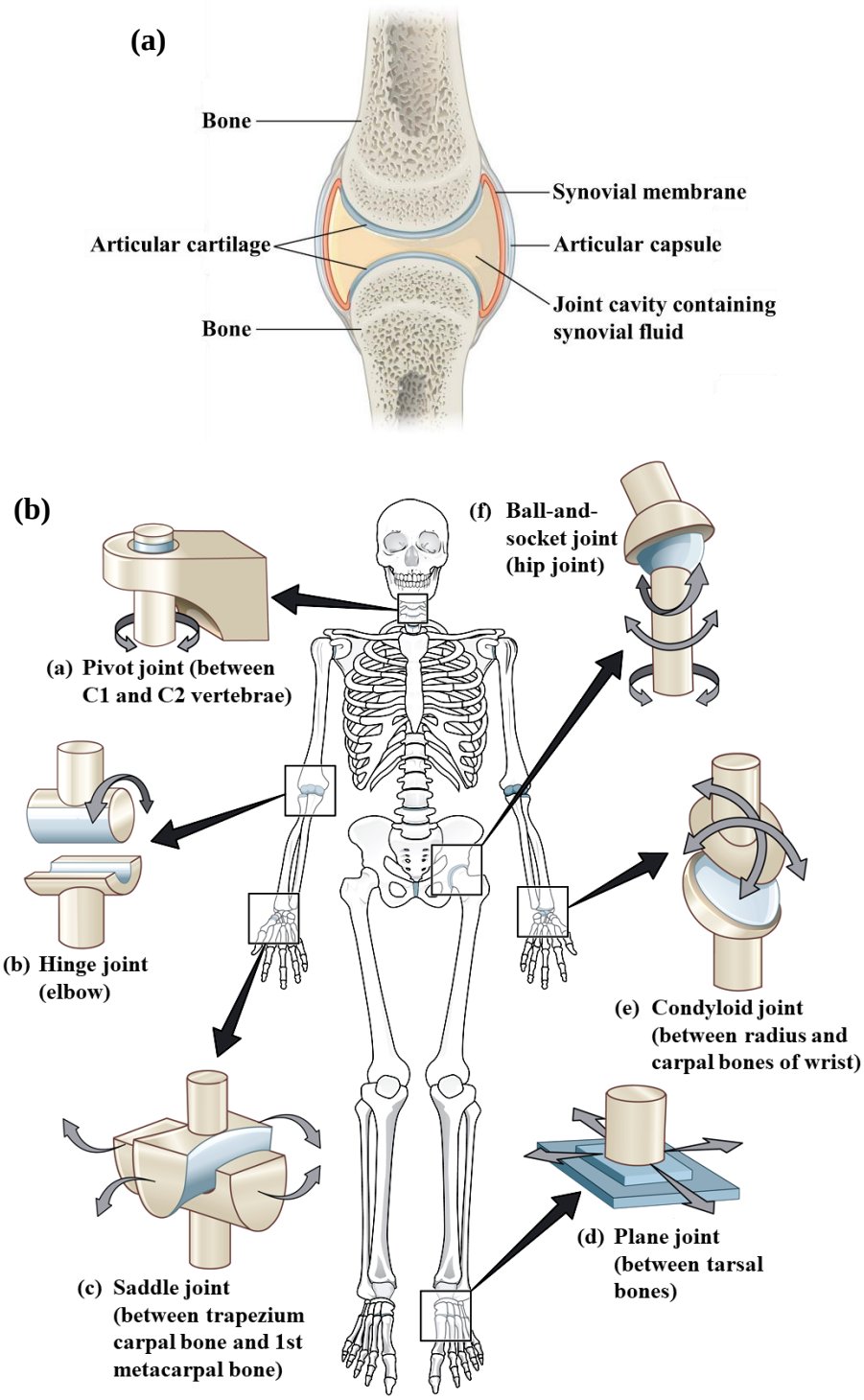

Figure 1-1. (a) A Synovial Joint; (b) Types of Synovial Joints.
Image source: https://opentextbc.ca/anatomyandphysiology/chapter/9-4-synovial-joints/ under a Creative Commons Attribution 4.0 International License.

1.1.2. Key Parameters for Joint Monitoring

The physiologic joint movement occurs through the isotonic contraction of the muscles and the contractile force is closely related to the change in muscle length at the joint location [12]. During the contraction, the change in muscle length varies with different joint angles, motions and postures. By measuring the range of motion of a joint, it is possible to determine the maximum force generated by the muscle as one measure of the health condition of a joint. Similarly, the joint angles and postures at different activity levels also depict muscle strength and endurance [13]. Therefore, one of the main goals of developing a joint monitoring system is to track and record the joint activities in the form of meaningful data such as angle, range of motion (ROM), motion, orientation, and other important physiological parameters such as local skin temperature, sweat rate or muscle pressure around the joint. This could potentially be used to estimate the joint health status and provide feedback to the person whose joint is being monitored.

Joint Angle and ROM

Each movable body joint has an optimal range of joint angle for a specific activity or motion. To reach that optimal angle, the muscle should have the correct length to bear the maximum strength [14]. There are several published reference values of the active range of joint angles or range of motions [15]–[17] for a healthy adult. However, the ROMs may vary depending on sex, age, physical structure and daily activities [18]. A pictorial view of the 5 joints' movements and the normative values of normal joint range of motion (ROM) in 674 normal subjects by gender (54% females and 46% males) and four different age groups (2-8, 9-19, 20-44 and 45-69 years) measured in degrees [19] are presented in Appendix A (Figure A-1 and Table A-1). The reference values were calculated along with 95% confidence intervals for normal range of motion for 11 different movements measured on 5 joints. From Table A-1, for all joints, a downtrend of ROM values is visible with aging, for both male and female subjects. The greatest change was seen in knee flexion, with a 15° difference in mean ROM between the age groups of 2–8 years and 45–69 years. Although ROMs are generally affected by aging, there can be other reasons such as injuries

or other health-related problems which can cause a reduction in the ROM of a joint. Therefore, it is very important and useful for therapists and physicians to study joint angles for the early detection of joint issues or determine the progress in joint rehabilitation.

Joint Motion

The motion of a joint describes its movement from the center of the joint location [19], [20]. Joint motion includes flexion (bending), extension (straightening), adduction (movement towards the center of the body), abduction (movement away from the center of the body) and rotations (inward and outward movements) [21]. The measurement of a joint's motion in different activities includes both its angle and orientation in a 3D space which can provide useful clinical information related to joint health. Therefore, for joint health assessment and rehabilitation, continuous motion monitoring is very important.

Other Physiological Parameters

Along with angle and motion, there are some other physiological parameters related to joints that can provide important information about joint health status. For example, changes in local skin temperature around the joint can be an indication of pathology. Local temperature change occurs due to the changes in blood flow in that region. Generally, the skin temperature of an inflamed joint is higher (1.1°C – 2.8°C) than a normal joint [22]. Therefore, monitoring joint skin temperature can be a useful clinical indicator in evaluating the health status of a joint.

Muscle pressures/forces around a joint during several activities and movements are also closely correlated to the corresponding musculoskeletal health. Muscle pressure changes around a joint with every movement (flexion, extension, etc.) and the values are different for different activities. Muscle pressure plays a crucial role in determining the force balance, contact force and pressure distribution of the joint [23]. Any imbalance in muscle forces can result in joint pain and stress. Muscle forces around the joints can be easily estimated by utilizing flexible pressure sensors or electromyography (EMG) sensors [24], [25].

For joint monitoring, another important parameter is the sweat rate of the joint skin. It can provide the necessary estimation about the thermal status and other physiological condition such as blood circulation of joints. Stress and perspiration in the joint are related to the local blood flow and the activities of the sweat gland which can be interpreted by measuring the sweat rate. The galvanic skin response (GSR) sensor is one of the common types of sweat rate sensors. This sensor is used to measure skin conductance which varies with the change of skin moisture caused by sweating [26].

1.2. Importance of Knee Joints

Among all the body joints, the knee is the largest and the most complex joint in human body [27]. Knee joints provide stable support to our whole body and flexibility in our legs to ease our lower limb activities. It is a type of synovial joint (hinge type) [28], which joins the upper leg bone (femur) to the lower leg bones (tibia and fibula). There are two C-shaped cartilages (medial and lateral menisci) between the femur and tibia which act as shock absorbers and another bone called the patella (kneecap) that make the knee joint. Ligaments join the knee bones to provide joint stability, and tendons connect the knee bones to the leg muscles to support joint movements (Figure 1-2) [29], [30].

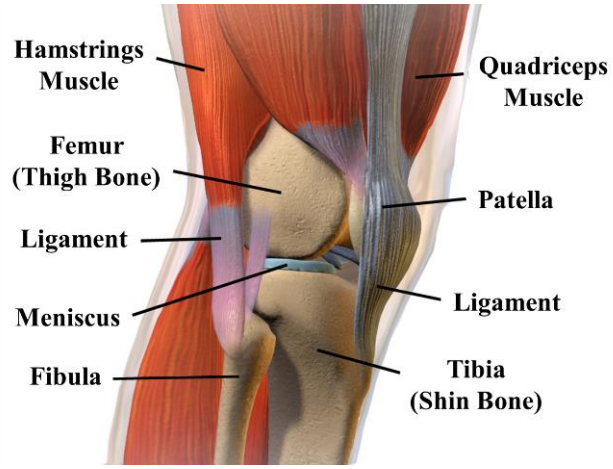

Figure 1-2. The knee joint in the human body.
Image source: https://en.wikipedia.org/wiki/Knee under a Creative Commons Attribution 4.0 International License.

Knees experience a large range of motion (up to ~140°), bear most of the body weight and absorb a huge amount of pressure during several daily activities. While walking across level ground, the average force on each knee is the equivalent to 1.5 times our body weight. The pressure is even greater when we climb up or down (can be of two to three times our body weight) the stairs, and squat (up to four to five times our body weight) to tie a shoelace or pick up an item from the ground [31]. Due to that enormous pressure, plus regular wear and tear, there is always a high chance of having knee problems during many labor-intensive jobs, sports or recreational activities. Knee joints also deteriorate due to overweight, aging or diseases such as osteoporosis or arthritis [29]. Moreover, being the largest weight-bearing and somewhat unstable joints of the human body, knees have high exposure to injuries. Knee injuries may be caused from abnormal twisting or bending the knee, falling on the knee, or by a direct blow from accidents [29].

Limited range of motion, pain, stiffness, swelling and inflammation are the most common signs of knee problems and injuries [32]. In addition, they may catch or lock up. Many knee-related issues also cause deformity, weakness and instability in knee joints. The common knee disorders and injuries include osteoarthritis, rheumatoid arthritis, gout, knee bursitis, Baker's cyst, osteochondritis dissecans, sprains and strains, dislocation, fractures, torn ligament, meniscus injury, and patellofemoral syndrome [32]. Although older adults are more prone to have knee disorders, they can occur in people of all ages. Mobility is highly affected by having knee problems which gradually leads to a lack of independence, depression, reduced productivity, weakened ability in handling daily activities, and worsening quality-of-life [33]. Therefore, proper functioning of the knee joints is essential for good mobility and is considered one of the most important and critical health assessment parameters.

1.3. Research motivation

Worldwide, musculoskeletal disorders are one of the major causes of loss of work, early retirement, reduced retirement wealth [2] and diminished productivity [3]. According to the

Global Burden of Disease Study 2010 (GBD 2010), the impact on the global disability burden due to musculoskeletal conditions is enormous, and it is the top-ranked common cause of disability among older adults [34]. Among musculoskeletal disorders, arthritis is one of the most common, and it is a major contributor to the world's disability burden. From 1990 to 2013, it increased by 75% across the world's population [34], [35]. There are more than 100 different types of arthritis [35] which can affect virtually any joint [36], and people of all ages, genders and races can have arthritis-related problems. Knee osteoarthritis (KOA) is the most common form of arthritis and is a substantial cause of disability affecting millions of people around the world [37]. In osteoarthritis, the natural cushioning between joints and cartilage wears away, and the bones of the joints begin to rub more closely against each other with less of the shock-absorbing benefits from cartilage. As a result, people experience pain, swelling, stiffness, decreased ability to move, and sometimes, the formation of bone spurs. Although the prevalence of knee osteoarthritis increases with age, it can occur even in young people. According to the Arthritis Foundation [35], about 14 million individuals in the U.S. have knee osteoarthritis. There are several factors such as aging, obesity, inherited abnormalities in the shape of the leg bones, repetitive stress on knee joints, athletics and other illness can increase the risk of developing osteoarthritis of the knee. Eventually, this leads to physical impairment and loss of mobility which have severe physical, mental and social consequences among the people with KOA.

Monitoring and assessing the mechanical and physiological characteristics of the knee joints during daily living activities in the natural environment may provide valuable insight into understanding the initiation and development of KOA in an individual. Therefore, development of a smart wearable knee monitoring and assistive device can help a person by regularly monitoring the joint health and mobility status as well as assisting to maintain regular physical activities/exercises and proper diet [38] to prevent KOA. This device can also extract important parameters for early diagnosis leading to early treatment of KOA and other knee-related issues. For knee injuries, during the recovery period following treatment, patients need to go through several rehabilitation programs depending on the

improvement in their knee health status. Current methods to assess the healing process during rehabilitation comprise a series of qualitative physical examinations, which are infrequent and subjective. An accurate, easy-to-use, cost-effective, non-invasive wearable knee joint monitoring system that can be operated outside the clinical environment would be able to improve the rehabilitation outcomes by ensuring the correct execution of the exercise and quantifying the progress towards the recovery of knee health. Moreover, such a monitoring system is desirable for other human activity-related programs such as sports medicine, human performance assessment and virtual guided training [39].

There are several sensing technologies capable of detecting joint parameters and movements. Among them the most common clinically used joint monitoring systems are based on goniometers (mechanical or electromechanical) [40]–[45] or video/imaging systems [46]–[49]. However, inflexibility and low accuracy are the major drawbacks of such goniometer-based systems. On the other hand, video/imaging systems [46], [48]–[50] use complicated image processing algorithms and machine learning techniques to track joints and analyze mobility characteristics. Typically, a complex and expensive infrastructure with sophisticated image acquisition and analyses tools is required for such kinds of systems. Moreover, such a system is only effective with a pre-equipped lab environment, which restricts the users' normal movements and makes it unsuitable for continuous or long-term knee joint monitoring during daily activities.

Fortunately, with the advances in sensor technology, the monitoring process has become easier, more convenient and less costly to implement. Also, wearable sensors are now very reliable, and are extensively used for healthcare, entertainment, security and consumer applications [51]–[53]. Thus, advanced sensors have opened the door of opportunity to develop a miniaturized wearable knee joint monitoring device that is accurate, durable and able to connect wirelessly with smart devices for easy, fast and seamless operation [54]. However, the selection of the sensors is critical, and depends upon several associated factors related to performance, cost, calibration and service of the entire system. Finally, to implement a comprehensive knee joint monitoring system, we need to integrate the selected sensors with a data transmission device and a feedback system.

To accomplish the abovementioned objectives, this research focuses on the development of a non-invasive and wearable smart knee monitoring device that can provide a complete set of data related to knee health and mobility including joint range of motion, walking parameters and the state of adjacent joint muscles. We investigated different sensing technologies and designed our wearable monitoring system by fusing multiple types of sensors (IMU – inertial measurement unit, temperature, pressure, and GSR - galvanic skin response). Inertial motion sensors (gyroscopes and accelerometers) are capable of measuring the mechanical parameters such as knee angle, rotation and speed of movement by measuring rotation and acceleration. Other sensors are used to record and monitor other important parameters such as knee skin temperature, skin conductance and the pressure by the muscles around the knee joint. All sensors used to build the system are low-cost, low-power, miniature and light-weight with wireless connectivity. We used an Android smartphone to gather and store the sensors' data wirelessly and later applied efficient signal analysis and features extraction techniques for reducing the computational complexities for continual knee monitoring. Thus, our system is suitable for real-time monitoring using minimum processing resources and the processed data can provide useful information about the overall knee health status of an individual.

1.4. Research contributions

The research work conducted in this thesis focuses on developing a comfortable, easy-to-use, low-cost, wearable smart knee joint monitoring system to facilitate continuous monitoring in real living conditions and to provide important health analysis related to knee joints and mobility. The major contributions of this work are summarized as follows.

- **The development of a multi-sensor-based smart wearable knee joint monitoring system.** The system was designed by fusing multiple low-cost, miniaturized sensors: inertial measurement unit (IMU), temperature, pressure, and galvanic skin response (GSR) sensors. The combined system is capable of measuring important mechanical

and physiological parameters related to knee joints and has wireless connectivity to transfer the recorded data to a smart device simultaneously.

- **The implementation of different signal processing and analysis techniques to extract the necessary joint and gait parameters.** Knee angle, stride length, minimum foot clearance (MFC), gait speed and cadence (steps per minute) were estimated from the IMU data, and knee skin temperature, skin conductance and the pressure by the muscles around the knee joint were calculated from the other three sensors. Besides these mechanical and physiological parameters, a set of statistical, temporal and energy features of knee joint movement were also extracted from the preprocessed IMU signals.
- **Creating a database using the developed monitoring system, and validating the measurements and proposed methods.** A total of 70 healthy subjects in the age range from 18 to 86 years participated in this study. Different validation techniques were used to determine the concurrent validity of the estimated joint and gait parameters from the proposed monitoring system.
- **Characterization of the knee joint and gait parameters with respect to different age groups and gender.** Characteristics of several key extracted features were found to be varied for different subject groups participated in this study. Comparisons of these joint and gait-related features between different age groups and genders are reported in this work to show the changing trends in joint and gait behaviors with age and gender.
- **Classification of knee data into different classes according to their common characteristics.** The support vector machine (SVM) was used in this study to train and classify the data corresponding to different subject groups. The groups of the subjects were defined according to their age, gender, BMI, as well as their knee and leg health conditions. The performance of the classifier was evaluated using a 10-fold stratified cross-validation.

Publications:

- A. I. Faisal, S. Majumder, T. Mondal, D. Cowan, S. Naseh, and M. J. Deen, "Monitoring Methods of Human Body Joints: State-of-the-Art and Research Challenges," Sensors, vol. 19, no. 11, p. 2629, Jun. 2019.

1.5. Thesis organization

In Chapter 1, an overview of human body joint monitoring including important body joints for mobility and key joint parameters is presented. Then, the importance of knee joints and the motivation of developing a simple, easy-to-use, cost-effective, non-invasive and unobtrusive knee monitoring system are presented. Finally, a brief summary of the main contributions of this research and the structure of this thesis are described.

In Chapter 2, an extensive literature review was conducted including traditional methods for human joint monitoring, state-of-the-art sensors and technologies for joint monitoring, and several sensor fusion methods. The research challenges of the currently available systems for joint monitoring are also addressed in this Chapter.

In Chapter 3, the details of design and development of the multi-sensor-based smart wearable knee joint monitoring system are presented. A brief overview of all the sensors (IMU, temperature, pressure and GSR) used to build the system is also described. Later, we have discussed the experimental protocol as well as data acquisition methods from the sensing system.

In Chapter 4, signal processing and data analysis techniques are demonstrated. We used different preprocessing techniques for the raw signals and then applied feature extraction methods to extract usable joint and gait-related features from the preprocessed data. We also calculated important joint parameters such as knee angle, stride length, MFC, gait speed, cadence, knee skin temperature, skin conductance and the pressure by the muscles

around the knee joint. Finally, different validation techniques are described which verified the correctness of the measurements by the proposed system.

In Chapter 5, the characteristics of extracted features and parameters from the knee data are analyzed and compared with respect to different subject groups. Later, we applied a feature selection algorithm (mRMR – minimum redundancy maximum relevance) and principal component analysis (PCA) to select the key features and reduce the dimensionality of the feature vector. We then exploited and trained the support vector machine (SVM) with the reduced feature vector, classifying the data corresponding to different subject groups. The classification accuracy was evaluated using a 10-fold stratified cross-validation.

In Chapter 6, this thesis is concluded with a summary of the research work and several research and technology development recommendations for future improvements to make the knee joint monitoring system more precise, efficient and user-friendly.

Chapter 2
Literature Review*

Advances in sensor technology have opened the door of opportunity to develop a miniaturized wearable joint monitoring device that is accurate, durable and able to connect wirelessly with smart devices for easy, fast and continuous operation [54]. For wearable applications, the selection of the sensor is critical. It depends upon several associated factors related to performance, size, cost, calibration and service of the entire system. To implement a complete joint monitoring system, we need to combine relevant sensors with a data transmission device as well as a data analysis and feedback system. Various types of joint monitoring devices based on different sensing techniques and algorithms are suggested in the literature [17], [28], [39]-[42], [48]-[70]. The main focus of many researchers is to make the system simple, easy-to-use, cost-effective, non-invasive, unobtrusive and wearable with wireless communications [92]. With these features, the system can be used in real-time for monitoring and analyzing the continuously collected data based on detailed input, requirements and specifications of the person being monitored [38], [93]–[96].

In this Chapter, we present a detailed survey of different proposed and developed technologies and methods of joint monitoring. Following the review on traditional methods used for joint monitoring, various types of modern sensors and technologies commonly used to develop joint monitoring systems are explained and compared highlighting their working principles, measurement parameters, data gathering and processing, and validation techniques. In addition, we also review several proposed sensor fusion methods for

* Adapted from A. I. Faisal, S. Majumder, T. Mondal, D. Cowan, S. Naseh, and M. J. Deen, "Monitoring Methods of Human Body Joints: State-of-the-Art and Research Challenges," Sensors, vol. 19, no. 11, p. 2629, Jun. 2019. Under a Creative Commons Attribution 4.0 International License.

developing joint monitoring systems. Finally, research challenges including shortcomings and limitations of these monitoring systems and algorithms are discussed.

2.1. Traditional Methods of Joint Monitoring

Most of the traditional joint monitoring and angle measurement systems were based on goniometer which is simple to use, noninvasive and inexpensive [42]–[45]. This device can be used to determine the range of angular motion of different human body joints such as the knee, elbow or waist [45] in a two-dimensional space. A photograph of the universal goniometer is shown in Figure 2-1.

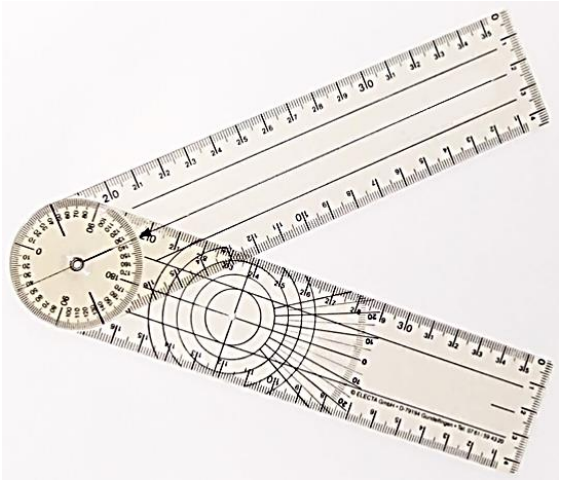

Figure 2-1. Universal goniometer**.**
Image source: https://commons.wikimedia.org/wiki under a Creative Commons Attribution 4.0 International License.

Recent goniometer-based joint monitoring systems use mechanical or electromechanical goniometers, which are based on resistive potentiometers or strain gauges [44]. This type of goniometer consists of a flexible measuring element (resistive potentiometers or strain gauges) attached between two end blocks, one fixed and the other moving on a light spring. However, The main disadvantages of these kinds of goniometers are lower accuracy, large size, imprecision, flimsiness and fixed center configuration which does not provide flexibility with the natural joint movement [43]. To overcome these difficulties in joint related research and clinical monitoring, researchers are now using different types of

sensors to build joint monitoring systems that are flexible, unobtrusive and of higher precision [44], [45].

2.2. State-of-the-Art Sensors and Technologies

Sensors are the fundamental elements of a joint monitoring system to measure the physiological parameters - angle, range of motion and posture - of joints. Various research groups [16], [17], [28], [39]-[42], [48]-[70] have used different sensor types to build joint monitoring systems. Some systems were developed using a single sensor [44], [55]–[57], [71], [90], [97]; others were assembled with a combination of multiple sensor technologies using data fusion methods [39], [75], [98], [99]. The selection of sensors is crucial when developing an accurate and reliable monitoring system. The key features to be considered while developing such a system are high efficiency and accuracy, good reliability, high sensitivity, small size, light-weight, lower energy consumption, and low processing resources [54]. In this Section, we will discuss various state-of-the-art sensor technologies used to develop joint monitoring systems.

2.2.1. Optical Sensors

Most of the common implementations of optical sensor-based joint monitoring system used either intensity modulation or optical navigation methods [44], [45], [89], [100]. Optical fiber sensors (OFSs) were used for intensity modulation [88], [90], [101]. The basic working principle of OFS-based systems is to detect the attenuation of the transmitted optical signal power due to bending of the optical fiber [90]. On the other hand, the systems using optical navigation sensors detect planar motion with joint movement. The optical navigation-based monitoring device is also known as optical-based goniometer [44], [45], [102].

Optical fiber sensors are now often used for designing various health monitoring systems [88], [101], [103]–[105], and several categories of OFSs were developed for both health-related academic research and commercial products. Depending upon the measuring

techniques of the physical parameters and their conversion methods from optical data, OFS can be categorized into four different types: single-point, long-gauge, quasi-distributed and distributed sensors [88]. Optical fiber sensors are made of flexible plastic optical fibers through which optical signals are transmitted. The basic components of an OFS-based system are a light source, flexible optical fiber and a photodetector. The light source generates the optical signal that travels through the flexible optical fiber and is received by the photodetector at the end of the fiber. By measuring the attenuation of the optical signal, it is possible to determine the bending angle of the fiber [89]. Due to this simple sensing principle and structure, optical fiber sensors can be easily integrated into a monitoring system for measuring human joint angles [101]. Basic configurations and working principles of an optical fiber and OFS-based joint monitoring system are shown in Figure 2-2(a) and (b).

The main benefits of OFS are high resolution, flexibility, light-weight and immunity to electromagnetic interference. Different techniques were developed to improve the sensitivity and accuracy of OFS-based joint angle measurements [89]. For example, roughening or polishing the surface on one side [72] of an OFS is a common method to improve the sensitivity by enhancing the optical signal attenuation with bending [106]. In the work described in [89], a wearable knee motion monitoring system using a flexible plastic OFS placed in a commercial knee brace was developed. The change of transmittance (the ratio of the light energy incident on an object to that transmitted through it) was measured while bending the plastic optical fiber. One side of the fiber was polished to improve the performance as macro-bending creates more attenuation [100], [107]. This device was made wearable and wireless by integrating a wireless communication board based on Bluetooth technology with the main controller board. A comparative analysis with a reference video-based monitoring system was made and the average deviation of angle measurement between the two systems was 2.1°.

Another optical fiber sensor-based human joint monitoring system is presented in [90]. In this system, the authors used a fiber-optic curvature sensor with a different sensitive zone configuration and the diameter of the configured optical fiber was 1.5 mm. A “teeth-like”

configuration was created by drilling precisely on one side of the fiber [108] to make the sensitive zone (Figure 2-2(c)). Due to this sensitive zone, when the optical fiber bends while keeping the teeth on the convex side, the light intensity on the outer side decreases. Conversely, the light intensity increases when the teeth are on the concave side. LabVIEW software and ZigBee-based wireless communication were used to complete the system. The optical intensity was exponentially dependent on the curvature angle and the angle range of the system was -120° to 120° with a 1 Hz sampling rate. However, a linear characteristic was found between -45° and 25°, with an average sensitivity of 20 mV/° (voltage change per angle) and a resolution of 1° [90]. The sensor had a high operating temperature limit (up to 70 °C) without any deformation or characteristics change. Therefore, within certain ROM limitations, the proposed sensor was suitable for developing a low-cost and simple wearable joint monitoring system with wireless communication capabilities.

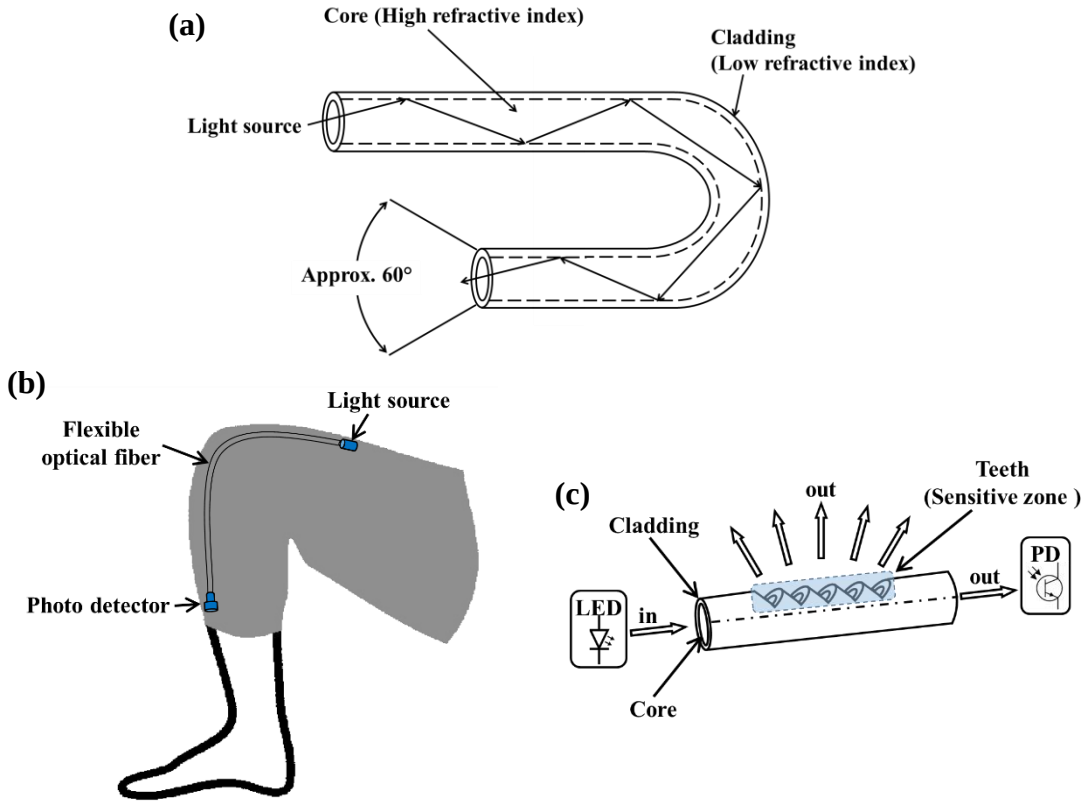

Figure 2-2. (a) Optical fiber configuration and working principle; (b) Construction and operation method of the fiber-optic curvature sensor with a "teeth-like" sensitive zone; (c) Flexible OFS-based joint monitoring system configuration.

An optical fiber-based goniometer presented in [44] was made of a single-mode optical fiber. Intensity modulation of a propagating laser beam was used to detect the changes in polarization due to the rotation of adjacent portions of fiber. Controlled birefringence was induced by a fiber loop with a fixed radius. The components of the reported goniometer and its working principle are shown in Figure 2-3. A trans-impedance amplifier with a high gain-bandwidth product gave a high-precision output signal with high sensitivity. A sample-and-hold circuit, an acquisition board and a computer-based software program were designed to gather and process the data. The goniometer was combined with a fabric to build a flexible, compact and accurate wearable joint monitoring system with several applications such as testing an athlete's performance and training status.

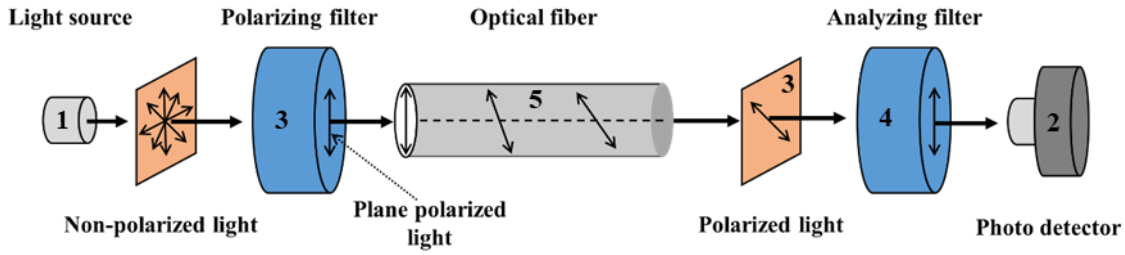

Figure 2-3. Components and working principle of optical-based goniometer system. The system was composed of five components: (1) a semiconductor laser as light source, (2) a Si p-i-n photodiode as photo detector, (3,4) two linear polarizers as polarizing and analyzing filters, and (5) a single-mode optical fiber as stress-induced birefringence polarization controller (SIBPC).

In [45], another wearable system using optical-based goniometer for joint monitoring was proposed. These authors used a technique similar to the optical mouse which has a small camera to identify two-dimensional planar motion by detecting the displacement. They chose the elbow joint for their experiments and their system consisted of two units: hardware and firmware. The hardware unit had three components: the sensor, microcontroller and the joint module (a flexible strip). The firmware unit was for communication and data gathering. The proposed sensing system setup for elbow joint measurement is shown in Figure 2-4. The flexible strip was placed around the joint with one end fixed, and the sensing unit was placed on the other end. The sensing unit was able to move freely along with the strip and measured the uniaxial displacement during bending

of the elbow joint. The angle (α) was calculated from this linear displacement (Δx) that is directly correlated with the bending (equation (2-1)).

$$\alpha = \frac{\Delta x}{R} \cdot \frac{360°}{2\pi}. \tag{2-1}$$

The joint radius (R) was assumed to be constant for this calculation. The proposed sensing module is light-weight and easy to assemble as a joint monitoring system. However, the system can only monitor one-dimensional movement which can affect the angle measurement's accuracy for human body joints.

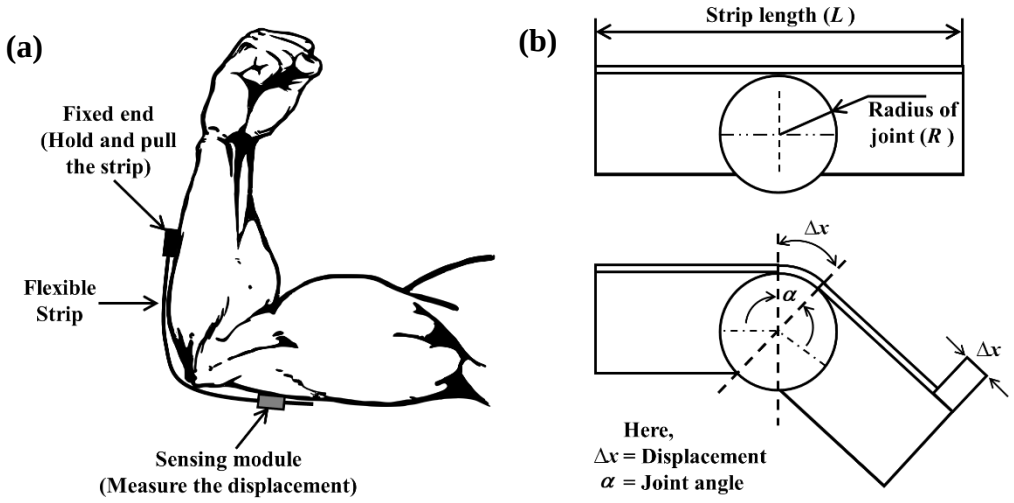

Figure 2-4. (a) Sensing setup of optical-based goniometer system for human elbow joint measurement; (b) Operation method of the system.

2.2.2. Imaging and Video-based Tracking System

Imaging and video-based human skeletal tracking is a well-accepted method for human joint monitoring because of its broad applicability and reliability [47]–[49], [55], [91], [109]–[115]. One or more cameras are the core components of this system. The process flow of this method is to capture the visual data of several human actions by using a single [47] or multiple camera network [91], and then track the joints using anthropometric constraints (size, shape and composition of the human body) and known joint locations in reference images/videos with the same action. These applications comprise various fields of research such as biomechanics, image processing, machine learning and pattern

recognition [46]. The main challenge of this system is to construct a three-dimensional human model using a single static camera. A new image processing method was proposed in [116] where they used 2D images to create a 3D model. They introduced a new image descriptor based on discrete cosine transform (DCT), which was used in the pose-matching procedure for finding appropriate action in the reference database using an interpolation and tracking process. The descriptor matrix was divided into three frequency regions for different levels of tracking: (1) Low-frequency region containing the general shape and intensity information of the joint; (2) Middle-frequency region with general edge information; and (3) High-frequency region consisting details of the tracked joints. Both discriminative and tracking algorithms were used in this method to increase joint tracking accuracy. A block diagram of an imaging-based human skeletal tracking is presented in Figure 2-5.

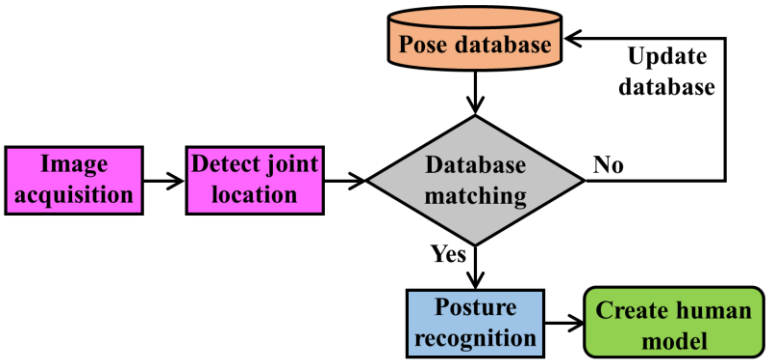

Figure 2-5. Block diagram of imaging-based human skeletal tracking.

A single camera-based system can only detect the joint location within its field of view, thus limiting the range of observations. To solve this problem and track human joint motion in a large area with multiple fields of view, a distributed camera network system was used in [91]. They set up multiple cameras to make the network and used an information-weighted consensus filter (ICF) as a distributed estimation algorithm to track human motion in a camera network inside the sensing range. The distributed camera network setup is shown below in Figure 2-6(a). They used the Microsoft Kinect image sensor instead of a usual camera to build the camera network [91] because Kinect can measure the joint locations without any markers [47]. Kinect is a high-end imaging device with an RGB

camera, a multi-array microphone and a built-in laser projector combined with a monochrome CMOS sensor that makes it capable of capturing color images and depth images (Figure 2-6(b)). In addition, it has a skeletal tracking tool which is able to recognize 20 different joints' locations of a human body. Therefore, instead of a usual camera, Kinect has been chosen by many researchers who are working on vision-based human joint monitoring and analysis problems [47]–[49], [55], [91].

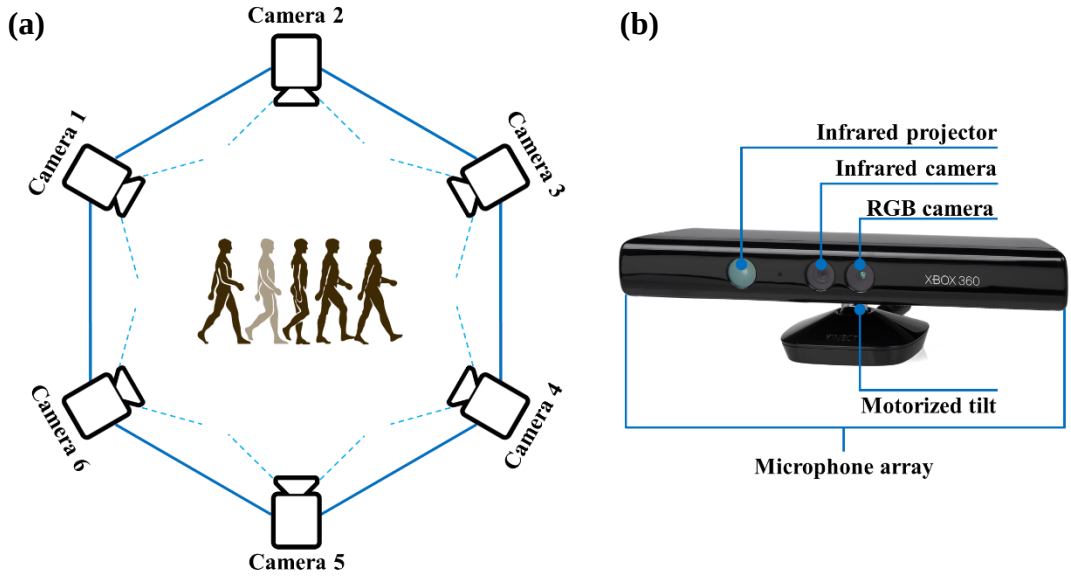

Figure 2-6. (a) Sensing setup of optical-based goniometer system for human elbow joint measurement; (b) Operation method of the system.

Although imaging and video-based joint tracking system is a popular and reliable monitoring technique [47]–[49], [55], [91], [109]–[115], it requires complex, expensive infrastructure and sophisticated analyses of data-intensive video streams. Also, this system is only effective with a pre-equipped environment and setup, restricting users' usual movements, which makes it unsuitable for continuous and long-term joint monitoring in daily activities.

2.2.3. Textile-based Sensors

Textile-based sensors (e.g., flexible conductive wire sensors, flex sensors, strain sensors, etc.) are very suitable for developing a wearable joint monitoring system. The working

principles of all these sensors are similar. In all cases, changes of resistance are measured, and these changes are directly related to the corresponding joint angles [57]. To develop a long-term and regular wearable monitoring device, textile-based sensors can be a good choice because of their flexibility and simple sensing principle. Furthermore, they can be easily integrated into stretchable skin-tight fabrics around the joints [57], [56].

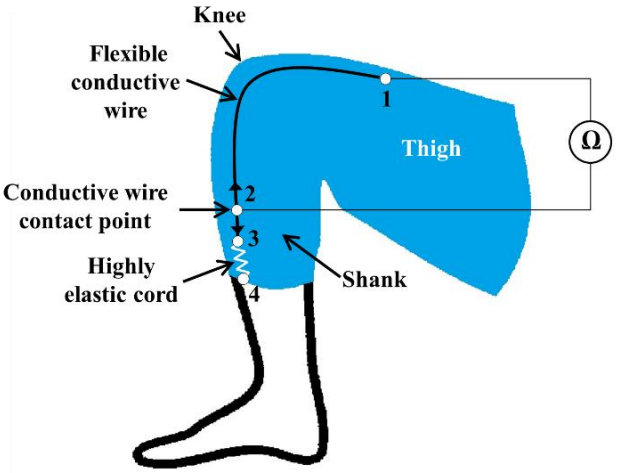

Figure 2-7. Schematic design of conductive wire sensor-based wearable joint monitoring device.

A flexible conductive wire sensor-based method was proposed in [56] where the authors incorporated flexible conductive wires in flexible and comfortable fabrics for joint monitoring. They implemented a single-axis arrangement with a single conductive wire designed for the knee joint (Figure 2-7). The parameter measured was the resistance changes of the conductive wire with the movements of the joints. Figure 2-7 shows the implementation of the system where one end of the flexible conductive wire was fixed to the fabric above the knee at point 1 and the other end was connected with an elastic cord at point 3. The elastic cord was attached to the fabric below the knee at point 4 and helps the conductive wire slide freely with bending and stretching. There was a wire contact point between point 2 and 3 along the fiber and it was permanently stitched into the fabric at point 2 to keep it fixed. The fiber slides with the movement of the knee, causing the change of conductive thread length between 2 and 3 as well as the resistance in that portion [56]. The resistance value at a specific point is directly proportional to the knee angle. They also proposed a multiple conductive wires-based system to monitor multi-axis joint (e.g., hip

and shoulder) angles. Their future focus in this research is to improve the accuracy of the system by applying a more precise technique of incorporating conductive wires into flexible, skin-tight fabrics and adding a wireless module for data transmission.

Flex sensor is another type of textile-based sensor which is usually made of a conductive material with flexible and stretchable properties [57]. The shape of the sensor will change with the applied force, causing the resistance change between two measuring points. Therefore, the flex sensor is convenient for wearable joint monitoring systems by integrating it with comfortable garments [57]–[60]. The flex sensor is usually stitched to the flexible and skin-tight garment across the joint to be monitored. Whenever the joint bends or stretches, the pressure changes on the sensor which causes the variation of its electrical properties (resistance). This resistance variation due to the joint movement can be measured using an electronic system to quantify the joint angle [59]. Textile-based highly stretchable strain sensors are also used by some researchers for human joint monitoring [62]–[64], [117]–[119]. Conductive yarns were employed as the conductive part of the strain sensor. Different textile materials with preferable elasticity and conformability were used to fabricate the system comfortable for human joints [63], [117]. Another type of textile-based sensor was developed in [64] by using flexible and stretchable CCF (chopped carbon fiber)/PDMS (polydimethylsiloxane) conductive yarns. The CCF/PDMS composite sensors were integrated into the textile structures and used the piezoresistive (resistance-strain) behavior of the sensors for detecting human joint motion.

2.2.4. Inertial Measurement Unit Sensors

An inertial measurement unit (IMU) is a combination of three sensors (accelerometer, gyroscope and magnetometer) and is used to measure the three-dimensional acceleration, angular velocity and the magnetic field vector in their own coordinate systems. As a unit, the three sensors are calibrated in such a way that each of their individual coordinate system acts as an orthogonal base which typically remains well aligned with the outer casing of the unit [73]. Moreover, there are some commercially available IMU sensors with built-in algorithms to fix the sensors' orientation with respect to a global fixed coordinate system

(e.g., [120]) which can be represented by a rotation matrix, a quaternion, or Euler angles. For developing a wearable measurement system for human joint motion, IMUs are the most promising and compact devices for both clinical assessment and research studies, because of their small size and capability to measure joint motion with precision and accuracy [73]–[78], [87]. To detect position and orientation, three-dimensional angular velocities and linear accelerations are measured using the IMU sensors. Most of the IMU-based joint monitoring systems use two calibrated IMUs placed below and above a joint [73]–[78]. Relative data from those two IMUs are compared for tracking the joint angle and motion.

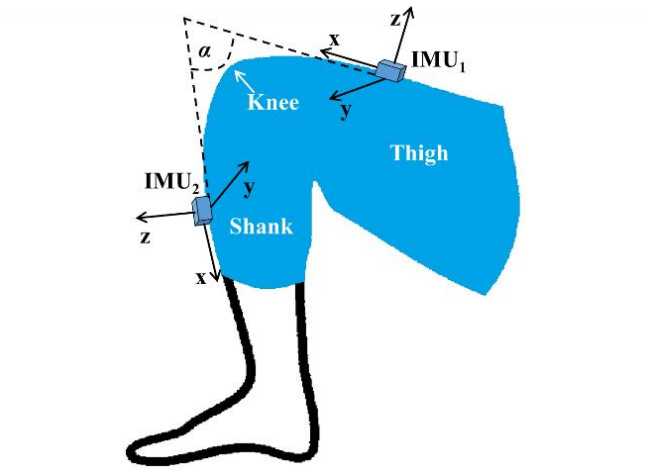

Figure 2-8. IMU sensors' orientation and position for knee angle measurement.

For accurately computing a joint angle, we need to compensate for joint alignment using the two IMUs method described in [75]. These authors proposed a manual method using a set of predefined postures of different leg movements to align two IMUs attached on the thigh and shank. A fusion algorithm was then applied to measure the 3D knee joint angle. The measurement was then validated against the Liberty magnetic motion capture and tracking device (Polhemus, USA). Later they added a functional calibration procedure which only relied on the IMUs data and made an error assessment by comparing the results obtained from the combined method to the reference system [79]. This method can be applied to monitor complex joints e.g., knee, ankle or elbow. A similar system was developed in [74] where Bluetooth technology was added for wireless communication. The system was evaluated by comparing it with an infrared motion capture system having an

average deviation range of 0.08° to 3.06° from each other. Figure 2-8 illustrates two IMU sensors-based configuration for measuring the knee angle (α).

In [80] two IMUs-based joint angle measurement methods were presented. There, they transformed the measured data from both sensors into a joint coordinate system by aligning the IMUs' local coordinate axes with the joint axis. Their first approach included the magnetometer readings (magnetic field vectors) to get a precise alignment. In the second technique, they relied only on the accelerometer and gyroscope data. Indoor measurements can suffer from magnetic disturbances due to other magnetic devices that may be present. Therefore, the authors excluded the magnetometer data for indoor monitoring and achieved equally accurate results. Thus, they were able to increase the accuracy of joint angle measurements by two IMUs having a precise calibration and alignment technique.

An IMU-based auto-calibration method was proposed in [82]. First, the limitations of an existing position calibration method were identified by performing a theoretical analysis (evaluation of observability by computing the Fisher Information Matrix). Based on that analysis, a new method to continuously determine the IMUs' relative position with the joints was introduced. Then, based on the simulated and captured data, an experimental evaluation was performed to present the enhancement of the calibration method. In [78], another IMU calibration and alignment protocol based on simulation and experimental analyses was proposed. These authors simulated a computer-based lower body anatomical frame with four IMU sensors to estimate the angles of hip and knee. In the simulation, the sensors were placed on the pelvis, right thigh, right shank and right foot, and aligned with the associated limbs' coordinate system. They also made a joint model using two semi-spheres interconnected by a universal goniometer and placed IMU sensors on each sphere. They used this model to evaluate the accuracy and repeatability of the system while measuring angular movements. Finally, they performed a real gait test involving five healthy volunteers and validated the method by comparing the results from experiment with simulations.

The drift effect is another concern when using IMU sensors to calculate joint angles and estimate orientations. A random bias drift which builds up over time and affects the sensors'

tracking accuracy [81]. A new kinematic model was proposed in [81] to minimize this drift error. There [81], they considered natural physical constraints (age, gender and bone structure) while measuring the range of motion for each joint with their system. They modeled the sensor's random drift and used zero-velocity updates. To avoid the complex linearization process, they implemented an improved version of the Extended Kalman Filter (EKF) which is called Unscented Kalman Filter (UKF). Instead of estimating nonlinearity, it approximates the distribution of the measured data. They validated the algorithm by comparing their inertial tracker's result with a reference optical tracking system and a high-precision industrial robot arm.

Instead of conventional two IMUs-based joint monitoring system, a single IMU-based system was developed in [83] to monitor hip and knee joint angles. The single IMU was placed on the shank and the collected data was utilized to estimate the 3D lower-limb (pelvis, thigh and shank) joint kinematic quantities during five different lower limb motions with the help of the least-squares identification algorithm. It achieved an average accuracy of 3.2° and a correlation coefficient above 0.85 by comparing with reference data from a stereophotogrammetric system. One limitation of this method was the degradation of joint angle estimation due to the IMU's motion artifact. Moreover, no pelvic motion was assumed in this approach. Thus, the quality of the result might be reduced with large pelvis movements.

By using an IMU-based system, we can measure not only joint angles, but also other important gait parameters such as cadence, step length, step variability, and lateral and vertical excursion of the center of mass [77] for gait analysis. IMU sensors are very convenient to develop such a system because of their miniature size, low-cost and flexibility to use without space restrictions compared to traditional gait analysis methods such as semi-subjective techniques, imaging or floor sensors [121]. Moreover, most modern commercial IMUs have an integrated wireless module which makes it more appropriate to develop a wearable system for continuous joint monitoring and gait analysis [76], [77], [84], [92], [122]–[126]. A fundamental process flow of measuring joint angles using IMU devices (adapted from [76]) is described below in Figure 2-9.

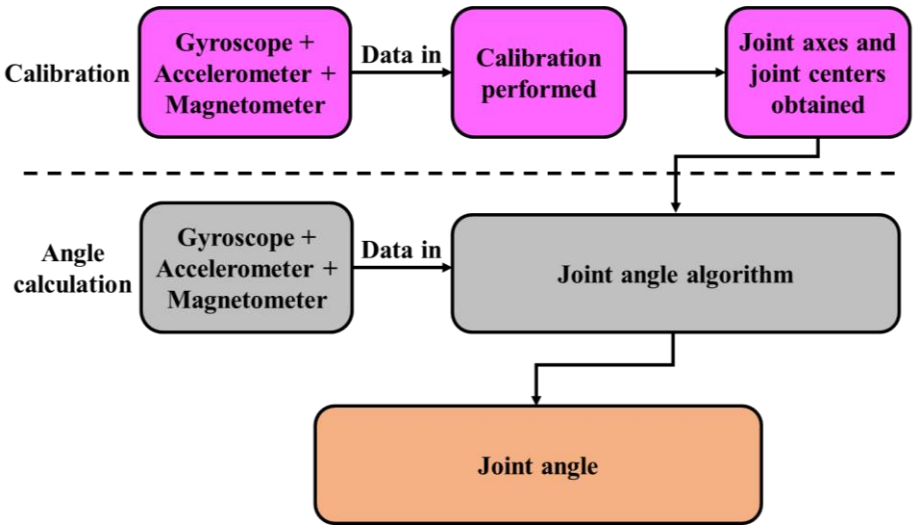

Figure 2-9. Process flow of joint angle measurement with IMU devices.

In [70], the authors used only gyroscope sensors to measure human joint angles. Gyroscopes in modern IMUs can measure 3-axes angular rate with movements. For measuring the joint angle, two gyroscopes were placed above and below the joint location and calibrated before joint motion. Movement angles of each gyroscope were calculated by integrating the angular rate. Then, the joint angles were extracted by comparing the changes in angle between two gyroscopes using trigonometric functions. Two optimization filters were used. One was a Median filter [70] which is a non-linear digital filtering technique to remove noise from the sensor signal. The other was a Kalman filter [70], an algorithm that uses a series of measurements gathered over time, having statistical noise and other inaccuracies, and produces estimates of unknown variables that tend to be more accurate than those based on a single measurement alone, by estimating a combined probability distribution over the variables for each timeframe. Both filters were used to mitigate the noise and drift in the sensors to yield optimized output signals [70], [127].

Some other research groups have proposed using only a magnetometer-based sensing system to measure magnetic fields to determine movement. A wearable field generator design was introduced in [128] to build a fingertip glove equipped with magnetic tracking sensors. Another magnetic sensor-based hand glove in [129] was designed with 20 Hall-effect sensors embedded. This glove was used to assess hand orthopedic disorders by

detecting the relative and absolute orientation of the fingers. In [71], a magnetometer-based nonobtrusive system for monitoring the wrist and hand movement was proposed. A magnetic (neodymium) ring worn on the index finger and two triaxial magnetometers mounted in a watch-like unit were used to measure the magnetic field produced by the magnetic ring and send the data to a wireless device. The movement of the finger was then calculated from the reading of the magnetic field which was correlated to the finger motion. The accuracy of the proposed system was analyzed by comparing it with a traditional goniometer-based system. An average accuracy of 92%–98% with a 19%–28% standard deviation was obtained.

2.2.5. Other Sensors and Techniques

Some studies have proposed acoustic emission (AE) sensor-based joint monitoring systems where they used piezoelectric-films or MEMS (micro-electro-mechanical systems) based microphones to record the sound produced by a moving joint [97], [130]–[133]. This acoustic emission from joints also known as vibroarthrographic signals (VAG) are considered as clinically relevant biomarkers for joint health [132]. The researchers utilized the recorded signal to quantify the consistency of acoustic emissions from joints with respect to joint angle and position [131]. The emitted acoustic signal from an over-exercised joint during motion produces higher amplitude and shows a different pattern in the frequency domain compared to the healthy joints [97]. However, one of the major challenges is the background and interface noise that need to be mitigated to improve the signal-to-noise ratio (SNR) of the emitted signal [132].

A few research groups [65]–[69] have used different inbuilt smartphone sensors and cameras to measure joint angle and motion. Several applications (apps) were used to access and analyze the sensor data. These apps are mostly based on inbuilt smartphone sensors such as the accelerometer [65], [67], gyroscope [67], [68], magnetometer [69] or camera [66]. In all cases, the results from the apps have shown adequate validity when compared against universal goniometer or inclinometer. In addition, a comparison study between two smartphone-based apps (inclinometer and camera) was published in [66]. In this study, the

camera-based app provided higher precision and accuracy (a mean difference of <1° and 1/50 difference >3°) compared to the inclinometer-based app (a mean difference of <7° and 16/50 difference >10°). These researches suggest that the newly developed smartphone-based apps show potential as a useful tool for joint health monitoring [134].

2.3. Sensor Fusion

Recently, some researchers have used sensor fusion methods (combination of multiple types of sensors) to develop more precise and reliable joint monitoring systems. Sensor fusion is the process of combining multiple sensor data in such a way that the combined output shows better performance than individual sensor results [135]. Thus, sensor fusion allows multiple viewpoints with improved resolution, greater spatial and temporal coverage, reduction in ambiguity, and greater precision in measurements. A simplified block diagram of sensor fusion (adapted from [135]) is shown in Figure 2-10.

In [86], a sensor fusion method combining both flex and gyroscopic sensors was proposed. Multiple flex sensors and a MEMS gyroscope were mounted on a supportive fabric worn by the subjects. To fuse the measurement by multiple sensors and estimate accurate joint angles, Kalman filtering was used. The authors built a behavioral model of joint movement over time and updated the system data using the model in Kalman filtering. The main purpose of using multiple sensors was to minimize sensor errors and reduce measurement noise.

Another method proposed in [39] was a fusion of textile electro-goniometer and accelerometer based on the Kalman filter. The purpose of this approach was to avoid pre-estimation of the accelerometer position and alignment. The focus was to measure knee angle during various motion activities and the system was standardized by comparing it with a commercial IMU-based system. Their technique used the data from the accelerometer to continuously adjust the goniometer reading and did periodic calibration. Thus, the fusion system showed more accurate angular measurement (RMSE: mean, μ = 1.96° and standard deviation, σ = 0.96°) compared to the individual derived estimation by

the accelerometer (RMSE: $\mu = 6.55°$ and $\sigma = 2.87°$) or textile electro-goniometer (RMSE: $\mu = 5.15°$ and $\sigma = 0.47°$).

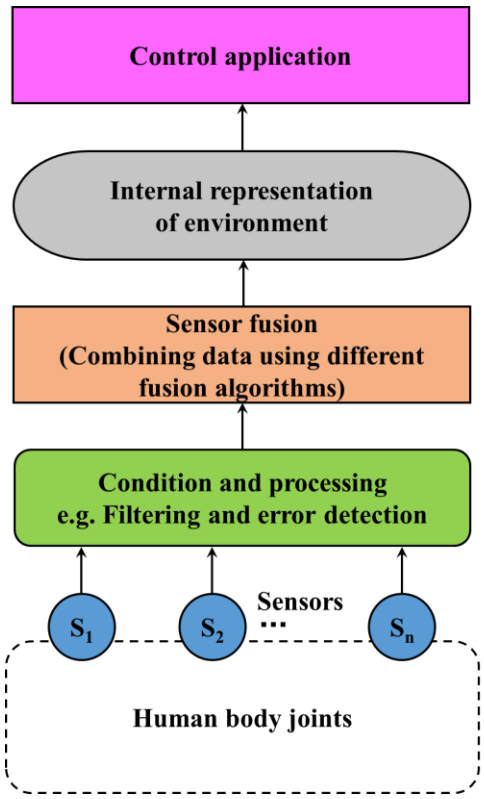

Figure 2-10. A simplified block diagram of sensor fusion methods.

A study on data fusion from wearable IMUs and surface EMG sensors to monitor and assess human motor function was presented in [136]. To estimate a motor function abnormality, a group of machine learning algorithms was used on the fusion data. To validate the algorithms' effectiveness, two parameters: normal data variation rate (NDVR) and the determination coefficient (DC) were derived. A lower NDVR value represents better validity and a larger DC value represents a higher consistency and reliability of the system. Through experiments, these authors proved that the fusion result was superior to the sensors' separate data: a reduced NDVR and a better DC from a regression analysis performed between the derived indicator and the routine clinical assessment score were obtained.

A fusion of data from optical sensors and inertial measurement units (IMU) to analyze human movement and design human kinetic energy harvesting systems was presented in [98]. High-speed cameras were used as optical sensors to determine the positions and angles of the joints. IMUs were used for acceleration, angular rate and magnetic field vector measurements. The fusion data was used to compute actual orientation and linear acceleration. The authors used this result to estimate the kinetic energy generated in different joints during several body motions. The purpose of this analysis was to design an energy harvesting system by converting human kinetic energy to electrical energy and then find the recommended joints (knees and ankles while walking) to place the energy harvesting module.

From the discussions above, the main purpose of fusing data from multiple sensors in a joint monitoring system is to overcome physical limitations of the sensing system and improve measurement accuracy as well as reliability. This is done by minimizing the error rate and enhancing the signal-to-noise ratio (SNR) while maintaining practical usability. In addition, sensor fusion offers several other advantages such as improved resolution, increased confidence in results, robustness against interference, and reduced ambiguity and uncertainty. Although it is in the early stages of development, current research results suggest that fusion systems are superior to other means of measuring and monitoring joint movement using one or a few sensors.

2.4. Research Challenges

After evaluating all these technologies and methods, it seems that the development of a viable joint monitoring system can turn joint-related study (clinical and non-clinical) in a new direction. Wearable light-weight devices with miniature sensors and wireless connectivity appear to have the greatest potential in terms of ease of use, cost and the measurement of accurate and clinically relevant information. Despite the enormous technological advances in the past few decades, their application for joint activity

monitoring in the real world is hindered by several research challenges including the following:

- Most of the joint monitoring researches are focused on developing the sensing system using different technologies and sensing combinations. There is much less research emphasizing the data post-processing techniques and building predictive models. More work is needed to define an efficient prediction and feedback model depending on the properties of the data set and the experimental settings.
- One of the main challenges is to extract and select features in real-time systems since the modeling techniques can handle the raw extracted features. This causes unnecessary redundancies which reduce the accuracy and efficiency of the system. This can be resolved by integrating cloud server communication with the system for real-time data mining. Therefore, the cloud server can handle all sets of data by using proper algorithms.
- The majority of the studies reported in the literature employed different methods to assess validity and reliability which makes it difficult to compare these devices. In addition, clinical acceptance is questioned due to the lack of enough involvement of medical professionals during the design and evaluation process. Therefore, a standard validation criterion and protocol should be developed by the major regulatory bodies to evaluate the accuracy and reliability of a device. These standards would provide guidelines for researchers to develop high-quality devices for both research and commercial use.
- The accuracy of joint health assessment using a monitoring device is heavily affected by the variety of training data and it is highly recommended that the training data set must contain as many varieties as possible. However, it is challenging to coordinate human subjects of different ages and musculoskeletal conditions in real-time to collect a diversified joint dataset. This is a major barrier to evaluating the efficacy of the devices and rigorous clinical trials are required to address this issue.

- Although sensor fusion technique is an advanced approach, very few research studies are conducted in the field of joint monitoring. The major challenges of using multiple sensors in one system are data acquisition and processing, simultaneous wireless communication and synchronization. To solve the communication problem, we need to install a wireless communication module that supports multiple connections for different sensors. We also need to calibrate all the sensors efficiently and use data standardization methods to overcome the difficulties related to data processing and management. Moreover, the selection of a proper sensor combination in a multi-sensor system is crucial to enhance the performance of a joint monitoring system.
- The hardware and computational resources for a monitoring system can be a crucial factor for long term communication and data acquisition. Therefore, high configuration hardware support is needed with an efficient algorithm which can deal with large data set resourcefully. However, more resources will consume more power which is one of the most critical factors to be considered while building a system. To develop a balanced system, the power requirement of the system should be minimized by selecting power-efficient components and a more efficient power supply. Energy harvesting can also be an option to solve this problem.
- As the system requires processing and transmitting health information of users, information security is a key aspect to consider. It includes data privacy, security as well as ethical requirements recommended by responsible regulation bodies. The scope of security and ethical requirements need to be clearly defined and specified. Besides, more efficient and secure algorithms are needed in order to ensure highly secured communication channels in existing low power, short range wireless platforms.
- Finally, for getting widespread acceptance among users, the systems need to be simple, wearable, easy-to-use, cost-effective, non-invasive, unobtrusive and inter-operable among various operating platforms. Therefore, more research and development efforts are needed to enhance the systems' acceptance from both medical, user and business perspectives.

Chapter 3
Knee Monitoring System Design and Methodologies[†]

In order to design and develop a simple, efficient and low-cost wearable smart knee monitoring device, we investigated several sensing technologies and then selected a set of different miniaturized sensors (IMU, temperature, pressure and GSR) which, when combined, can provide the information related to joint angle and motion, as well as measure some other important physiological parameters such as local skin temperature, muscle pressure and sweat-rate of the joint skin that are related to joint health. The developed multi-sensor-based system can be wirelessly connected to a smart computing device with a continuously running software program to record and process all the knee joint and mobility-related parameters for further assessment related to knee joint health. In this Chapter, a brief overview with technical specifications of the selected sensors are presented, followed by the details of the proposed system design, experimental protocol and data acquisition methods from the sensing system. Moreover, based on the literature review, a comparison among our developed system and several published knee monitoring systems is presented at the end of this Chapter.

3.1. Sensors

Our developed knee monitoring system consists of four types of miniaturized sensors wirelessly connected to a smart computing device with a real-time software program to

[†] Part of this work will be submitted for consideration for publication as: A. I. Faisal, S. Majumder, R. Scott, T. Mondal, D. Cowan, and M. J. Deen, A Simple, Low-Cost Multi-Sensor-based Smart Wearable Knee Joint Monitoring System, March 2020. (in preparation).

record and process knee joint and mobility-related parameters. For measuring the mechanical parameters such as knee angle, rotation and speed of knee joint movement we used the IMU sensors due to their compact size and capability to measure joint motion and orientation with precision and accuracy. In order to measure other important physiological knee joint parameters such as local skin temperature, muscle pressure and sweat rate of the joint skin, we included three other sensors: temperature, pressure and GSR. Thus, our knee monitoring system with these four sensors would represent the first of its kind which can non-invasively and simultaneously monitor both the mechanical and physiological parameters related to knee joint health.

3.1.1. Inertial Measurement Unit Sensors

Inertial measurement units (IMU), also known as inertial sensors, comprise multiple 3-axes sensors (usually accelerometers, gyroscopes and magnetometers) to measure linear acceleration, angular velocity and the magnetic field vector in their own three-dimensional local coordinate system. In our system, we only used the accelerometer and gyroscope data collected from two IMUs to monitor the movements of a knee joint. We selected the MetaWear CPro IMU from MbientLab Inc. for our system because of its small size, low-cost, good energy efficiency and low-power wireless connectivity. The IMU has dimensions of 24 mm diameter x 6 mm thick and it is powered by a small coin-cell battery. The accelerometer and the gyroscope have full-scale ranges of ±16g and ±2000 degrees per second (dps), respectively, and can acquire the signal at the highest sample rate of 100 Hz. A photograph of the CPro IMU board with its dimensions is shown in Figure 3-1 and the technical specifications of the sensor are presented in Table 3-1. In addition to the on-board sensors (accelerometer, gyroscope and magnetometer), the MetaWear CPro is also equipped with general-purpose input/output (GPIO) pins which can be used to connect additional sensors to the board (Appendix B). The GPIO pins are represented by the pin interface and accessed through the GPIO interface. Therefore, we used another CPro to connect another three sensors described below using the GPIO pins and to collect their data.

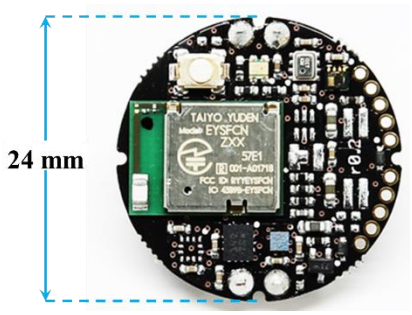

Figure 3-1. MetaWear CPro IMU board.

Table 3-1: Technical specifications of MetaWear CPro IMU board.

Sensor Parameters	Value
Weight	Ultra-lightweight at just 0.2 oz
Size	24 mm diameter x 6 mm thick
Power consumption	Sleep mode supports 6 months idle time
Power Source	200mAH coin-cell (CR2032) replaceable
Synchronized timestamp	Supports multiple devices simultaneously
Data Transfer	Bluetooth Low Energy Smart®
Range	± 2, ± 4, ± 8, ± 16 g → Accelerometer ± 125, ± 250, ± 500, ± 1000, ± 2000°/s → Gyroscope
Resolution	16bit
Sample Rate	0.001Hz – 100Hz

3.1.2. Temperature Sensor

For the measurement of the knee skin temperature, a thermistor was used. Thermistors are linear resistors whose resistance varies with temperature. The thermistor used in this project is a 135-104LAG-J01 discrete thermistor (NTC) manufactured by Honeywell Sensing and Productivity Solutions. This is a high-quality glass-encapsulated unit of 100,000 Ohm resistance with ±10.0% tolerance and 25/85 BETA = 3974 (a constant of the thermistor). A photo of the sensor is shown in Figure 3-2 and its technical specifications are presented in Table 3-2.

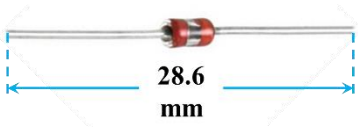

Figure 3-2. Temperature sensor (135-104LAG-J01 Discrete Thermistor).

Table 3-2: Technical specifications of temperature sensor (135-104LAG-J01 Discrete Thermistor).

Sensor Parameters	Value
Resistance at 25°C	100,000 Ohm
Resistance tolerance	±10.0%
Operating Temperature	-60 °C to 300 °C [-76 °F to 572 °F]
Size	2.0 mm diameter, 28.6 mm lead length
Beta	3974

3.1.3. Pressure Sensor

In order to measure the muscle pressure around the knee, a force sensitive resistor (FSR) whose resistance varies with the force applied to it, is used. Therefore, by measuring the resistance value, the pressure on the sensor can be estimated. We used FSR® 402 Short (Figure 3-3) manufactured by Interlink Electronics which is a sensitive single-zone force sensing resistor that is circular in shape with a diameter of 18.28 mm. The diameter of its active area is 12.7mm. The response time of the sensor is 3µs and the resistance decreases with the increasing force applied to the surface of the sensor. The technical specifications and device characteristics of the sensor are presented in Table 3-3.

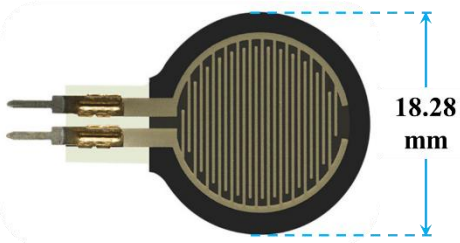

Figure 3-3. Pressure sensor (FSR® 402 Short).

Table 3-3: Technical specifications of Pressure sensor (FSR® 402 Short).

Sensor Parameters	Value
Actuation Force	0.1 Newtons
Force Sensitivity Range	0.1 - 10.02 Newtons
Force Repeatability	± 2% (single part) and ±6% (part to part)
Non-Actuated Resistance	10 MW
Response Time	3µs
Size	18.28mm diameter (active area 12.7mm diameter)
Thickness Range	0.2 - 1.25 mm
Operating Temp. Range	-30 - +70 °C

3.1.4. Galvanic Skin Response Sensor

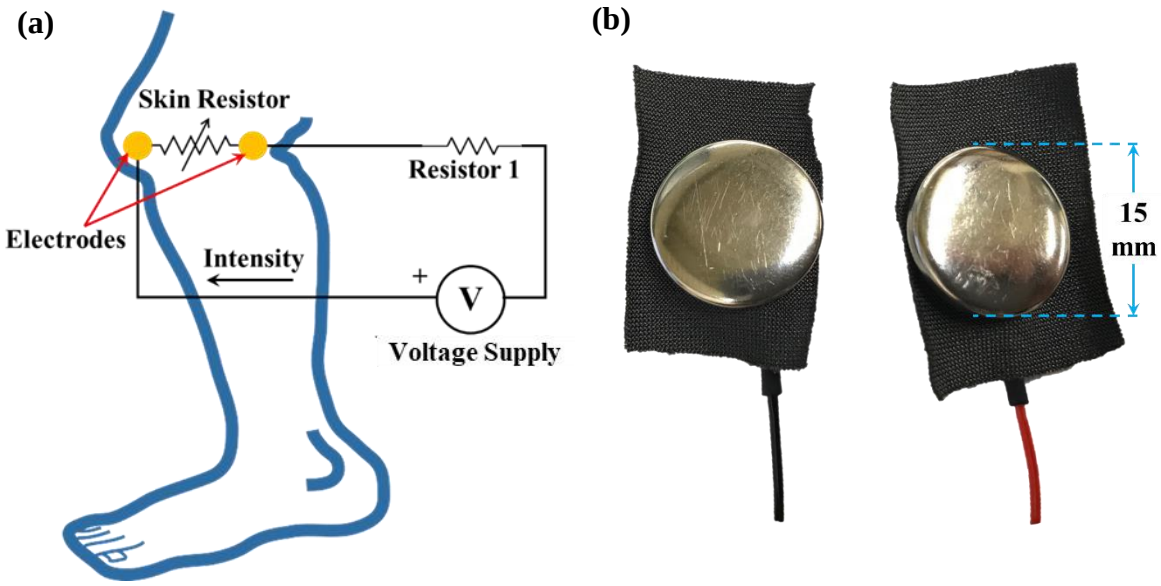

Figure 3-4. (a) GSR Sensors Schematics; (b) GSR Electrodes.

We used a two-electrodes-based Galvanic skin response (GSR) sensor for the measurement of local skin sweat gland activity, which is related to skin stress and perspiration. It measures the skin conductance around the knee which represents the sweat gland activity. The greater the sweat gland activity, the higher the skin conductance. The most common method to measure a GSR signal is based on a constant voltage system. A constant low

voltage is applied to the two electrodes that are in contact with the skin. The circuit also contains a very small resistance compared to the skin resistance that is in series with the voltage source and the electrodes (Figure 3-4(a)). In our system, we used the MetaWear CPro IMU board as the voltage source and connected two commercial electrodes (Figure 3-4(b)) with the power supply and GPIO pin of the board. With this setup, any fluctuation in the current flow due to a change in the electrical properties of the skin can be detected.

3.2. Knee Monitoring System

3.2.1. Integration of External Sensors with IMU Board

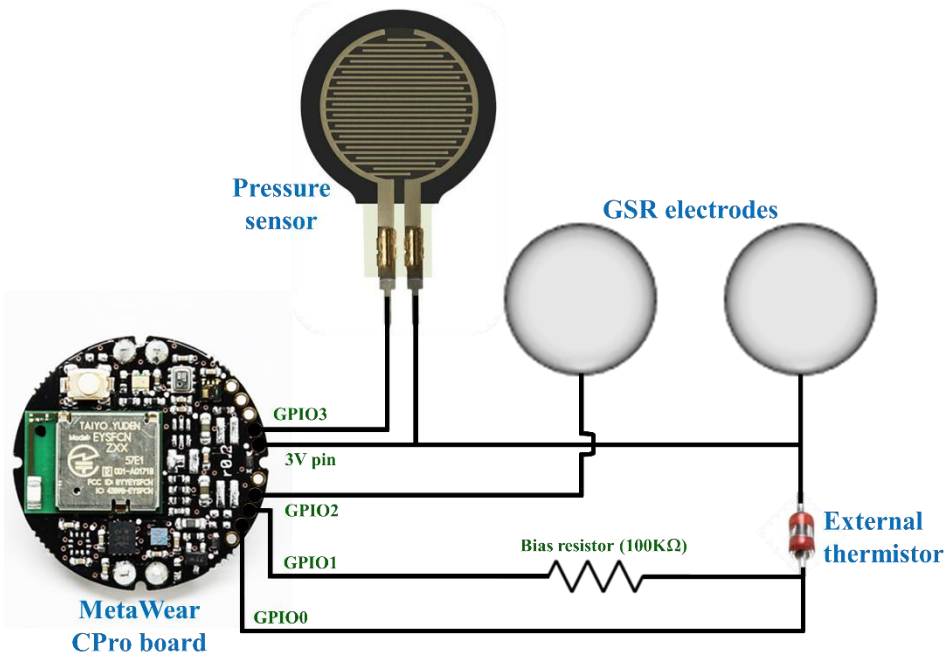

Figure 3-5. Integration of external sensors with MetaWear CPro IMU board.

First, we built a combined sensing module with temperature, pressure and GSR sensors by connecting those sensors externally to a MetaWear CPro IMU board using its GPIO pins. Here, the MetaWear CPro IMU board performs as the central processing unit and power supply and collects the readings from all three sensors and transfers the data wirelessly into a smart device for further analysis. We connected the temperature sensor to the GPIO0 (pin

2) and the 3V pin (pin 6) on the CPro board. A 100 kΩ bias resistor was also connected in series between GPIO1 (pin 3) and GPIO0 (pin 2). To measure the temperature, we measured the resistance of the temperature sensor (the variable resistor) by using the simple voltage divider rule. In this case, GPIO1 is on low (connected to ground – 0V) and then the analog value of GPIO0 is recorded. We attached two GSR electrodes to the CPro board, one to GPIO2 (pin 4) and another to the 3V pin (pin 6). The circuit of the sensor becomes complete to flow the current when both the electrodes come in direct knee skin contact. Then, the analog value of GPIO2 is recorded to calculate the skin conductance. As both the GSR and pressure sensors work with the same mechanism (resistance variation with the sensed signal), the circuit configuration for the pressure sensor setup is the same as GSR sensor. We used the GPIO3 (pin 7) and the 3V pin (pin 6) to connect our FSR to the CPro board. Then, the analog value of GPIO3 is recorded to calculate the pressure on the sensor. The integration of all these external sensors with MetaWear CPro IMU Board is presented in Figure 3-5.

3.2.2. Implementation of Multi-Sensors-based System

We used the aforementioned sensing module and two additional IMU boards to implement the prototype of our simple, easy-to-use, cost-effective, non-invasive and unobtrusive wearable wireless knee monitoring system with signal acquisition and processing software. A breathable, non-sweating, adjustable and comfortable knee brace (SLS 306 Patella Knee Support Brace from Soles) and two Velcro straps were used to attach all the sensors. Each Velcro strap has one IMU board. One strap needs to be placed above the knee (thigh) and another is below the knee (calf) to measure the mechanical parameters such as knee angle, rotation and speed of knee movement. Another CPro board along with the other three external sensors (temperature, pressure and GSR) are attached on the inner side of the knee brace (placed on knee patella) to collect the data related to the skin temperature, skin conductance and pressure by the muscles around the knee joint. The brace and the straps with the sensors can be put comfortably on around the knee without hindering a user's normal movements. With this system, we can easily and wirelessly collect and store

simultaneous knee joint data from all the sensors in a smartphone or a portable computer. A combined photograph of all the sensors and the prototype of our smart wearable wireless knee joint monitoring system is presented in **Figure 3-6.**

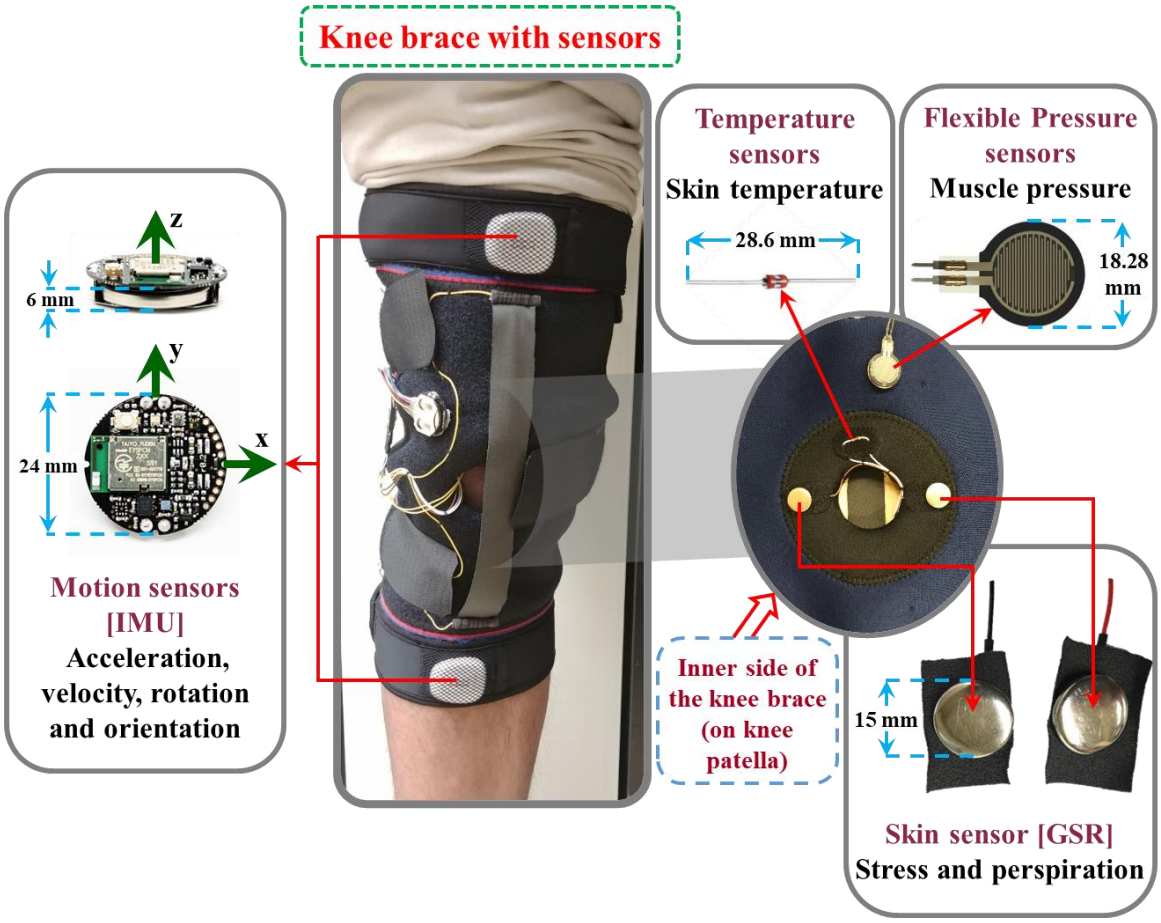

Figure 3-6. Multi-sensor-based smart wearable wireless knee joint monitoring system.

3.3. Data Acquisition System and Protocol

The smart knee monitoring system needs to be worn around the knee joint with the sensors positioned at the frontal section for monitoring the joint parameters. Prior to acquiring the joint data using the system, a letter of consent and the study protocol including some key information such as the motivation for the study, data acquisition procedure, data security and privacy protocols were prepared and reviewed by the University's Research Ethics

Board (Appendix B). A total of 70 healthy adult subjects with their ages ranging from 18 to 86 years participated in this study. Each participant was requested to answer a questionnaire form prepared by a physician to collect some key physical information which includes sex, age, weight, height, leg length, knee perimeter and some general clinical histories. Although, all subjects in our study were healthy and did not have any diagnosed health issues, 15 persons among them had reported prior histories or undiagnosed issues in their knees or legs. A summary of the subjects' characteristics are presented in Table 3-4.

Table 3-4: Summary of the subjects' characteristics.

Categories	Subject groups	Number of subjects
Gender	Male	56
	Female	14
Age (years)	18-40 (avg. 27)	52
	41-86 (avg. 59)	18
BMI (kg/m^2)	19-29	56
	<19 and >29 – Having health risk	14
Knee and leg health conditions	No issues	55
	Having histories or undiagnosed issues (knee or leg)	15

The types of tests involved the subjects strapping the knee brace on, and performing normal walking exercises for approximately 200 meters on a well-illuminated, obstacle-free wide ceramic tiled walkway (Figure 3-7) at their preferred walking speed. These walking experiments allowed for the acquisition of stable data related to joint movement while walking. The two IMUs were positioned in such an orientation that the x, y and z-axis respectively point towards the upright direction (longitudinal), the outward direction (mediolateral) and the forward direction (anteroposterior). To maintain the consistency of measurements among all subjects, the brace was always strapped with the same orientation keeping the knee in the middle and the IMUs were attached just below and above the brace maintaining same distance (14 cm) from the knee joint (Figure 3-6).

Figure 3-7. Walkway for the walking exercise.

We used an Android smartphone for real-time wireless data collection and storage from our system through Bluetooth communication. We installed "MetaBase" Android app developed and provided by MbientLab Inc. to configure our IMU boards and access the accelerometer and gyroscope sensors data. "MetaBase" is also available in Windows and iOS app stores for free. This app allows for connecting multiple IMU sensors at the same time which gave us the advantage of gathering synchronous data from both IMU sensors (Appendix B). For acquiring data from the other three sensors (temperature, pressure and GSR), we used another Android app called "MetaWear" (Appendix B). This is a development app with a free codebase [137] providing examples of different MetaWear APIs and their functionalities [138]. With the help of these examples, we customized the Android app according to our requirements to access and collect data form our other three sensors attached with the GPIO pins of the 3rd CPro board. Both the "MetaBase" and "MetaWear" Android apps can be run in parallel using the same Android smartphone. This

made our system suitable for simultaneously collecting data from all the five sensors from a subject performing the walking experiment.

All the sensors' data are stored in an easily readable file format (*.csv) which can be readily used for post-processing and further analysis. We developed several MATLAB programs to process these data and extract useful features related to gait and knee joint activities. Then, statistically significant features selection and dimensionality reduction of the features were performed for reducing the computational complexities and efficient analysis. Finally, the reduced features were classified using the support vector machine (SVM). A short list comparing our developed knee monitoring system with different published joint monitoring systems including their advantages and limitations is presented below in Table 3-5 and a block diagram showing the complete process flow of the proposed knee joint health analyzer is presented in Figure 3-8.

Table 3-5: List of different joint monitoring systems, and their advantages and limitations.

Ref.	Types of Sensor	Human Joint	Parameter	Advantages	Limitations
[40]–[43]	Electrogoniometer	Knee, ankle	Resistance / Strain	1. Based on resistive potentiometers or strain gauges application 2. Straightforward measurement	1. Large size, imprecision and fixed center configuration 2. High cost (hardware and software sold separately)
[44], [45]	Optical-based goniometer	Knee, elbow	Optical navigation	1. Compact and light-weight 2. High reaction speed	1. Sensitive to the placement location 2. 3D motion tracking may not be possible
[89], [90]	Optical fiber sensors	Knee	Signal attenuation	1. High resolution, flexibility and light-weight 2. Immunity to electromagnetic interference	1. Limited measurement range 2. Sensitive to temperature and humidity
[47], [48], [55], [91]	Video imaging-based systems	Knee, hip, elbow, shoulder	Visual data	1. Able to detect movements of multiple joints simultaneously 2. No body-worn sensors are needed	1. Limited coverage area 2. Complex method with expensive setup and sophisticated analyses
[56]–[61], [63], [117]–[119]	Textile-based sensors	Knee, hip, elbow, fingers	Resistance / Strain	1. Low-cost, flexible and suitable for long-term monitoring 2. Simple mechanism and easy integration with comfortable garments	1. Nonlinearity, low accuracy and ineligible to detect 3D movement 2. Performance degradation due to large mechanical strains and rigorous deformations
[132]	Acoustic sensors	Knee	High-frequency soundwave	1. Light-weight and easily attachable around joints 2. Wireless monitoring is possible	1. Significant background and interface noise 2. Nonlinearity and low accuracy
[73], [74], [76], [77], [83], [87], [126]	IMU sensors (accelerometer, gyroscope and magnetometer)	Knee, hip, elbow, shoulder	Linear acceleration, angular velocity and magnetic field vector	1. Low-cost, light-weight, compact, high accuracy and easy to install 2. Reliable for 3D joint movement and orientation detection	1. Signal drift 2. Sensors alignment is required in a multiple IMUs-based system
Our System	IMU sensors (accelerometer, gyroscope and magnetometer), temperature, pressure and GSR sensors	Knee	Linear acceleration, angular velocity, local skin temperature, muscle pressure and sweat-rate of knee joint skin	1. Low-cost, light-weight, compact, high accuracy and easy to install 2. Reliable for 3D joint movement and orientation detection 3. Capable of measuring other important physiological parameters (local skin temperature, muscle pressure and sweat-rate of the joint skin) related to joint health 4. Sensor fusion methods are applied to overcome signal drifts and alignment issues	1. Data analysis accuracy can be enhanced with a larger balanced dataset. 2. A stand-alone smart program is required for data acquisition, analysis and real-time feedback applications.

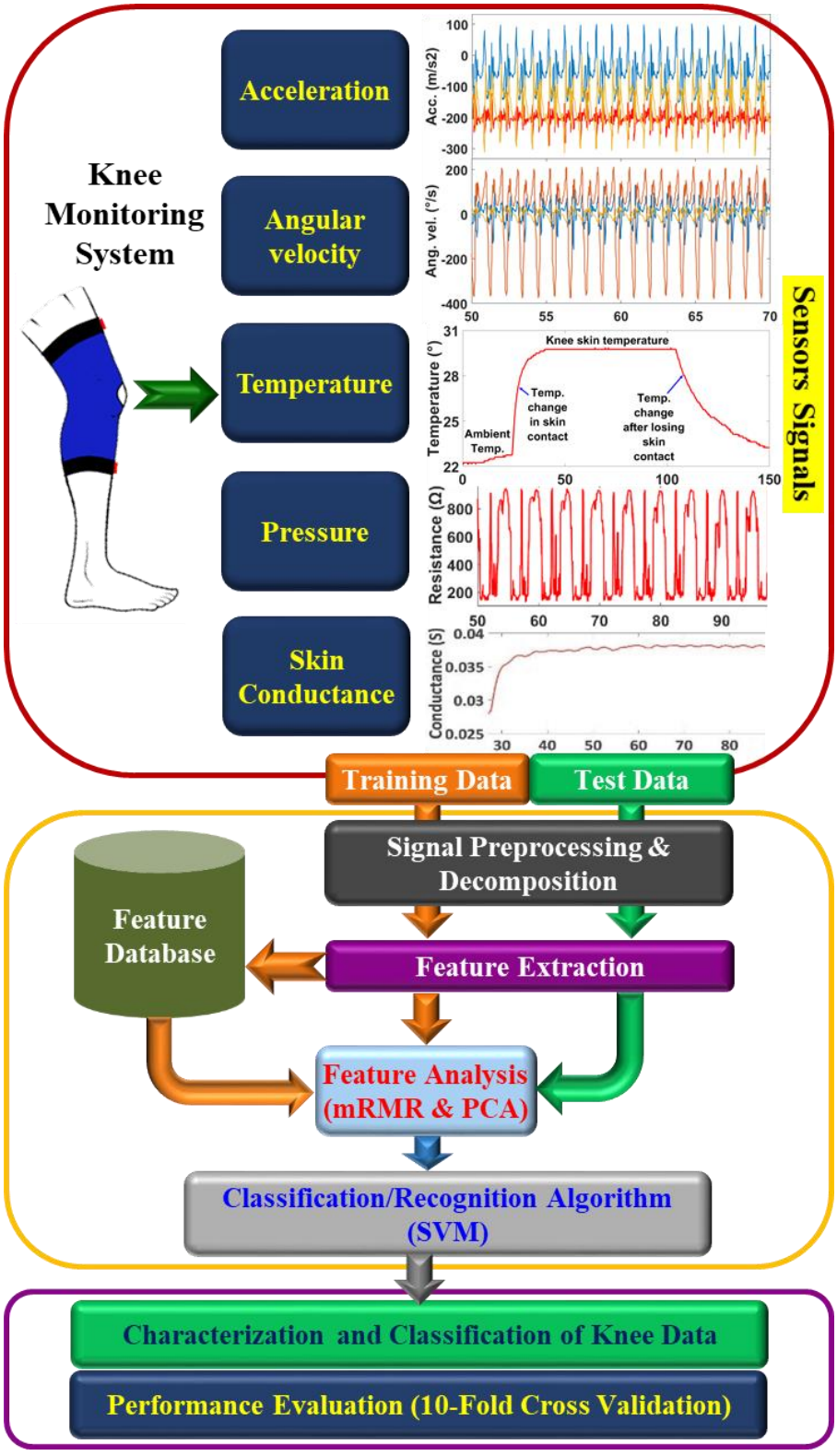

Figure 3-8. Block diagram (process flow) of the knee joint health analyzer.

3.4. Conclusions

As a summary, in this research work, we have adopted the IMU-based method and included some additional relevant sensors (temperature, pressure and GSR) to develop a simple, easy-to-use, efficient and low-cost wearable knee monitoring device. By using this device it is possible to extract valuable features related to joint angle and motion, as well as to measure other important physiological parameters such as local skin temperature, muscle pressure around the knee joint and sweat rate of the joint skin that are related to joint health. All the sensors used to develop the device are low-cost, low-power, miniature and light-weight with wireless connectivity and we followed a simple integration and data extraction process to make our system suitable for continuous or long-term knee joint monitoring during daily activities as well as joint activity analysis. Therefore, all the measured data using our multi-sensor-based knee monitoring system can be compiled to deliver valuable information and assessment related to knee joint health.

Chapter 4

Signal Processing and Data Analysis*

The collected data from the developed knee monitoring system undergoes several signal preprocessing and signal analysis steps to extract usable joint parameters and assess the mobility status of an individual. In this Chapter, we will discuss these signal processing and analysis techniques implemented for the collected data and determine important joint parameters such as knee angle, stride length, minimum foot clearance (MFC), gait speed, cadence (steps per minute), knee skin temperature, skin conductance and the pressure by the muscles around the knee joint. Besides these parameters, a set of statistical, temporal and energy features of knee joint movement were also extracted from the acquired IMU signals (linear acceleration and angular velocity). Different validation techniques that were used to validate the measurements of joint and gait parameters from our proposed monitoring system are also described.

4.1. Preprocessing

The raw data from the IMUs include random high-frequency noise from the vibration of the device and ambient environment which degrades the sensor readings and in turn, affects its accuracy [73], [139], [140]. To get a cleaner signal by removing this high-frequency noise, the sensor data is filtered using a fifth-order digital low-pass Butterworth filter. Since most of the significant features of the knee joint motion signals remain in the low-frequency region, we set the cut-off frequency of the filter at 12 Hz. Although both IMU sensors are calibrated to gather simultaneous data with a fixed sample rate (50 Hz for our work), the

* Part of this work will be submitted for consideration for publication as: A. I. Faisal, S. Majumder, R. Scott, T. Mondal, D. Cowan, and M. J. Deen, A Simple, Low-Cost Multi-Sensor-based Smart Wearable Knee Joint Monitoring System, March 2020. (in preparation).

total sample counts are not always the same for a longer set of data. Therefore, the filtered data from two IMU sensors are resampled with respect to a single time-array having a predefined sample rate (50 Hz) in order to time-align the data with each other. This alignment procedure is necessary for precise knee angle and motion calculation. A flowchart depicting the IMU signal preprocessing is shown in Figure 4-1.

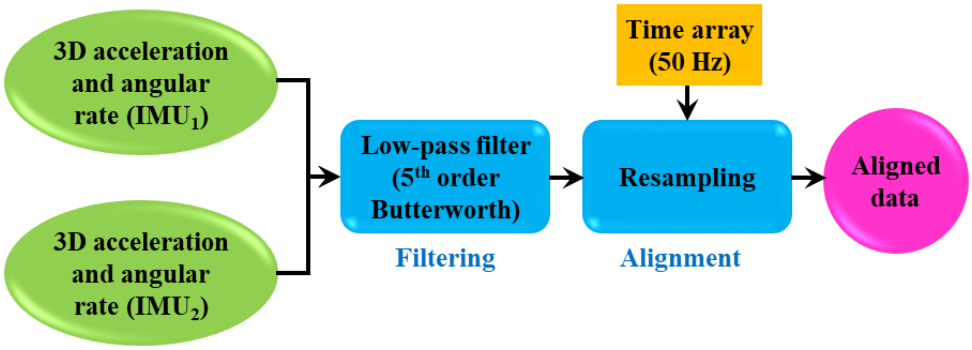

Figure 4-1. IMU signal preprocessing flowchart.

4.2. Estimation of Knee Joint and Gait Parameters

4.2.1. Knee Angle

We used the calibrated time-aligned data from two IMU sensors (IMU_1 and IMU_2) to measure the angle of knee flexion or extension (Figure 4-2). This angle calculation is useful for estimating the range of motion (ROM) of the knee joint which can vary depending on sex, age, physical structure and daily activities [19]. First, we used the accelerometer and gyroscope data individually to calculate the knee angle. The calculation from the accelerometer's data provides more absolute angle information due to sensors' orientation independence from each other. However, the measurement accuracy can be affected by the high-frequency noise in the sensors' data. On the other hand, it is simpler to calculate knee angles using the gyroscope data because its data is less impacted by high-frequency noise. However, the gyroscope data suffers from low-frequency drift over time. Therefore, we applied a fusion method (complementary filter) that combines both accelerometer and

gyroscope data to remove accelerometer noise and overcome gyroscopic drift while computing the knee angle during walking (Figure 4-3).

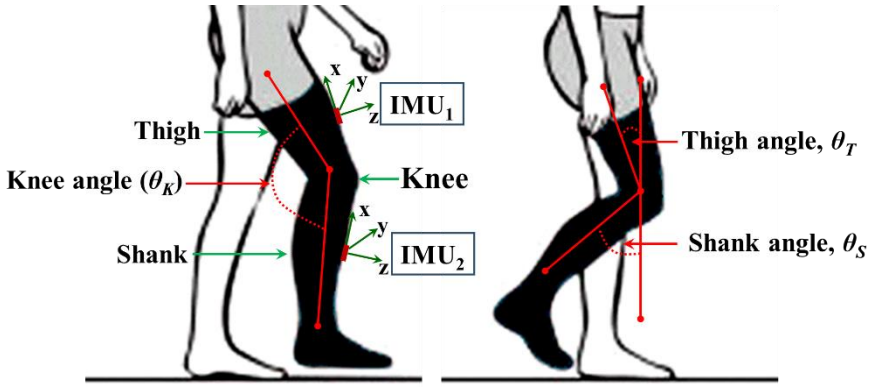

Figure 4-2. Knee angle from IMU sensors.

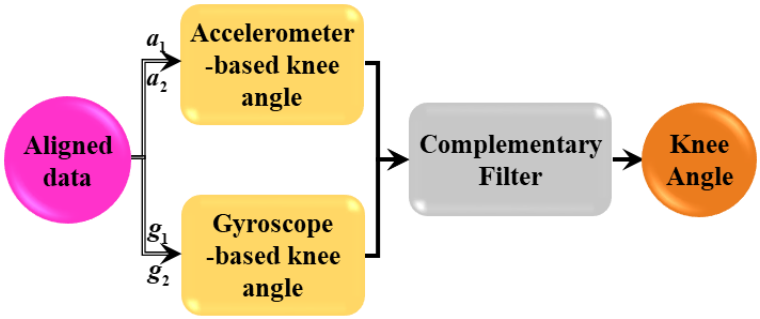

Figure 4-3. Sensor fusion to calculate knee angle.

For extracting knee angles from the accelerometer readings while walking or during other activities, first, it is necessary to estimate the IMUs' orientation vectors on the shank and thigh with respect to ground in a stationary position (straight standing with maximum knee extension). Second, we used the accelerometer readings while walking to compute the angle change between two vectors (stationary and walking) for both shank and thigh. The angle change from the accelerometer data was calculated using equation (4-1)

$$\theta_{acc} = \cos^{-1}\left(\frac{\overrightarrow{a_{st}} \cdot \vec{a}}{\left|\overrightarrow{a_{st}}\right| \cdot \left|\vec{a}\right|}\right), \tag{4-1}$$

where θ_{acc} is the angle between the two acceleration vectors, $\overrightarrow{a_{st}}$ and $\vec{a}$. The vector in stationary position (different for thigh and shank) is $\overrightarrow{a_{st}}$, and the vector during walking is

$\vec{a}$, whose value and direction changes with the sagittal movement of the thigh and shank. Thus, we can calculate the angle change for both thigh ($\theta_{T_{acc}}$) and shank ($\theta_{S_{acc}}$) while walking. We also determined the knee angle $\theta_{st_{acc}}$, in a stationary position from $\overrightarrow{a_{T_{st}}}$ (thigh) and $\overrightarrow{a_{S_{st}}}$ (shank) using the same equation. The walking knee angle $\theta_{K_{acc}}$, was then calculated using equation (4-2)

$$\theta_{K_{acc}} = \theta_{st_{acc}} - \left(\theta_{T_{acc}} + \theta_{S_{acc}}\right). \tag{4-2}$$

Calculation of the knee angle is straightforward using the angular velocities derived from two gyroscope data. The difference between the angular velocities around the joint axis was integrated with respect to time to calculate the angle. The knee angle $\theta_{K_{gyr}}$, from the gyroscope data [73] is defined as:

$$\theta_{K_{gyr}}(t) = \int_0^t \left(g_1(\tau)\cdot j_1 - g_2(\tau)\cdot j_2\right) d\tau\,. \tag{4-3}$$

In equation (4-3), j_1 and j_2 denote the joint axes for IMU$_1$ and IMU$_2$ devices, and g_1 g_2 represent their respective gyroscope values.

The calculated angles from both accelerometer and gyroscope data are then combined, using sensor fusion, in a way such that the limitations of each sensor are mitigated. We used a complementary filter which is a simple method of implementing sensor fusion for knee angle estimation with a very low computational complexity (Figure 4-4) [141].

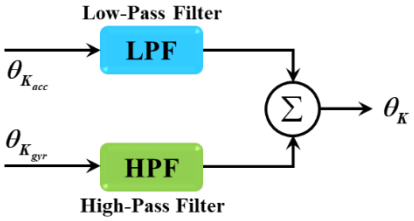

Figure 4-4. Complementary filter.

Complementary filters have the effect of low pass filtering the accelerometer data and high pass filtering the gyroscope data, then combining them to give the result. Complementary filters can be implemented by using equation (4-4)

$$\theta_K(t) = \alpha * \theta_{K_{gyr}}(t) + (1-\alpha)(\theta_{K_{acc}}(t)), \quad (4\text{-}4)$$

where θ_K is the knee joint angle and α is the filter constant. It is a tunable parameter between 0 and 1 which determines the cut-off time for trusting the gyroscope and filtering in the accelerometer data. By selecting an appropriate time constant, τ for the filters, the value of α can be obtained by using equation (4-5)

$$\alpha = \frac{\tau}{(\tau + T_S)}. \quad (4\text{-}5)$$

In our work, we tried different cut-off time for the complementary filter to select the appropriate time constant, τ for achieving the highest accuracy. We obtained the optimal value of α is 0.93 for a time constant (τ) of 0.25 s (4 Hz cut-off frequency) and sampling time (T_S) of 20 ms. This indicates that for time periods shorter than 0.25 s, the gyroscope data takes precedence and the accelerometer data is filtered out while for time periods longer than 0.25s, the accelerometer data takes precedence.

4.2.2. Stride Length and Minimum Foot Clearance

Stride length and minimum foot clearance (MFC) are two very important parameters for knee joint functionality assessment as well as gait analysis [142], [143]. A short stride length and a low MFC usually indicate reduced knee joint movement and angle during walking. Stride length is calculated by measuring the distance covered in one stride cycle (Figure 4-5). On the other hand, MFC denotes the vertical distance of foot bottom/shoe sole above the ground during the mid-swing phase (shank is perpendicular and foot is parallel to the ground) of a gait cycle (Figure 4-5). The movement of the foot during the mid-swing phase is considered as the most critical event while walking due to having the maximum horizontal velocity and minimum vertical distance above the ground [144]. Therefore, having a low MFC can trigger the possibility of trips and falls [145]. We utilized the gyroscope data from the shank's IMU to calculate the horizontal and vertical movement of the sensor during walking for stride length and MFC estimation. For these, we segmented the continuous motion signal into a series of stride cycles where each cycle consists of one

swing and one stance phase by applying a simple signal peak detection method (Figure 4-6).

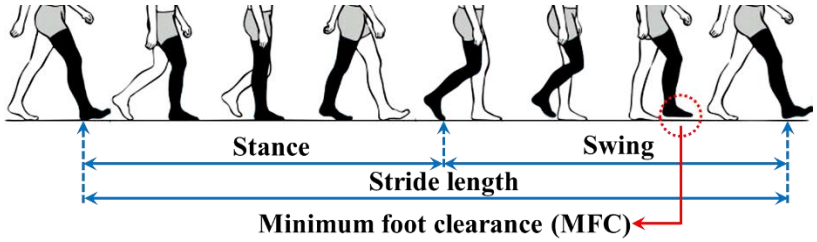

Figure 4-5. Stride length and minimum foot clearance in one gait cycle.

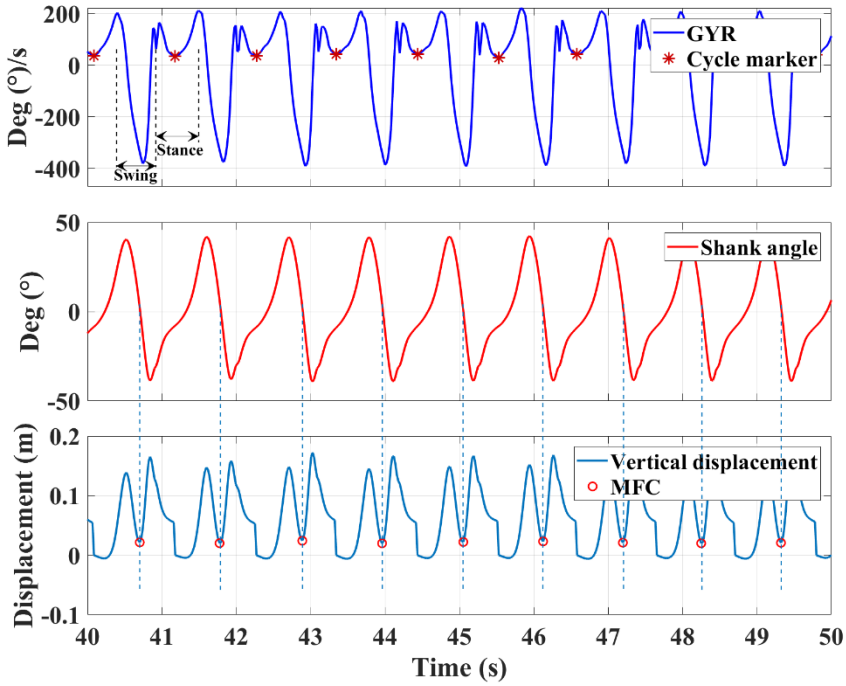

Figure 4-6. Minimum foot clearance (MFC) detection from vertical displacement.

To compute the displacement along the horizontal and vertical ground axes for each cycle, we first computed the shank angles both in the sagittal and transverse planes by integrating the gyroscope-measured angular velocities (equation (4-6))

$$\theta_S(t) = \int_0^t \omega(\tau) d\tau + \theta_S(0). \tag{4-6}$$

We also calculated the linear velocity v, by multiplying the angular velocity ω, with the radius r, of the angular rotation (equation (4-7))

$$v(t) = \omega(t) * r\,. \tag{4-7}$$

In this case, the radius of the angular rotation r, is equal to the length from the knee to the bottom of the heel. We then resolved the calculated linear velocity v, into horizontal (v_{hor}) and vertical (v_{ver}) components with respect to the earth, according to equation (4-8) and (4-9)

$$v_{hor}(t) = v(t) * \cos\theta_S(t)\,, \tag{4-8}$$

$$v_{ver}(t) = v(t) * \sin\theta_S(t)\,. \tag{4-9}$$

While considering the horizontal velocity, the sensor has the movements both in sagittal and transverse planes. Therefore, for precise estimation, we calculated linear velocity components $v_{hor,s}$ and $v_{hor,t}$, in both of these two planes by using equation (4-8) and then used these two components to obtain the magnitude of horizontal gait velocity v_{gait}, (equation (4-10))

$$v_{gait}(t) = \sqrt{\left(v_{hor,s}(t)\right)^2 + \left(v_{hor,t}(t)\right)^2}\,. \tag{4-10}$$

A simple trapezoidal integration of the horizontal gait velocity v_{gait}, during one stride cycle from $t = 0$ to $t_{one\ cycle}$, provides the horizontal displacement also known as stride length (equation (4-11))

$$Stride\ Length = \int_0^{t_{one\ cycle}} v_{gait}(\tau)d\tau\,. \tag{4-11}$$

Similarly, by integrating the vertical velocity v_{ver}, we obtained the vertical displacement s_{ver} (equation (4-12))

$$s_{ver} = \int_0^{t_{one\ cycle}} v_{ver}(\tau)d\tau\,. \tag{4-12}$$

The MFC occurs when the foot is parallel, and the shank is perpendicular to the ground. This means that the shank angle at the MFC is zero. Therefore, we used the calculated shank angle plot to identify the MFC location and then we determined the MFC in each stride cycle from the vertical displacement s_{ver} (Figure 4-6).

4.2.3. Gait Speed and Cadence

We are also able to measure gait speed and cadence (steps per minute) using our system. These two gait parameters are commonly used to evaluate the overall performance of walking [146]. To calculate the gait speed, the total distance of walking was divided by the travel time (equation (4-13)),

$$Gait\ Speed = \frac{D_{total}}{t_{stop} - t_{start}}, \tag{4-13}$$

where the total walking distance D_{total}, was calculated from the summation of stride lengths during each stride cycle from starting time t_{start}, to stopping time t_{stop}, (equation (4-14)).

$$D_{total} = \sum_{n=1}^{N} Stride\ Length. \tag{4-14}$$

In equation (4-14), *N* is the total number of gait cycles of an individual. We also used this number to calculate cadence using equation (4-15)

$$Cadence = \frac{N * 2 * 60}{t_{stop} - t_{start}}. \tag{4-15}$$

As each gait cycle consists of two steps, and cadence is expressed in steps per minute, therefore in equation (4-15), *N* is first multiplied by 2 and 60, and then divided by travel duration to determine the cadence of an individual.

4.2.4. Temperature, Pressure and Skin Conductance

We measured the knee skin temperature, skin conductance and the pressure by the muscles around the knee joint by using three different sensors attached on the inner side of the knee brace (see Figure 3-6). For measuring the knee skin temperature, we used an NTC Thermistor whose resistance value changes with temperature. We applied a simple voltage divider rule to resolve thermistor's resistance value R, from the ADC value (10-bit) obtained from MetaWear CPro board acting as the data acquisition unit of the sensor (equation (4-16)).

$$R = \frac{R_B * ADC_{Reading}}{1023 - ADC_{Reading}}. \quad (4\text{-}16)$$

The measured resistance R depends on the ADC reading, the bias resistor R_B in the voltage divider, and the ADC resolution which is 1023 in our system. To convert the resistance to a temperature measurement, we used "Steinhart–Hart Equation" also known as B (or β) parameter equation (equation (4-17)) which has been determined to be the best mathematical expression for the resistance-temperature relationship of NTC thermistors [147].

$$\frac{1}{T} = \frac{1}{T_0} + \frac{1}{\beta} \ln \frac{R}{R_0}. \quad (4\text{-}17)$$

In equation (4-17), R is the thermistor resistance at the skin temperature T in °C, R_0 is the resistance at T_0 = 25 °C and β is a constant of the thermistor, and it is 3974 for our sensor.

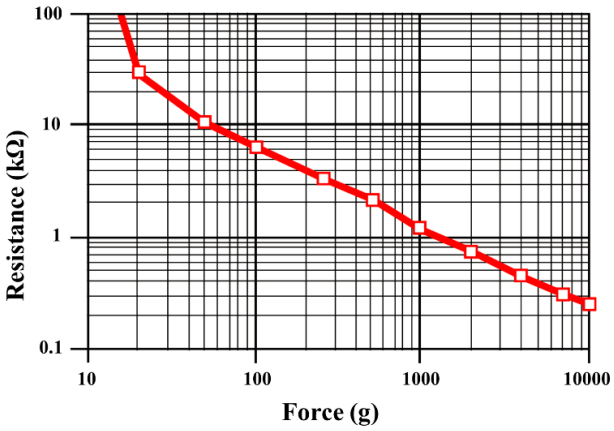

Figure 4-7. Force vs. resistance (FSR® 402 Short).

The working principle of the other two sensors, pressure and GSR, is the same as the temperature sensor – resistance variation with input stimulus. Therefore, we used the same method to determine the sensor resistance for further calculation. For the pressure sensor, we used the datasheet of FSR® 402 Short to determine the corresponding pressure from the resistance value. Figure 4-7 shows the resistance vs. force plot obtained from the datasheet.

Finally, we computed skin conductance G_{skin} (Siemens, S), around the knee by inverting the resistance value R_{GSR} measured by the GSR sensor (equation (4-18)).

$$G_{skin} = \frac{1}{R_{GSR}}. \tag{4-18}$$

4.3. Measurement Validation

4.3.1. Knee Angle

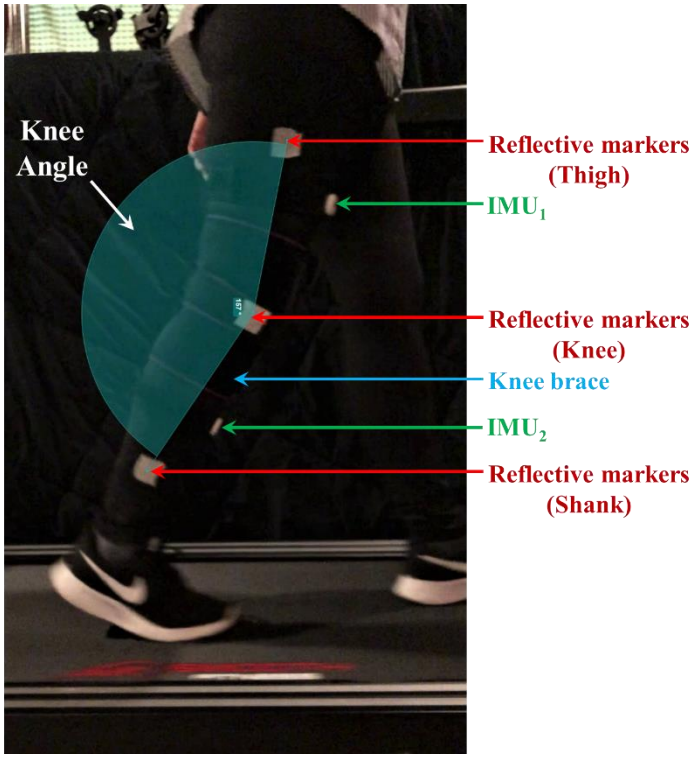

Figure 4-8. Reflective Markers attached on the subject's right lower limb (thigh, knee and shank) for knee angle measurement validation.

For knee angle measurement validation, the results from our IMU-based system were compared to a video-based motion analysis system. Video-based systems are widely used to quantify joint kinematic data for human gait in a controlled environment [49], [148]. We used a high-speed camera to capture two-dimensional (2D) videos of knee joint movements during walking on a treadmill and a freeware motion-analysis software Kinovea (version

0.8.26) [148] to analyze the video and quantify the knee joint angles during walking. Along with the knee monitoring system, three reflective markers were attached on specific lateral anatomical positions (thigh, knee and shank) of the subject's right lower limb as shown in Figure 4-8. These markers are detected by the motion-analysis tool to quantify the joint angles during walking. We initialized both the systems simultaneously to obtain synchronized data.

We used the concordance correlation coefficient ρ_C [77], [149] to compare the angle measurements from both systems. This coefficient measures the agreement between two readings from the same sample by determining the variation from the concordance line (45° line through the origin). With this method, we can assess the reliability of a new algorithm or a device by comparing to another known technique. The calculation of ρ_C, comprises a measurement of precision ρ, and accuracy C_b, and is

$$\rho_C = \rho * C_b . \tag{4-19}$$

Here, ρ is the Pearson correlation coefficient that measures how far each observation deviates from the best-fit line and it represents a measure of precision. C_b is a bias correction factor which measures how far the best-fit line deviates from the 45° line through the origin and denotes a measure of accuracy. The value of ρ_C ranges from 0 to 1, where 1 represents perfect concordance and a value of zero denotes complete disagreement. A descriptive scale for values of the concordance correlation coefficient is proposed in [150] and is reproduced in Table 4-1.

Table 4-1: Descriptive scale for values of the concordance correlation coefficient.

Value of ρ_c	Strength of agreement
< 0.90	Poor
0.90 - 0.95	Moderate
0.95 - 0.99	Substantial
>0.99	Almost perfect

The results obtained from the developed knee monitoring system showed substantial consistency with the readings from the video-based motion analysis system (Figure 4-9 and Table 4-2).

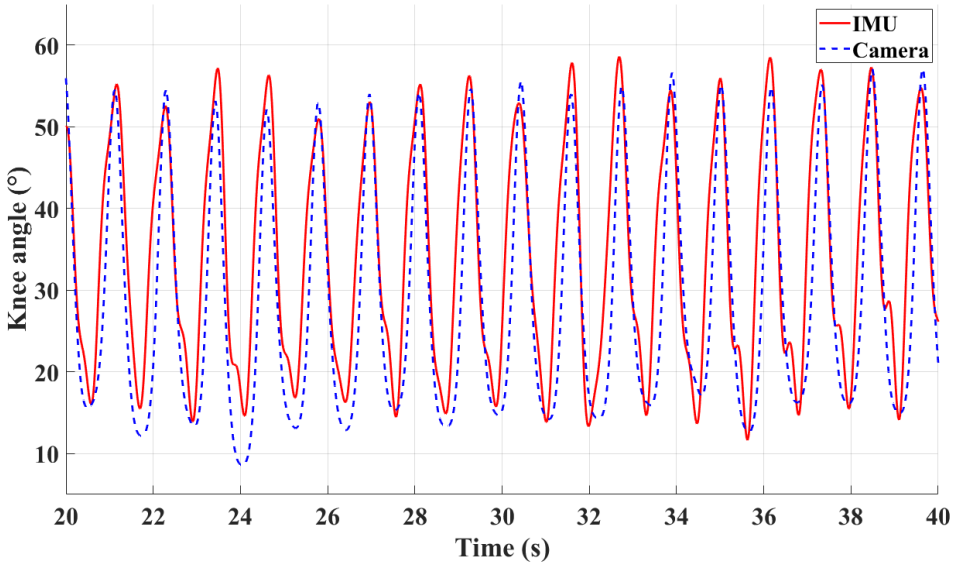

Figure 4-9. Knee joint angle of a walking test on treadmill.

Table 4-2: Concordance correlation coefficient ρ_c for walking test.

ρ_c : Concordance correlation coefficient	C_b : Bias correction factor	ρ : Pearson correlation coefficient
0.9577	0.9820	0.9753

4.3.2. Stride Length, Gait Speed and Cadence

The proposed stride length, gait speed and cadence calculation algorithms were validated using the traditional manual method. In this method, the steps of the subjects were manually counted while performing the walking exercise and the total distance was measured using a measuring tape. Therefore, the average stride length was calculated using,

$$Stride\ Length_{avg.} = \frac{D}{\left(\frac{number\ of\ steps}{2}\right)}, \tag{4-20}$$

where D is the measured distance for walking exercise. As one stride consists of two consecutive steps, the total number of steps was divided by two to get the total number of strides. Time information (total duration T) of the walking exercise was retrieved from the IMU readings. Gait speed and cadence were then calculated using equations (4-21) and (4-22).

$$Gait\ Speed = \frac{D}{T}, \tag{4-21}$$

$$Cadence = \frac{number\ of\ steps * 60}{T}. \tag{4-22}$$

This validation process included 10 subjects walking data to compare the results obtained from our developed system with manually calculated values for stride length, gait speed and cadence. The walking distance for each subject was 65 meters straight. Figure 4-10 shows the comparison and estimation errors (in cm) of the stride length calculation between two techniques.

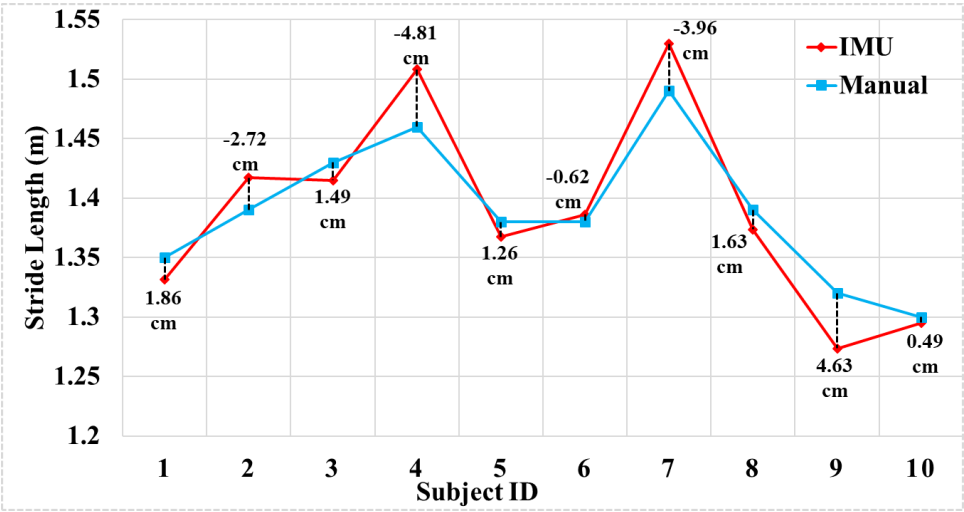

Figure 4-10. Comparison and estimation errors (in cm) of the stride length calculation.

As shown in Figure 4-10, in the worst case (subject 4) the estimation error for stride length was 4.81 cm (3.3%) and the mean error for 10 subjects was 1.7%. Similarly, for gait speed, the highest estimation error was 3.8% (5.1 cm/s) and the mean error was 2.1%. The cadence calculation using the knee monitoring system was also quite accurate with a mean error of 1.2%. Thus, these results proved the reliability of our system and the algorithm for determining stride length, gait speed and cadence.

4.3.3. Minimum Foot Clearance

Figure 4-11. MFC measurement validation using video-based motion analysis system.

We used the same video-based motion analysis system to validate the MFC measurement (Figure 4-11). In this case, one reflective marker was attached on the lateral side of the shoe to track the motion of the foot in the walking video. Then, we extracted the MFC (vertical distance between shoe sole and ground while the foot was parallel to the ground) from the tracked video to validate our measurement system. We measured MFC using both the systems simultaneously for normal and fast walking speed on the treadmill. In Table 4-3, a comparison between MFC calculations from the two systems is presented.

Table 4-3: MFC comparison.

	Avg. MFC from Video (mm)	Avg. MFC from IMU (mm)	Mean Error	
			(mm)	(%)
Normal walk	19.86	20.07	0.21	1.1
Fast walk	26.21	27.40	1.19	4.5

All the comparison results showed that the estimation of knee joint angle and gait parameters using our developed system were accurate and robust enough to be considered as a reliable device for knee joint and gait monitoring as well as assessment. We also

collected multiple knee data from the same subjects walking under similar conditions but at different times and compared those data in order to ensure the reproducibility of the measurement using our system. For each case, the acquired data from all the sensors showed high consistency and small variations with the highest standard deviation of ±7.5% from the mean values.

4.4. Feature Extraction

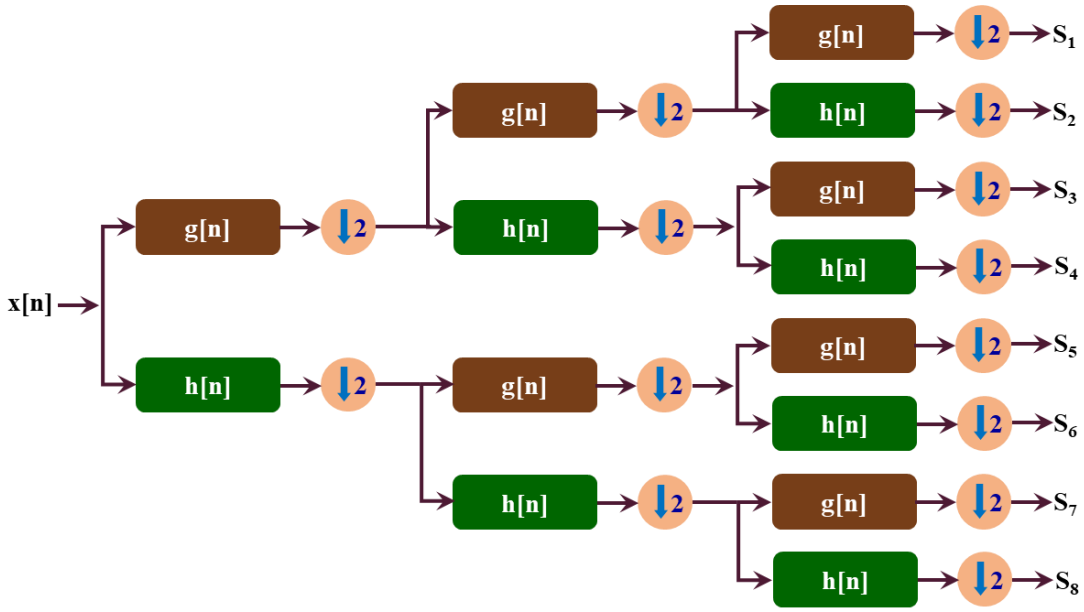

Figure 4-12. Wavelet packet decomposition tree up to 3rd level.

The feature extraction stage involves deriving relevant, informative and non-redundant data structures known as feature vectors from the sensors' signals for further analysis and better interpretation. We extracted a large set of time and frequency domain features from the preprocessed signals which included the energy features of each signal, timing and statistical parameters of the knee motion signals. Joint motion signals, being complex, non-linear and non-stationary, and having variable spectral characteristics, can be effectively analyzed by decomposing them into their spectral components.

To get the spectral components, we used wavelet packet decomposition (WPD) because of its fast and hierarchical tree-like decomposition algorithm, which makes it suitable for real-time applications. WPD is a wavelet transform where the signal is passed through more filters than the discrete wavelet transform (DWT). In the DWT, approximation coefficients and detail coefficients are decomposed by passing the discrete time-domain signal through a discrete-time low- and high-pass quadrature mirror filters in the first level. Then, the following levels are calculated by passing only the previous wavelet approximation coefficients i.e. the lower frequency components through the similar low- and high-pass filters [151]. The detail coefficients or the higher frequency components from each level remain unaltered. However, in the WPD, both the detail and approximation coefficients are further decomposed to create the full binary tree (Figure 4-12) and allow the signal to decompose evenly throughout its whole spectrum [152]. All components of a gyroscope signal around the mediolateral axis decomposed at level 2 are presented in Figure 4-13.

In our study, we used WPD at level 8 to decompose the preprocessed signals of the sensors and calculated the energy information E of each decomposed signal using equation (4-23). Those energy features derived from the signal components are closely related to the mechanical work done during knee joint movements [153], [154].

$$E = \frac{1}{M}\sum_{n=1}^{N}[S(n)]^2 \tag{4-23}$$

In equation **Error! Reference source not found.**, M represents the total number of gait cycles in the signal, N is the total number of samples and S denotes a decomposed signal component from the sensors.

We also extracted the timing parameters of knee motion which are important because of their variation with age, gender, BMI as well as knee health condition [122]–[124]. Other relevant statistical features such as mean, maxima/minima, correlation coefficient, standard deviation and signal ratio are also calculated to realize discriminating information between various states or classes of the sensors data. In total, a 159-length feature vector was extracted from the sensors signals and Table 4-4 presents a list of the key features extracted for further joint analysis.

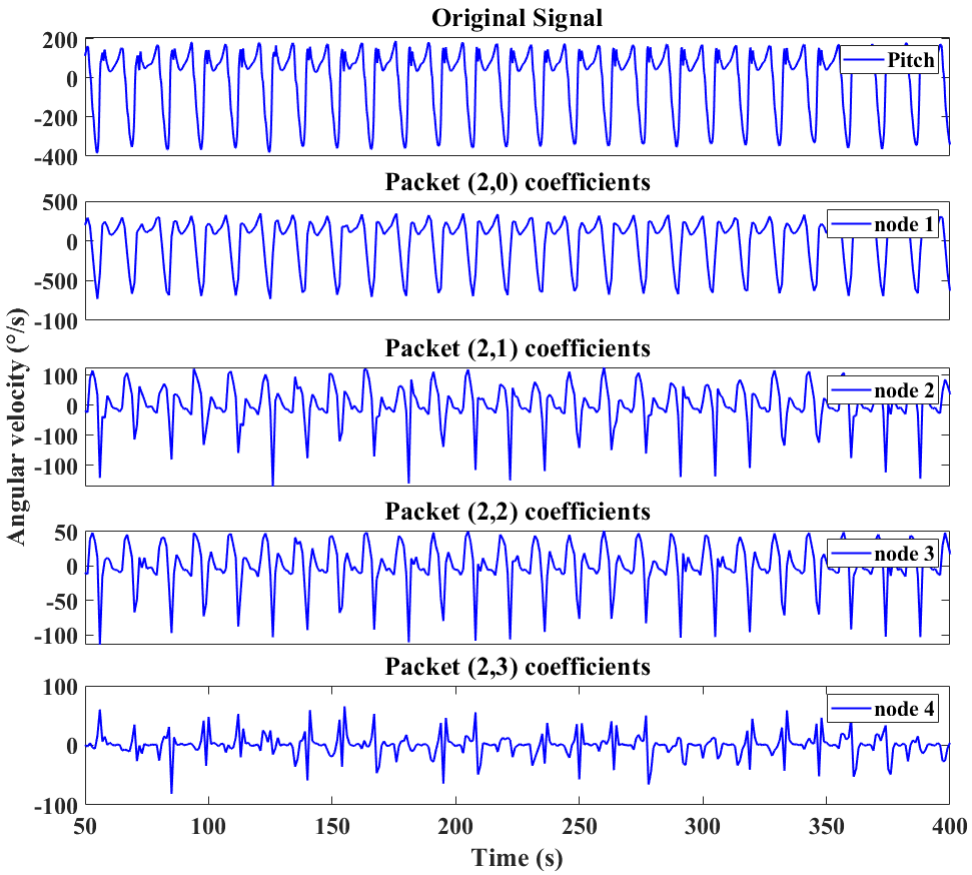

Figure 4-13. Original and four components of the mediolateral signal decomposed at 2nd level with wavelet packet decomposition.

Table 4-4: Extracted features.

Physiological	Temporal	Energy	Statistical
• Angle (knee, thigh and shank) • Stride length • MFC • Gait speed • Cadence • Knee skin temperature • Knee skin conductance • Muscle pressure around knee joint	• Stride time • Swing time • Stance time	• Acceleration • Angular velocity • Wavelet packet decomposed signal components	• Mean • Maxima/Minima • Correlation (thigh and shank IMU signals) • Linear correlation coefficient • Standard deviation • Ratio between two IMU signals

4.5. Conclusions

In summary, the signal processing and analysis of the acquired data is a vital phase of this research to retrieve necessary information related to knee joint health monitoring. There were four major steps involved: (1) Preprocessing of the raw sensor data; (2) Important knee joint and gait parameters estimation; (3) Validation of these measurements; and (4) Other relevant features extraction such as statistical, temporal and energy features of knee joint movement. In the preprocessing step, noise in the raw signals from the knee monitoring system were filtered out and then the "cleaned" signal were resampled to make them aligned with each other. Next, the clean signals were used to calculate different knee parameters such as knee, thigh and shank angle change, knee skin temperature, muscle pressure, and skin conductance during walking. We also estimated several gait parameters such as stride length, MFC, gait speed and cadence which are also important for gait analysis. In addition, we used different feature extraction techniques to obtain statistical, temporal and energy features from the preprocessed signals. These features are important to formulate the relationship between the key characteristics of the knee joint and prepare the model for prediction and diagnostic decision making.

Chapter 5
Characterization and Classification of Knee Data*

The extracted features from the knee monitoring systems are used for characterization of the knee joint behavior and classification according to their common characteristics for different subject groups. In order to select more discriminative and statistically significant features, and reduce the dimensions of input data, we applied different feature selection and dimensionality reduction algorithms. After completing the feature selection step, we used the key parameters and statistically significant features to characterize the data and retrieve meaningful information such as anomaly, outliers and alarms detection which can be used for further prediction, diagnostic decision making and feedback applications. The support vector machine was then exploited and trained with the reduced feature vector and their corresponding classes. The classes of the subjects' data were specified with respect to their age, gender, BMI, as well as their knee and leg health conditions. It was observed that the hyperplane determined by the SVM can successfully cluster the data into two separate classes with a high degree of accuracy which correspond to their class identities. The classification accuracy of the applied technique was evaluated by a 10-fold stratified cross-validation.

* Part of this work will be submitted for consideration for publication as: A. I. Faisal, S. Majumder, R. Scott, T. Mondal, D. Cowan, and M. J. Deen, A Simple, Low-Cost Multi-Sensor-based Smart Wearable Knee Joint Monitoring System, March 2020. (in preparation).

5.1. Feature Selection and Dimensionality Reduction

In order to reduce the redundancy and high dimensionality of the feature vectors, and for efficient analysis, dimensionality reduction was performed in two steps. First, we applied a feature selection algorithm (mRMR – minimum redundancy maximum relevance) [155], [156] to rank all the extracted features with respect to their importance score and then a 36-length feature vector was derived based on their statistical significance ($p < 0.05$). The feature importance of a given feature X_i ($i \in \{1, 2, ..., m\}$), among total m (=159 in our work) features based on mRMR can be expressed as:

$$f^{mRMR}(X_i) = I(Y, X_i) - \frac{1}{|S|}\sum_{X_S \in S} I(X_S, X_i), \tag{5-1}$$

where Y is the response variable, S is the set of selected features, $|S|$ is the number of features and $X_S \in S$ is the features out of the feature set S. The function $I(.,.)$ is the mutual information (equation (5-2)).

$$I(Y, X) = \int_{\Omega_Y}\int_{\Omega_X} p(x, y)\log\left(\frac{p(x, y)}{p(x)p(y)}\right)dxdy, \tag{5-2}$$

where Ω_Y and Ω_X are the sample spaces corresponding to Y and X, $p(x, y)$ is the combined probability density, and $p(.)$ is the marginal density function. For discrete variables Y and X, the mutual information function is expressed as:

$$I(Y, X) = \sum_{y \in \Omega_Y}\sum_{x \in \Omega_X} p(x, y)\log\left(\frac{p(x, y)}{p(x)p(y)}\right). \tag{5-3}$$

In this mRMR feature selection process, at each level, the feature with the highest feature importance score $\max_{X_i \in S} f^{mRMR}(X_i)$ is added to the selected feature set S. Thus, all the extracted features are ranked based on their importance score.

The second step is dimensionality reduction was accomplished utilizing principal component analysis (PCA) [157]. PCA is a mathematical technique that reduces the size of the data set and extracts the most important information from the data table. It compresses

the high dimensionality of the feature vector onto a lower-dimensional feature subspace by analyzing the covariance matrix of the data [158]. The definition of the covariance matrix for a data set with n dimensions can be expressed as:

$$C^{n\times n} = (c_{ij}, c_{ij} = \text{cov}(Dim_i, Dim_j)), \tag{5-4}$$

where $C^{n\times n}$ is a $n\times n$ covariance matrix and Dim_x is the x -th dimension. The covariance between two feature vectors X and Y presents the correlation between them. If the covariance value is positive, it indicates both vectors have the same directions and if negative, then they move to the opposite directions. If it is zero, then the two vectors are independent of each other. The formula to calculate covariance is

$$\text{cov}(X, Y) = \frac{\sum_{i=1}^{n}(X_i - \bar{X})(Y_i - \bar{Y})}{(n-1)}, \tag{5-5}$$

where $\bar{X}$ and $\bar{Y}$ are the mean values. After computing the covariance matrix of a data set, eigenvalues and eigenvectors for the covariance matrix are calculated to determine the variances for each component. In general, only first few components contain most of the variance of the original data. Thus, the new lower dimensional vector ensures minimal loss of relevant information. In our study, the 36-length feature vector was projected to the 2-length principal component space for each classification using the first two principal components that contain 81% - 87% of the total variance.

5.2. Characteristics of Key Extracted Features and Parameters

Although all subjects were healthy and performed their walking experiments for joint monitoring at their preferred pace and comfort, we found variations in the characteristics for several extracted features among different subject groups. Typically the bone density of a human body reaches its peak value around age 30, tends to remain stable with equal amounts of bone formation and bone breakdown from about age 30 to 50, and after age 50, bone breakdown starts to exceed bone formation, resulting in bone loss and joint health degradation [159], [160]. Therefore, we divided the subjects in our study into three age groups (18-30, 31-50 and 51-86 years) to compare their knee joint and gait-related features

($p < 0.05$). Each of these groups was also divided according to their gender to show the comparison between male and female subjects of the same age groups.

5.2.1. Angles and Gait Parameters

On average, the female subjects in our study walked with higher knee angle change (50.2°) compared to the male subjects (48.2°) while walking (Table 5-1). A higher knee angle change involves higher angular movements (flexion, extension) of knee joints within its range, thus causing increased generation or absorption of joint power during walking [161], [162]. Also, when we compared thigh and shank angle changes during walking (Table 5-1 and Figure 5-1), the female subjects exhibited higher thigh angle change (33.9°) than the male subjects (31.5°) due to their greater pelvic tilt and larger hip swing while walking [163], [164]. The structure of the female pelvis, commonly referred to as gynecoid pelvis, is distinctly different compared to male pelvis with a wider sacrum and pubic arch. This anatomical difference coupled with a relatively lax ligament of the female pelvis and hip joints results in a larger hip swing and thigh movement among the females. In contrast, the male subjects showed a slightly larger shank angle change (23.6°) than females (22.5°) (Table 5-1).

It was also observed that the average magnitude of overall knee angle changes as well as thigh and shank angle changes declined for the subjects in the older age range (Figure 5-1). This is because, with aging, joint movement becomes stiffer and less flexible due to a gradual reduction of the lubricating fluid inside the knee joints and the cartilage becoming thinner. Also, the ligaments tend to shorten and lose some flexibility, restricting joint movements [165].

We also compared different gait characteristics (average values) measured with our knee monitoring system and found them to be distinctly different among the three groups (Table 5-2 and Figure 5-2). It was observed that the female subjects had shorter stride length (1.27 m) and a higher cadence (116 steps/min) during walking, while the male subjects walked with longer stride length (1.33 m) and a lower cadence (110 steps/min) (Table 5-2). A

higher cadence and shorter stride length usually require increased joint torque and power during walking [166], thus showing a tendency among the females to expend more energy while walking.

Table 5-1: Knee, thigh and shank angles during walking.

Age	Knee Angle Change (°) (p = 0.034)			Thigh Angle Change (°) (p = 0.01)			Shank Angle Change (°) (p = 0.03)		
	Male (SD)	Female (SD)	Avg.	Male (SD)	Female (SD)	Avg.	Male (SD)	Female (SD)	Avg.
18-30	51.8 (10.6)	54.6 (8.8)	53.2	34.7 (6.5)	37.1 (6.7)	35.9	27.1 (4.3)	25.4 (1.9)	26.2
31-50	47.5 (9.3)	49.7 (2.8)	48.6	32.5 (3.3)	35.2 (4.4)	33.9	23.6 (5.2)	22.2 (4.2)	22.9
51-86	45.2 (6.2)	46.2 (2.3)	45.7	27.2 (2.6)	29.5 (2.4)	28.3	20.0 (3.1)	19.8 (1.9)	19.9
Avg.	48.2	50.2		31.5	33.9		23.6	22.5	

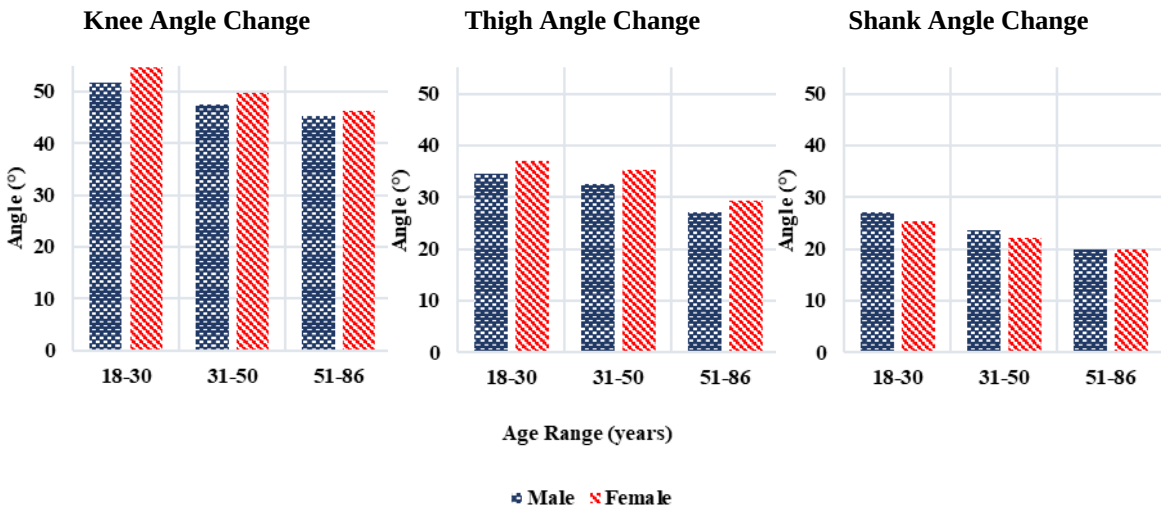

Figure 5-1. Comparison of magnitude of knee, thigh and shank angle changes for the three age groups.

Similarly, subjects from the older age group (51-86) walked with shorter stride length (1.26 m) and a higher cadence (116 steps/min) compared to the younger adults (Table 5-2). The gradual deterioration of joint health with aging affects balance and stability among the older adults and they tend to compensate for these issues by decreasing their stride length and increasing their cadence. This reduced stride length and knee joint movement among older adults also affect their MFC while walking. As a result, adults in the "51-86" age range in

our study showed the lowest MFC average (17.4 mm) among the three age groups (Table 5-2). MFC is a key gait cycle parameter for predicting the likelihood of tripping and falling. It occurs during the mid-swing phase in a walking cycle where the forward velocity of the foot is maximum. Thus, a high forward velocity coupled with a low MFC increases the possibility of unanticipated foot-ground contacts, resulting in trips and falls during walking [145]. Therefore, our knee monitoring system can potentially be used for continuous monitoring and analyzing of an individual's gait characteristics to identify the unsteady gait as well as to predict the possibility of trips and falls.

Table 5-2: Stride length, cadence and MFC of walking.

Age	Stride Length (m) (p = 0.037)			Cadence (p = 0.01)			MFC (mm) (p = 0.01)		
	Male (SD)	Female (SD)	Avg.	Male (SD)	Female (SD)	Avg.	Male (SD)	Female (SD)	Avg.
18-30	1.39 (0.08)	1.29 (0.13)	1.34	107 (6)	114 (4)	111	19.19 (3)	19.18 (4)	19.19
31-50	1.33 (0.12)	1.27 (0.12)	1.30	110 (5)	115 (2)	113	18.71 (3)	18.83 (2)	18.77
51-86	1.27 (0.05)	1.25 (0.04)	1.26	112 (4)	119 (2)	116	17.66 (2)	17.17 (1)	17.41
Avg.	1.33	1.27		110	116		18.52	18.39	

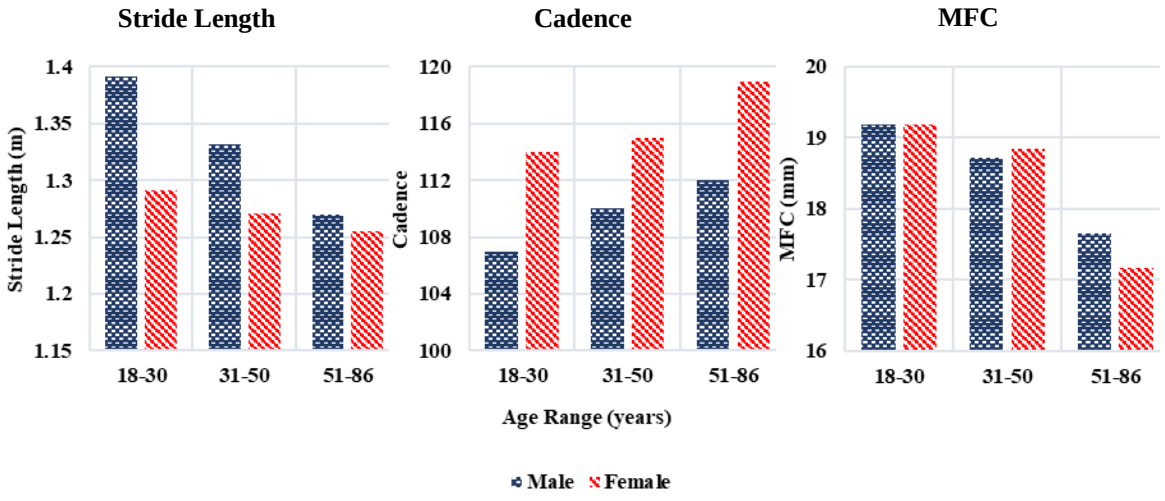

Figure 5-2. Comparison of magnitude of different gait-related features among the three age groups.

5.2.2. Energy Features

We also calculated and compared the energies of the significant components ($p < 0.009$) of the decomposed signals from the gyroscope (Figure 5-3 and Table 5-3) and accelerometer (Figure 5-4 and Table 5-4) data for all three axes. It was observed that the average energies of the mediolateral (y-axis) and anteroposterior (z-axis) acceleration were significantly higher for female subjects than the male subjects (Figure 5-4). As discussed earlier, females tend to have larger hip and knee flexion as well as higher mediolateral movement which causes higher power absorption during the gait cycle. Moreover, as females walk with a higher cadence and shorter stride length compared to males, their knee joints and adjacent muscles need to perform higher amounts of mechanical work than males during walking for a fixed distance in the same time. The female subjects also exhibited higher rotational energy around the mediolateral (y-axis), longitudinal (x-axis) and anteroposterior (z-axis) directions compared to their male counterparts (Figure 5-3). The distinct higher magnitudes of mediolateral (y-axis) acceleration energy (Figure 5-4), and rotational energy around mediolateral (y-axis) and longitudinal (x-axis) axes (Figure 5-3) of females represent their larger hip and knee joint movements while walking.

Table 5-3: Rotational energy.

	Gyroscope ($p < 0.009$)								
	Around x-axis*			**Around y-axis***			**Around z-axis***		
Age	**Male (SD)**	**Female (SD)**	**Avg.**	**Male (SD)**	**Female (SD)**	**Avg.**	**Male (SD)**	**Female (SD)**	**Avg.**
18-30	50.37 (13.97)	50.97 (12.41)	50.67	170.96 (23.38)	212.79 (33.78)	191.88	18.88 (6.94)	10.47 (3.07)	14.67
31-50	52.46 (16.35)	62.58 (13.55)	57.52	178.03 (31.11)	222.74 (25.91)	200.39	16.18 (4.38)	26.31 (10.37)	21.25
51-86	69.95 (12.54)	83.86 (6.15)	76.90	224.22 (35.13)	286.17 (39.99)	255.20	29.96 (12.49)	30.05 (14.69)	30.01
Avg.	57.59	65.80		191.07	240.57		21.67	22.28	

∗ Energy values of the gyroscope correspond to the value multiplied by 10^4.

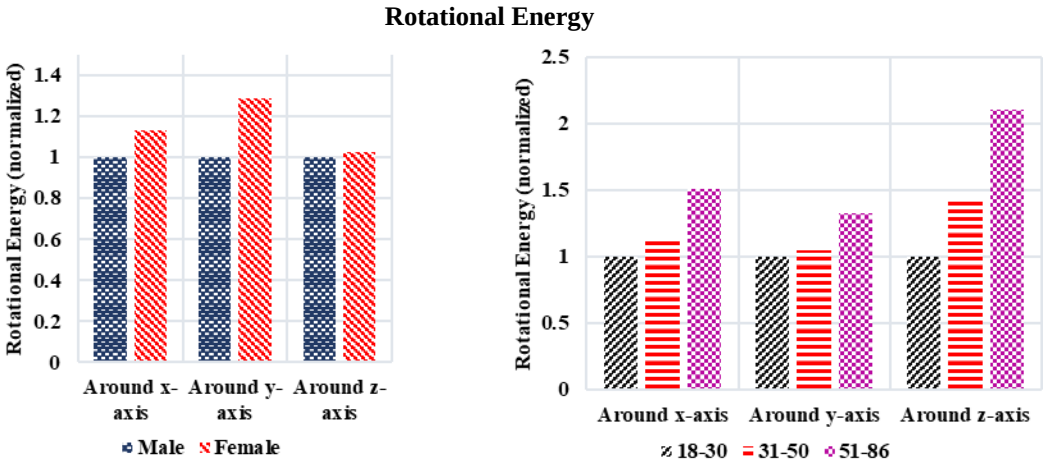

Figure 5-3. Comparison of rotational energy among different age groups.

Table 5-4: Acceleration energy.

Accelerometer ($p < 0.009$)									
	Along x-axis			**Along y-axis**			**Along z-axis**		
Age	**Male (SD)**	**Female (SD)**	**Avg.**	**Male (SD)**	**Female (SD)**	**Avg.**	**Male (SD)**	**Female (SD)**	**Avg.**
18-30	123.45 (18.77)	106.98 (14.32)	115.21	29.13 (4.72)	42.05 (5.65)	35.59	38.17 (9.73)	44.31 (7.79)	41.24
31-50	139.71 (22.66)	143.32 (9.16)	141.51	20.46 (2.35)	38.76 (1.37)	29.61	41.41 (9.13)	48.81 (6.36)	45.11
51-86	63.39 (5.97)	61.59 (5.71)	62.49	85.17 (6.01)	105.16 (5.84)	95.17	40.44 (9.26)	48.50 (3.61)	44.47
Avg.	108.85	103.96		44.92	61.99		40.00	47.21	

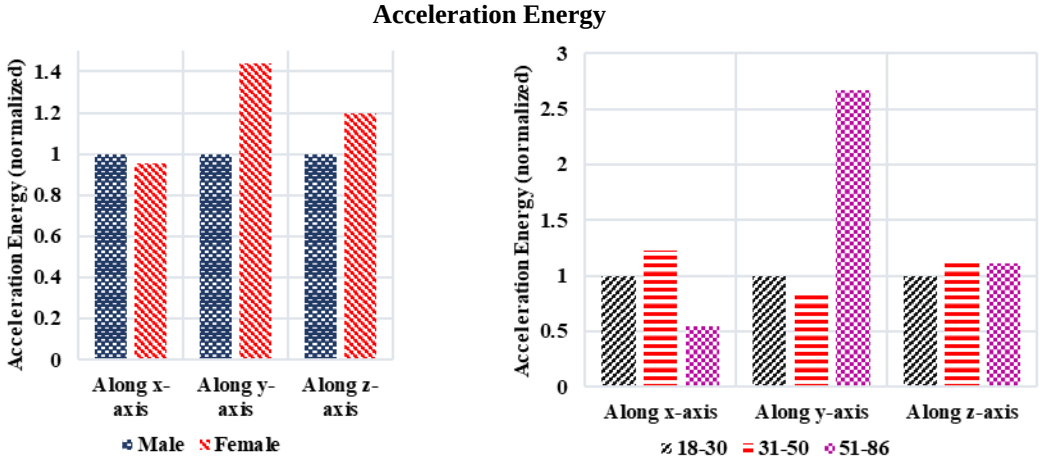

Figure 5-4. Comparison of acceleration energy among different age groups.

A significantly higher average (270%-320%) mediolateral (y-axis) acceleration energy and a lower average (45%-55%) of longitudinal (x-axis) acceleration energy among the older (51-86) age group can be attributed to their reduced balance and stability while walking [122] (Table 5-4). Their postural balance and alignment are affected due to larger mediolateral sway and lower longitudinal movements (low ground clearance). In addition, higher rotational energy around all three axes in older adults could be attributed to their increased asymmetry and variability in gait [122]. Generally, the younger adults possess better musculoskeletal health and an unimpaired somatosensory system. Therefore, their basal energy expenditure remains well controlled with better postural balance and alignment, as well as superior motor-cognitive coordination [167]. As a summary, a significant decline in knee joint angle, stride length as well as gait symmetry among older age groups demonstrates an overall deterioration of knee joint health along with weaker gait compared to the younger age groups.

5.2.3. Other Physiological Parameters

As we mentioned earlier that knees absorb a large amount of pressure during daily activities and the average force on each knee while walking is the equivalent to 1.5 times our body weight [31]. Therefore, in our study, we also analyzed the pressure change of the anterior compartment muscles of the thigh (directly connected with knee patella) while walking and made a comparison between different gender and age groups (Table 5-5 and Figure 5-5). It was observed that the male subjects exhibited stronger muscle pressure in comparison with the female subjects. Usually, males tend to have larger thigh muscle mass than females. Besides, men's muscles are more solid, due to having a higher proportion of Type 2 fast-twitch fibers [168], [169]. This kind of muscle fiber contains a lot of protein but less amount of blood. It has the ability to expand and contract rapidly with great force and generate its own energy. As men have about 50% more Type 2 muscle fibers than women's, they produce more pressure while walking [168]. It is also known that muscle mass and volume among older adults decrease gradually with age [170]. As a result, the force generated due to muscle expansion and contraction begins to decline which signifies the deterioration of

musculoskeletal health among older adults. In our experiments, we also found that the older adults with an age group from 51-86 years had the lowest thigh muscle pressure in comparison with the younger age groups during walking.

Table 5-5: Thigh anterior compartment muscle pressure while walking.

	Muscle Pressure (N/m^2) ($p < 0.05$)		
Age	**Male (SD)**	**Female (SD)**	**Avg.**
18-30	1802 (175)	1460 (163)	1631
31-50	1637 (91)	1359 (131)	1498
51-86	1439 (109)	1136 (52)	1287
Avg.	1626	1318	

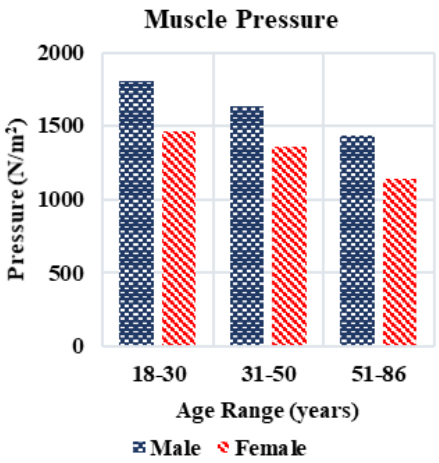

Figure 5-5. Comparison of thigh anterior compartment muscle pressure between different subject groups.

Using our system, we also measured local knee skin temperature and skin conductance during walking experiments. Usually, changes in knee skin temperature occur due to the changes in blood flow in that region and this change can be an indication of abnormality. For example, the skin temperature of an inflamed knee is usually higher (1.09 °C – 2.77 °C) [171], [172] than a normal or healthy knee (~30.6 °C on average) [22]. Similarly, stress and perspiration in the knee joints are related to the local blood flow and the sweat gland activities which vary due to external and internal stimuli. These variations can be assessed by measuring the changes in the skin conductance. However, for both these cases, long-time monitoring is needed to detect any noticeable changes. Therefore, in our current study,

we could not distinguish these kinds of variation as all participants were clinically healthy and we only collected each knee data for a short period of time. Instead, we have calculated the average value from our collected data for normal knee skin temperature which was 30.26 °C with a standard deviation of 0.93 °C. We also performed dry (normal) and wet knee (after workout) skin conductance measurement tests for two participants where the average conductance for dry skin was 38 μS and 46 μS for wet skin. In every measurement, the two GSR electrodes and the temperature sensor were placed on the knee patella (Figure 3-6) for better skin contact. The gap between two GSR electrodes was 6 cm (side by side).

5.3. Classification and Cross-Validation of Knee Data

The linear support vector machine (SVM) was used in our study to train and classify the data corresponding to different groups. SVM is a very well-known machine learning algorithm and it is very effective in classifying a two-class dataset with few samples [166], [173]. It is a supervised learning model that constructs a discriminative hyperplane or set of hyperplanes in a multi-dimensional space by maximizing the geometric margin between different classes. Hyperplanes are decision boundaries that help to classify the data points. Feature vectors determining the hyperplane with maximum margin are called support vectors. Other feature vectors do not alter the position and orientation of the hyperplane. We exploited and trained the linear SVM with our reduced 2-length vector, generating two distinct classes of baseline data with respect to two specific genders, age and BMI groups as well as knee and leg health conditions. The performance of the proposed technique for classification was evaluated using a k (=10)-fold stratified cross-validation. Each time, seven (10% of the total data) random subjects out of 70 were selected, without overlap. In our study, we chose k=10 which allows to evenly split our data sample and large enough to have low bias with a modest variance. On the other hand, the stratified cross-validation allows for increasing the accuracy for an imbalanced dataset by ensuring that each fold has the same proportion of observations from each class of the dataset. Thus, ten such non-overlapping balanced subsets were created to use as test data in each fold. Then, we used the remaining 63 subjects' data of each set to train the SVM. Finally, in each fold, the

excluded seven subjects were classified using the developed model. The results from each of the 10-fold validation were then combined to compute the overall accuracy of the classification model.

5.3.1. Gender

According to gender-based classification with 70 subjects (56 males and 14 females), most of the subjects' joint behaviors and gait patterns were found to be truly clustered to their corresponding groups (Figure 5-6(a)) and the classification results show a very high accuracy of ~97% from the 10-fold stratified cross-validation. Only 2 subjects (1 male, 1 female) were misclassified. This observation may suggest a potential difference (inherent or developing) in the joint and gait characteristics that prevented these two subjects from being truly classified according to his/her gender identity.

Figure 5-6(b) presents one-fold of classifying 7 subjects based on the SVM trained with the remaining 63 subjects, where one male subject was found to be wrongly classified. This misclassified male was found to exhibit some similar characteristics observed in healthy female subjects such as higher acceleration energy along the mediolateral axis (y-axis), larger rotational energy around the longitudinal (x-axis) axis, as well as lower pressure change around the muscles in the anterior compartment of the thigh. The confusion matrix for the gender-based classifier is presented in

Table 5-6 showing the high true positive rate (TPR: ~96% on average) and low false positive rate (FPR: ~4% on average) for two classes as well the high combined accuracy of the classifier.

Table 5-6: Confusion matrix for gender-specific classifier.

Gender	True positive rate (TPR)	False positive rate (FPR)	Accuracy
Male	98%	2%	97%
Female	93%	7%	

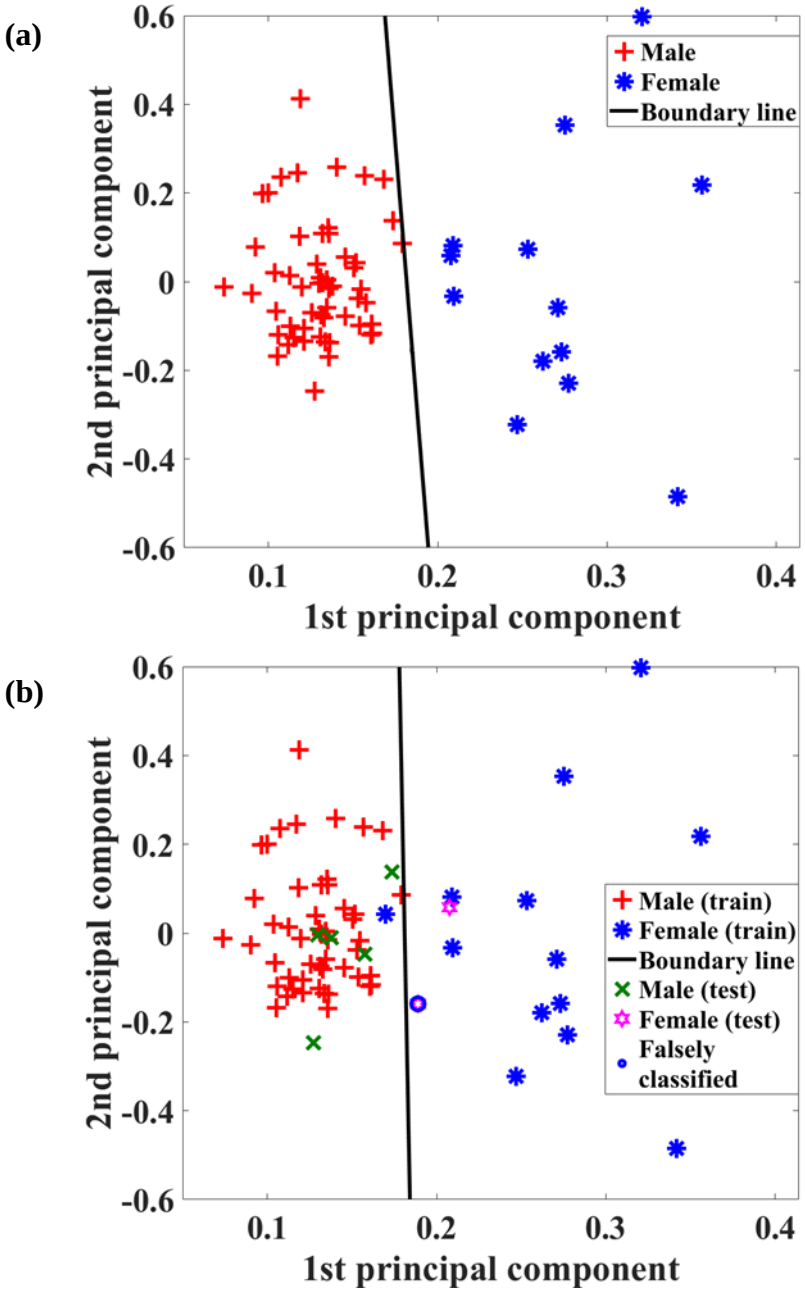

Figure 5-6. Classification results: (a) two distinct gender groups (excluding outliers – data fallen on the wrong side of the boundary); (b) One instance of cross-validation showing one subject is falsely classified.

5.3.2. Age

As we mentioned earlier that the linear support vector machine (SVM) is effective for classifying a two-class dataset. Therefore, in order to perform the age-based classification,

Table 5-7: Confusion matrix for age-specific classifier.

Age range	True positive rate (TPR)	False positive rate (FPR)	Accuracy
18-40 years	98%	2%	96%
41-86 years	89%	11%	

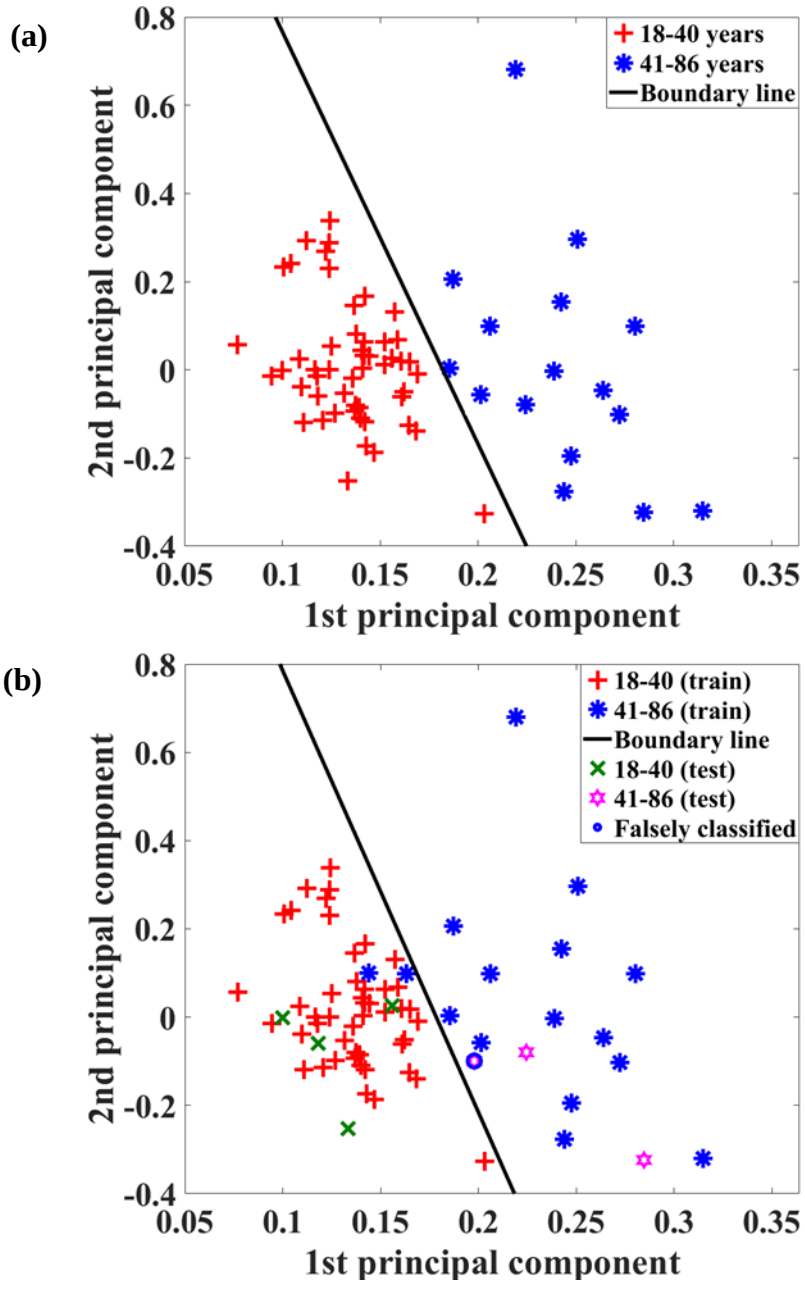

Figure 5-7. Classification results: (a) two distinct age groups (excluding outliers – data fallen on the wrong side of the boundary); (b) One instance of cross-validation showing one subject is falsely classified.

the subjects' data were divided into two new specific age groups. One group comprised persons with an age range from 18-40 years (52 adults) and the other group includes adults from 41-86 years (18 adults). We divided the subjects into these two groups because, knee joint disorders especially osteoarthritis (OA) is most common in adults over 40 [174]. Both of these groups were found to be distinctly arranged and separated by the boundary line created by the SVM (Figure 5-7(a)). However, 1 subject from the first group and 2 from the second were wrongly classified in this case. This anomaly among those subjects may be attributed to an altered knee joint movement and walking patterns in comparison with their own groups. For example, the misclassified younger adult showed lower knee angle change, stride length and MFC, whereas the two misclassified older adults had higher knee angle change as well as better stride length and MFC compared to other older adults. This classifier was also evaluated by a 10-fold stratified cross-validation. Figure 5-7(b) shows one instance of cross-validation where the subject aged below 40 years was falsely classified due to having joint characteristics similar to the older age group. The confusion matrix for the age classifier is presented in Table 5-7 showing an overall classification accuracy ~96%. The high TPR (~93% on average) as well as corresponding low FPR (~7% on average) of the classification outcomes prove the analyzer's capability in distinguishing the inconsistent knee joint behaviors with high confidence.

5.3.3. BMI

In addition to gender and age, we also performed a classification operation between two subject groups divided with respect to their BMI (body mass index). BMI is a weight screening tool (equation (5-6)) against height that can indicate whether a person has the correct weight for their height.

$$BMI = \frac{Weight(kg)}{height^2(m^2)}. \tag{5-6}$$

If a person's BMI is outside of the healthy range (underweight, excess weight or obese), their health risks may increase significantly and their joint health may be impacted. For instance, excess weight puts additional stress on the knee joint as the knee bears one of the

Table 5-8: Confusion matrix for BMI-specific classifier.

BMI	True positive rate (TPR)	False positive rate (FPR)	Accuracy
19-29 kg/m^2	95%	5%	93%
<19 kg/m^2 and >29 kg/m^2	86%	14%	

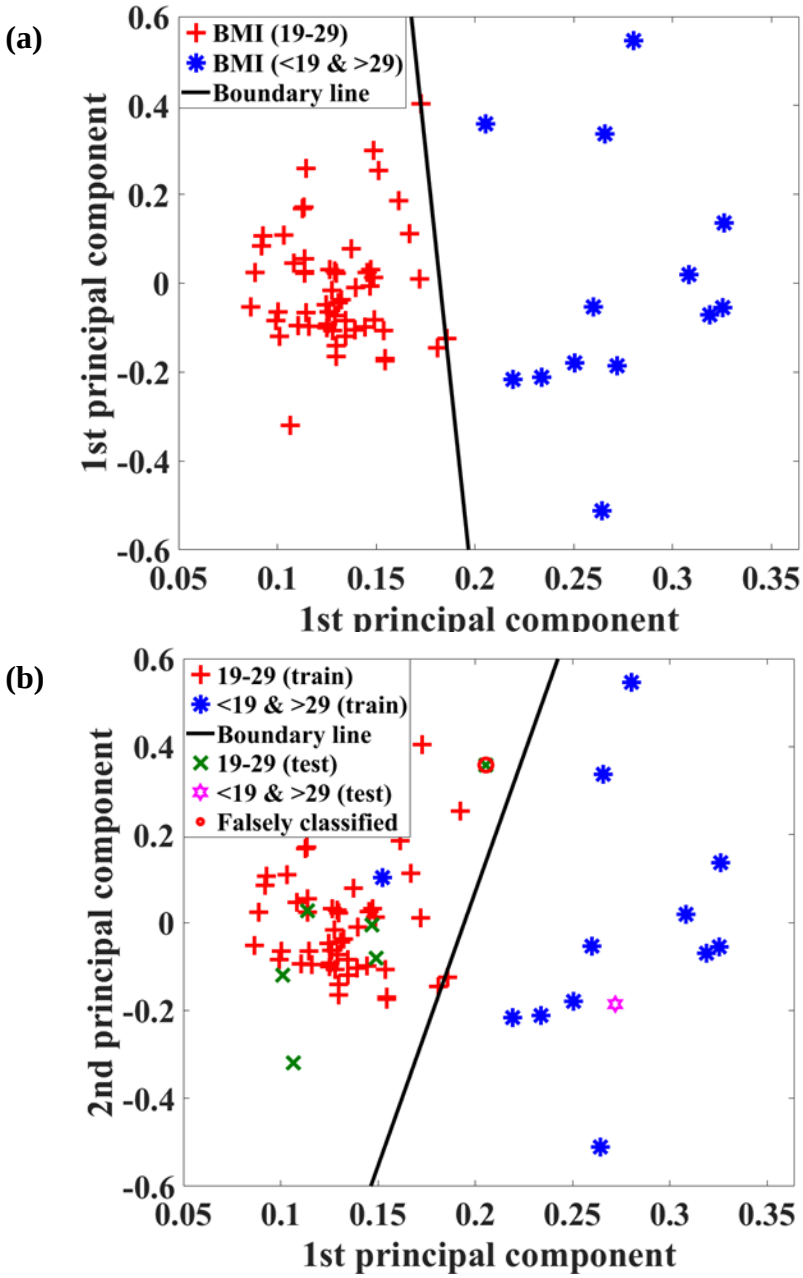

Figure 5-8. Classification results: (a) two distinct BMI groups (excluding outliers – data fallen on the wrong side of the boundary); (b) One instance of cross-validation showing one subject is falsely classified.

highest amounts of body weight during different daily activities [31]. Similarly, a weight that is too low can increase the risk of malnutrition, osteoporosis and anemia which can also cause the degradation of knee joint health. Therefore, we separated a subject group of 14 people with a BMI value less than 19 kg/m^2 (Underweight) and more than 29 kg/m^2 (obese) and performed classification operation utilizing their joint features. Hence, the other subject group of the classification comprised adults with a BMI range between 19 and 29 kg/m^2. The classification results showing two distinct BMI groups are presented in Figure 5-8(a). An overall classification accuracy of ~93% (Table 5-8) was achieved from the 10-fold stratified cross-validation (one-fold is presented in Figure 5-8(b)) which indicates a close relationship between the joint features and BMI. Also, the high TPR (~90% on average) and corresponding low FPR (~10% on average) indicate the classifier's reliability with high confidence.

5.3.4. Knee and Leg Health

Although all participants in our study had no clinically diagnosed knee joint issue or walking discomfort, 15 subjects among 70 had reported some histories related to knee health or injuries as well as problems such as occasional knee or lower back pain, bowed legs or flat feet. Any of these reported issues can be a future cause of knee related diseases and mobility degradation. Therefore, we applied our classification model (SVM) to distinguish those 15 subjects with undiagnosed issues using their data related to knee joint behavior and gait pattern. A clear clustering for each group (with and without issues) was found being separated by the boundary line created by the SVM (Figure 5-9(a)). The accuracy of the classifier was evaluated by a 10-fold stratified cross-validation. Figure 5-9(b) shows one instance of cross-validation where one healthy subject was classified as having issues related to knee joints and leg movement. Although there is no known problem reported by these subjects, this result can be an indication of potential developing issues related to knee joint and mobility. Thus, it is possible to use our monitoring system and classifier for prediction and early diagnosis of knee joint and mobility-related problems. The high TPR (~95% on average) and overall accuracy (~96%) as well as corresponding

Table 5-9: Confusion matrix for knee and leg health-based classifier.

Knee and leg health condition	True positive rate (TPR)	False positive rate (FPR)	Accuracy
No joint issue	96%	4%	96%
Undiagnosed joint/leg issue	93%	7%	

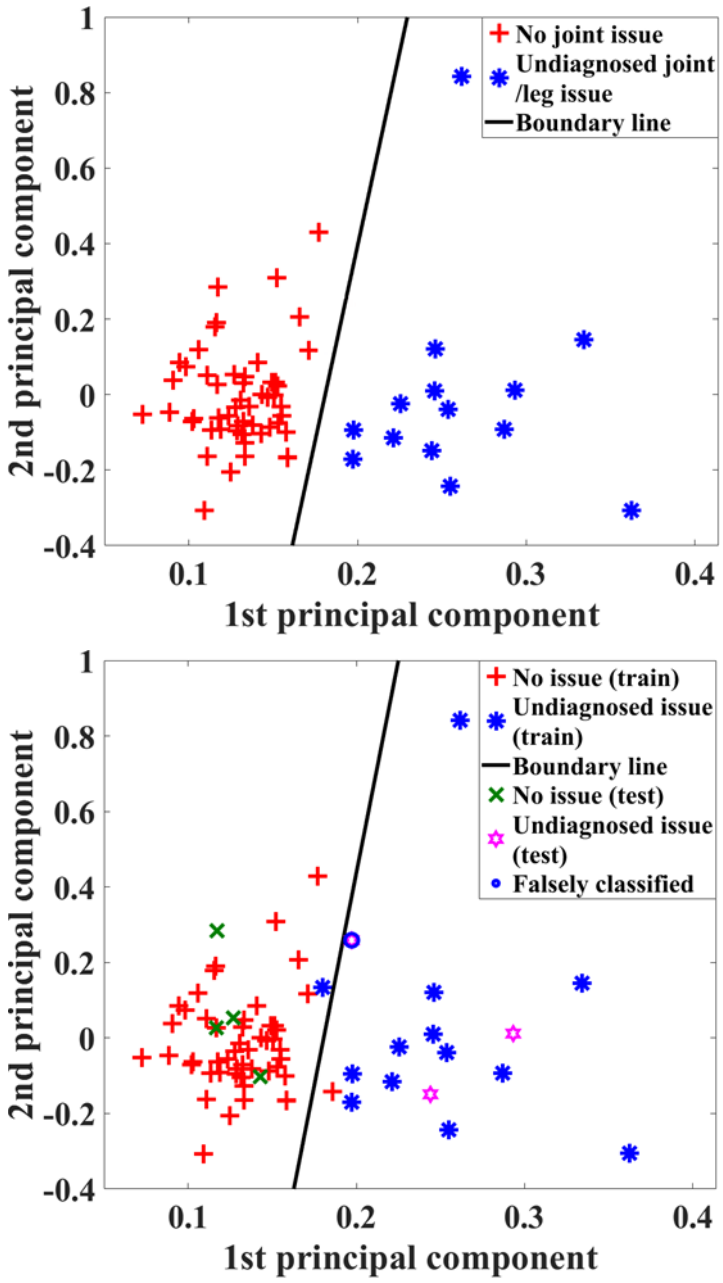

Figure 5-9. Classification results: (a) two distinct groups with (undiagnosed) and without joint issue (excluding outliers); (b) One instance of cross-validation showing one subject is falsely classified.

low FPR (~5% on average) of the classification results (Table 5-9) validates the capabilities of the analyzer in distinguishing anomalous joint behavior from healthy knee joints with high confidence.

5.4. Conclusions

In this Chapter, we applied several data processing and machine learning algorithms to utilize the extracted features from the knee monitoring systems and find useful information and correlation between different knee joint behaviors. In order to rank and select statistically significant features, the mRMR feature selection method was used. Then by applying PCA, the selected 36-length feature vector was projected on the 2-dimensional spaces using the first two principal components without much loss of information. Several key extracted knee joint and gait parameters such as angles, stride length, cadence, MFC, rotational and acceleration energy features, and other physiological knee features such as muscle pressure around the knee joint, local skin temperature and skin conductance are analyzed to show the comparisons between different subject groups. The reduced 2-length vectors extracted from PCA were utilized to train the linear SVM and classify the data corresponding to two specific subject groups. Different subject groups were defined based on genders, age, BMI as well as their knee and leg health conditions. The classification accuracy for each case was evaluated by a 10-fold stratified cross-validation. For each classification, distinct clusters with respect to their corresponding groups were observed which allows the analyzer to distinguish any potential anomaly in the data and identify any individual with the inconsistent knee joint characteristics for further analysis.

Chapter 6
Conclusions and Future Work

6.1. Conclusions*

The physical and health issues associated with the rapidly aging population are a rising socio-economic burden for many countries including Canada. Among these issues, the loss of mobility among older adults is especially serious as it has severe social, mental and physical consequences. Poor mobility, in turn, results in a lack of independence, depression, and a decrease in the ability to handle daily activities, which together lowers the quality-of-life. Factors that influence the loss of mobility include being elderly, poor or infrequent physical activity and/or poor diet that leads to obesity and some chronic diseases such as arthritis or diabetes. Aging, coupled with poor mobility, also leads to faster musculoskeletal weakening in the older adults. In addition, musculoskeletal weakness is a serious health risk as it can cause falls resulting in broken or fractured bones such as hips or thighs, which then leads to more serious health issues. With the aging population, the cost of services provided by social and healthcare workers for elderly daily welfare, and the cost of their direct treatment and hospitalization for different musculoskeletal disorders are posing a huge financial/social burden on government, society and family members. A major component of this high cost goes for controlling and treatment of these musculoskeletal-related elderly's health issues and injuries, which is also very demanding in terms of social and medical personnel and infrastructure.

The load-bearing joints in our human body bear a huge amount of loading pressure during normal everyday movements. Therefore, these joints are highly affected due to aging,

* Part of this work will be submitted for consideration for publication as: A. I. Faisal, S. Majumder, R. Scott, T. Mondal, D. Cowan, and M. J. Deen, A Simple, Low-Cost Multi-Sensor-based Smart Wearable Knee Joint Monitoring System, March 2020. (in preparation).

obesity and other musculoskeletal disorders and injuries. Among all the load-bearing joints, the knee joint is considered as the most important and critical for health assessment due to the massive amount of pressure it absorbs with every lower limb activity and high exposure to injuries. Therefore, continuous and long-term monitoring of knee joints during daily activities can provide a complete set of data related to mobility including knee joint range of motion, walking parameters and the state of muscles around the joint. These data, when analyzed, can then be utilized to detect the risk of certain musculoskeletal disorders that may not be noticeable at early stages through regular monitoring. For such knee monitoring, a simple, easy-to-use, reliable and cost-effective system would be of immense benefit for keeping track of the knee joint health status of elderly people as well as the persons undergoing rehabilitation towards healthier joints.

In this research, we developed a multi-sensor-based low-cost, wearable and easy-to-use knee joint monitoring device which can record and wirelessly transmit continuous knee data in real living conditions. The system is composed of MEMS-based inertial motion sensors, and temperature, pressure and skin conductance sensors which allow it to simultaneously measure knee movements as well as other important physiological parameters such as skin temperature, conductance and muscle pressure change around the joint during movements. These parameters can potentially be used by the medical personnel to determine the overall knee joint health and mobility status of an individual. The smart wearable knee monitoring system can also be used for early diagnoses and proper treatment of knee joint disorders such as osteoarthritis and osteoporosis, fall detection, and post-surgery monitoring of a patient's mobility and rehabilitation.

For signal processing and data analysis, different computationally efficient techniques were adopted which renders the analyzer suitable for systems with limited processing capabilities. The initial processing steps include filtering and resampling of the raw data to make the sensors' signal clean and aligned for further analysis. We applied a simple sensor fusion method – the complementary filter, to calculate the knee angle during walking. This fusion method is used to remove the high-frequency noise from the accelerometer data and reduce the drift from the gyroscope data. We also computed thigh and shank angles as well

as several gait parameters such as gait speed, stride length, minimum foot clearance (MFC) and cadence from the inertial motion sensors data. Besides joint movement and physiological parameters, a large set of statistical, temporal and energy features were also extracted from the system data. We used wavelet packet decomposition (WPD) which is a fast and hierarchical tree-like decomposition algorithm to get the spectral components from the joint motion signals.

The proposed analysis system is capable of identifying abnormalities in the knee joint behavior by assessing its features with respect to the baseline clusters corresponding to an individual's peer group. To highlight the important features and make the analysis efficient we used the minimum redundancy maximum relevance (mRMR) feature selection method and principal component analysis (PCA) for dimensionality reduction. Then, the linear support vector machine (SVM) was trained with these reduced feature components (principal component 1 and 2) followed by a 10-fold stratified cross-validation. The classification results showed high accuracy forming distinct clusters or patterns for different subject groups based on their age, gender, BMI and knee/leg health conditions and distinguishing abnormalities in joint behavior.

6.2. Future Work

This research work focused on developing a low-cost, easy-to-use multi-sensor-based wearable knee joint monitoring system to evaluate overall knee joint health and mobility status of an individual. However, to make the monitoring system more precise and efficient, we plan to address several important research challenges in our future work.

- This work only included healthy subjects who were supposed to possess comparably better joint functionalities than the people with known joint disorders or diseases. The knee joint functionalities and movement pattern change gradually through aging, different disease processes and at different severities; thus its characteristics are likely to deviate from those of healthy joints corresponding to an individual's peer group. Even though discrete clusters or distinct patterns of different subject groups are

reported in this work, further in-depth study on a larger balanced dataset including subjects having different knee joint-related issues or diagnosed diseases with a wider range of age and BMI would be beneficial to reinforce and expand our preliminary findings.

- This research involves human subjects and their health information, so it is mandatory to fulfill all the requirements set by the responsible regulatory bodies such as data privacy, information security and other ethical requirements. Therefore, before the monitoring system can be used on patients, additional approval from McMaster University's Research Ethics Board (REB) is required demonstrating the feasibility and reliability of the system.
- In this study, we mainly focused on the straight and flat surface walking of an individual under ideal condition to keep the analysis model simple and evaluate its feasibility. In the next step, we will include a diverse database based on walking signals from different surfaces, different conditions, different footwear, and more varied daily lower limb activities at home and in a community environment to extend our analysis and findings.
- In this research, we measured a single knee joint at a time which limits the asymmetry and variability analysis between two knee joints' characteristics while walking. These kinds of analyses are required in order to determine the degree of coordination between two knees as well as lower limb dominance. Therefore, we are going to duplicate another prototype which will allow us to collect simultaneous data from both the knee joints during walking and other lower limb activities.
- We also hope to introduce a health index for knee joints based on the extracted key features that can act as a base-line to distinguish between atypical and normal knee joint characteristics for different groups of subjects and activities. This index can be used as reference by medical practitioners and regular users to quickly determine their knee health condition. Also, we plan to establish a nomogram for different genders and people with different physical structures because of their distinct joint characteristics

during activities. Further, persons from different ethnicities may have different normative values which needs further study and quantification.

- Another major challenge is to make the system real-time to simultaneously acquire, process and analyze the data which can reduce unnecessary redundancies and increase the accuracy and efficiency for continuous monitoring. Therefore, we will work towards developing a stand-alone smart program integrated with a combined data acquisition process as well as analysis and modeling techniques for further feedback and prediction applications. A cloud server communication can also be set up for real-time data mining and handling large amounts of data using proper algorithms. Thus, we will be able to use the knee monitoring system for early diagnoses of joint disorders, real-time detection and prevention of falls, evaluation of athletes' performance and progress in rehabilitation.
- The developed knee monitoring system can be used to evaluate knee joint health and to extract several gait features that proves its feasibility as a gait analyzer. Since gait is correlated with human cognitive and cardiovascular activities, it is possible to use these extracted gait features to find a quantitative correlation with cognitive and cardiovascular functions. This correlation can potentially be exploited in predicting the development of neurodegenerative disorders such as dementia, Alzheimer's or Parkinson's, and diseases associated with the cardiovascular system.

Finally, an important long-term goal of this research is to develop an accurate, easy-to-use, low-cost, wearable smart knee joint monitoring and assistive system which can help persons at high levels of musculoskeletal health risk by tracking and assessing the knee joint function in a comfortable and non-intrusive manner. Therefore, instead of a knee brace, we are planning to integrate the sensing module inside regular garments such as pants or socks to reduce the cost and make the system smaller and user-friendly. By integrating efficient prediction and feedback models, the system can be further exploited for biofeedback applications such as fall detection and prevention, correcting errors or mistakes in joint exercises during rehabilitation, and real-time evaluation of athletes' performance. Moreover, the Internet of Things (IoT) is already unlocking the benefits of

advanced computing and communication technologies in the healthcare industry. Therefore, this smart system, taking advantage of the IoT, would also be able to provide important joint-related information to medical professionals for early and accurate diagnosis of joint-related problems and diseases as well as more efficient and effective medical intervention when needed.

References

[1] H. Gray, "Anatomy of the human body," *Am. J. Med. Sci.*, vol. 157, no. 5, p. 704, May 1919.

[2] D. Schofield, S. Kelly, R. Shrestha, E. Callander, M. Passey, and R. Percival, "The impact of back problems on retirement wealth," *Pain*, vol. 153, no. 1, pp. 203–210, Jan. 2012.

[3] D. J. Schofield *et al.*, "Lost productive life years caused by chronic conditions in Australians aged 45–64 years, 2010–2030," *Med. J. Aust.*, vol. 203, no. 6, p. 260, Sep. 2015.

[4] "Musculoskeletal conditions." [Online]. Available: https://www.who.int/news-room/fact-sheets/detail/musculoskeletal-conditions. [Accessed: 31-Jan-2020].

[5] S. Dadoun *et al.*, "Mortality in rheumatoid arthritis over the last fifty years: Systematic review and meta-analysis," *Jt. Bone Spine*, vol. 80, no. 1, pp. 29–33, Jan. 2013.

[6] Arthritis and Osteoporosis Victoria, "A problem worth solving - the rising cost of musculoskeletal conditions in Australia," Elsternwick, Victoria, Victoria, 2013.

[7] V. C. Mow and W. M. Lai, "Recent developments in synovial joint biomechanics," *SIAM Rev.*, vol. 22, no. 3, pp. 275–317, Jul. 1980.

[8] A. Y. Hui, W. J. McCarty, K. Masuda, G. S. Firestein, and R. L. Sah, "A systems biology approach to synovial joint lubrication in health, injury, and disease," *Wiley Interdiscip. Rev. Syst. Biol. Med.*, vol. 4, no. 1, pp. 15–37, Jan. 2012.

[9] BCcampus, *Anatomy and Physiology: Chapter 9.4 Synovial Joints*. 2017.

[10] "Aging & Health A to Z," *Health in Aging*, 2017. [Online]. Available: http://www.healthinaging.org/aging-and-health-a-to-z/topic:joint-problems/. [Accessed: 30-Aug-2018].

[11] A. M. Briggs *et al.*, "Musculoskeletal health conditions represent a global threat to healthy aging: A report for the 2015 world health organization world report on ageing and health," *Gerontologist*, vol. 56, no. Suppl 2, pp. S243–S255, Apr. 2016.

[12] B. Garner, "Joint anatomy and basic biomechanics," in *Chiropractic Technique*, 2010, pp. 11–34.

[13] M. Ha and D. Han, "The relationship between knee joint angle and knee flexor and extensor muscle strength," *J. Phys. Ther. Sci.*, vol. 29, no. 4, pp. 662–664, 2017.

[14] V. Baltzopoulos and D. A. Brodie, "Isokinetic Dynamometry," *Sport. Med.*, vol. 8, no. 2, pp. 101–116, Aug. 1989.

[15] "Anthropometry and biomechanics," *NASA*. [Online]. Available: https://msis.jsc.nasa.gov/sections/section03.htm. [Accessed: 07-Nov-2018].

[16] W. B. Greene and J. D. Heckman, *The clinical measurement of joint motion*. Illinois:

American Academy of Orthopaedic Surgeons, 1994.

[17] J. E. Slightam, "Modeling and simulation of biologically inspired 3D-printed fluid power robotic system architectures," Milwaukee School of Engineering, 2016.

[18] K. Moromizato, R. Kimura, H. Fukase, K. Yamaguchi, and H. Ishida, "Whole-body patterns of the range of joint motion in young adults: masculine type and feminine type," *J. Physiol. Anthropol.*, vol. 35, no. 1, p. 23, 2016.

[19] J. M. Soucie *et al.*, "Range of motion measurements: reference values and a database for comparison studies," *Haemophilia*, vol. 17, no. 3, pp. 500–507, May 2011.

[20] W. Zhang, M. Tomizuka, and N. Byl, "A wireless human motion monitoring system for smart rehabilitation," *J. Dyn. Syst. Meas. Control*, vol. 138, no. 11, p. 111004, Jul. 2016.

[21] C.-Y. Chiang, K.-H. Chen, K.-C. Liu, S. Hsu, and C.-T. Chan, "Data collection and analysis using wearable sensors for monitoring knee range of motion after total knee arthroplasty," *Sensors*, vol. 17, no. 2, p. 418, Feb. 2017.

[22] H. A. Ménard and D. Paquette, "Skin temperature of the knee: an unrecognized physical sign of inflammatory disease of the knee.," *Can. Med. Assoc. J.*, vol. 122, no. 4, pp. 439–40, Feb. 1980.

[23] Y. Y. Dhaher and L. E. Kahn, "The effect of vastus medialis forces on patello-femoral contact: a model-based study.," *J. Biomech. Eng.*, vol. 124, no. 6, pp. 758–67, Dec. 2002.

[24] T. F. Besier, D. G. Lloyd, and T. R. Ackland, "Muscle activation strategies at the knee during running and cutting maneuvers," *Med. Sci. Sport. Exerc.*, vol. 35, no. 1, pp. 119–127, Jan. 2003.

[25] T. F. Besier, M. Fredericson, G. E. Gold, G. S. Beaupré, and S. L. Delp, "Knee muscle forces during walking and running in patellofemoral pain patients and pain-free controls," *J. Biomech.*, vol. 42, no. 7, pp. 898–905, May 2009.

[26] J. Kim, S. Kwon, S. Seo, and K. Park, "Highly wearable galvanic skin response sensor using flexible and conductive polymer foam.," *2014 36th Annu. Int. Conf. IEEE Eng. Med. Biol. Soc.*, vol. 2014, pp. 6631–4, Aug. 2014.

[27] M. A. H. M. Adib and M. F. Jaafar, "Review: modelling of meniscus of knee joint during soccer kicking," *IOP Conf. Ser. Mater. Sci. Eng.*, vol. 50, no. 1, p. 012027, Dec. 2013.

[28] A. I. Faisal, S. Majumder, T. Mondal, D. Cowan, S. Naseh, and M. J. J. Deen, "Monitoring methods of human body joints: state-of-the-art and research challenges," *Sensors*, vol. 19, no. 11, p. 2629, Jun. 2019.

[29] G. M. Salim and M. A. Zawawi, "Knee joint movement monitoring device based on optical fiber bending sensor," *J. Telecommun. Electron. Comput. Eng.*, vol. 10, no. 1–3, pp. 25–29, 2018.

[30] M. Hoffman, "Knee (human anatomy): function, parts, conditions, treatments." [Online]. Available: https://www.webmd.com/pain-management/knee-pain/picture-of-the-knee#1. [Accessed: 06-Sep-2019].

[31] "Why weight matters when it comes to joint pain - Harvard Health." [Online].

Available: https://www.health.harvard.edu/pain/why-weight-matters-when-it-comes-to-joint-pain. [Accessed: 08-Jan-2020].

[32] "Knee pain - symptoms and causes - mayo clinic." [Online]. Available: https://www.mayoclinic.org/diseases-conditions/knee-pain/symptoms-causes/syc-20350849. [Accessed: 04-Apr-2020].

[33] S. L. Brennan-Olsen *et al.*, "Prevalence of arthritis according to age, sex and socioeconomic status in six low and middle income countries: Analysis of data from the World Health Organization study on global AGEing and adult health (SAGE) Wave 1," *BMC Musculoskelet. Disord.*, vol. 18, no. 1, p. 271, Dec. 2017.

[34] C. J. L. Murray *et al.*, "Disability-adjusted life years (DALYs) for 291 diseases and injuries in 21 regions, 1990–2010: a systematic analysis for the Global Burden of Disease Study 2010," *Lancet*, vol. 380, no. 9859, pp. 2197–2223, Dec. 2012.

[35] Arthritis Foundation, "Arthritis by the numbers," *Arthritis Foundation*, vol. 15, no. 4, pp. 1–70, 2017.

[36] E. Papi, A. Belsi, and A. H. McGregor, "A knee monitoring device and the preferences of patients living with osteoarthritis: a qualitative study," *BMJ Open*, vol. 5, no. 9, pp. 1–8, Sep. 2015.

[37] M. V. Hurley, D. L. Scott, J. Rees, and D. J. Newham, "Sensorimotor changes and functional performance in patients with knee osteoarthritis," *Ann. Rheum. Dis.*, vol. 56, no. 11, pp. 641–648, Nov. 1997.

[38] K. Nisar, A. A. A. Ibrahim, L. Wu, A. Adamov, and M. J. Deen, "Smart home for elderly living using wireless sensor networks and an Android application," in *2016 IEEE 10th International Conference on Application of Information and Communication Technologies (AICT)*, 2016, pp. 1–8.

[39] A. Tognetti, F. Lorussi, N. Carbonaro, and D. de Rossi, "Wearable goniometer and accelerometer sensory fusion for knee joint angle measurement in daily life," *Sensors*, vol. 15, no. 11, pp. 28435–28455, Nov. 2015.

[40] V. M. Pomeroy, E. Evans, and J. D. Richards, "Agreement between an electrogoniometer and motion analysis system measuring angular velocity of the knee during walking after stroke," *Physiotherapy*, vol. 92, no. 3, pp. 159–165, Sep. 2006.

[41] P. Piriyaprasarth, M. E. Morris, A. Winter, and A. E. Bialocerkowski, "The reliability of knee joint position testing using electrogoniometry," *BMC Musculoskelet. Disord.*, vol. 9, no. 1, p. 6, Dec. 2008.

[42] K. Rome and F. Cowieson, "A reliability study of the universal goniometer, fluid goniometer, and electrogoniometer for the measurement of ankle dorsiflexion," *Foot Ankle Int.*, vol. 17, no. 1, pp. 28–32, Jan. 1996.

[43] L. Tesio, M. Monzani, R. Gatti, and F. Franchignoni, "Flexible electrogoniometers: kinesiological advantages with respect to potentiometric goniometers," *Clin. Biomech.*, vol. 10, no. 5, pp. 275–277, Jul. 1995.

[44] M. Donno, E. Palange, F. Di Nicola, G. Bucci, and F. Ciancetta, "A new flexible optical fiber goniometer for dynamic angular measurements: application to human

joint movement monitoring," *IEEE Trans. Instrum. Meas.*, vol. 57, no. 8, pp. 1614–1620, Aug. 2008.

[45] C. K. Lim, Z. Luo, I.-M. Chen, and S. H. Yeo, "A low cost wearable optical-based goniometer for human joint monitoring," *Front. Mech. Eng. China*, vol. 6, no. 1, pp. 13–22, Dec. 2010.

[46] A. Gritai and M. Shah, "Tracking of human body joints using anthropometry," in *2006 IEEE International Conference on Multimedia and Expo*, 2006, vol. 2006, pp. 1037–1040.

[47] M. U. Islam, H. Mahmud, F. Bin Ashraf, I. Hossain, and M. K. Hasan, "Yoga posture recognition by detecting human joint points in real time using microsoft kinect," in *2017 IEEE Region 10 Humanitarian Technology Conference (R10-HTC)*, 2017, vol. 2018-Janua, pp. 668–673.

[48] W. Z. W. Z. Abiddin, R. Jailani, A. R. Omar, and I. M. Yassin, "Development of MATLAB kinect skeletal tracking system (MKSTS) for gait analysis," in *2016 IEEE Symposium on Computer Applications & Industrial Electronics (ISCAIE)*, 2016, pp. 216–220.

[49] A. Jalal, S. Kamal, and D. Kim, "A depth video-based human detection and activity recognition using multi-features and embedded hidden markov models for health care monitoring systems," *Int. J. Interact. Multimed. Artif. Intell.*, vol. 4, no. 4, p. 54, 2017.

[50] J. Z. Edwards, K. A. Greene, R. S. Davis, M. W. Kovacik, D. A. Noe, and M. J. Askew, "Measuring flexion in knee arthroplasty patients," *J. Arthroplasty*, vol. 19, no. 3, pp. 369–372, Apr. 2004.

[51] S. Majumder, T. Mondal, and M. Deen, "Wearable sensors for remote health monitoring," *Sensors*, vol. 17, no. 12, p. 130, Jan. 2017.

[52] S. Majumder, L. Chen, O. Marinov, C.-H. Chen, T. Mondal, and M. J. Deen, "Noncontact wearable wireless ECG systems for long-term monitoring," *IEEE Rev. Biomed. Eng.*, vol. 11, pp. 306–321, 2018.

[53] E. Nemati, M. J. Deen, and T. Mondal, "A wireless wearable ECG sensor for long-term applications," *IEEE Commun. Mag.*, vol. 50, no. 1, pp. 36–43, Jan. 2012.

[54] S. C. Mukhopadhyay, "Wearable sensors for human activity monitoring: a review," *IEEE Sens. J.*, vol. 15, no. 3, pp. 1321–1330, Mar. 2015.

[55] A. Mobini, S. Behzadipour, and M. S. Foumani, "Accuracy of kinect's skeleton tracking for upper body rehabilitation applications," *Disabil. Rehabil. Assist. Technol.*, vol. 9, no. 4, pp. 344–352, Jul. 2014.

[56] P. T. Gibbs and H. H. Asada, "Wearable conductive fiber sensors for multi-axis human joint angle measurements," *J. Neuroeng. Rehabil.*, vol. 2, no. 1, p. 7, 2005.

[57] J. H. M. Bergmann, S. Anastasova-Ivanova, I. Spulber, V. Gulati, P. Georgiou, and A. McGregor, "An attachable clothing sensor system for measuring knee joint angles," *IEEE Sens. J.*, vol. 13, no. 10, pp. 4090–4097, Oct. 2013.

[58] S. Bakhshi and M. H. Mahoor, "Development of a wearable sensor system for measuring body joint flexion," in *2011 International Conference on Body Sensor*

Networks, 2011, pp. 35–40.

[59] G. Gioberto, "Garment-integrated wearable sensing for knee joint monitoring," in *Proceedings of the 2014 ACM International Symposium on Wearable Computers Adjunct Program - ISWC '14 Adjunct*, 2014, pp. 113–118.

[60] M. Totaro *et al.*, "Soft smart garments for lower limb joint position analysis," *Sensors*, vol. 17, no. 10, p. 2314, Oct. 2017.

[61] H. Zhang, W. Niu, and S. Zhang, "Extremely stretchable, stable, and durable strain sensors based on double-network organogels," *ACS Appl. Mater. Interfaces*, vol. 10, no. 38, pp. 32640–32648, Sep. 2018.

[62] S.-M. Jeong, Y. Kang, T. Lim, and S. Ju, "Hydrophobic microfiber strain sensor operating stably in sweat and water environment," *Adv. Mater. Interfaces*, vol. 5, no. 24, p. 1801376, Dec. 2018.

[63] S. Park *et al.*, "Highly bendable and rotational textile structure with prestrained conductive sewing pattern for human joint monitoring," *Adv. Funct. Mater.*, vol. 29, no. 10, p. 1808369, Mar. 2019.

[64] H. Montazerian, A. Dalili, A. S. Milani, and M. Hoorfar, "Piezoresistive sensing in chopped carbon fiber embedded PDMS yarns," *Compos. Part B Eng.*, vol. 164, pp. 648–658, May 2019.

[65] M. P. Støve, T. S. Palsson, and R. P. Hirata, "Smartphone-based accelerometry is a valid tool for measuring dynamic changes in knee extension range of motion," *Knee*, vol. 25, no. 1, pp. 66–72, Jan. 2018.

[66] J.-Y. Jenny, A. Bureggah, and Y. Diesinger, "Measurement of the knee flexion angle with smartphone applications: Which technology is better?," *Knee Surgery, Sport. Traumatol. Arthrosc.*, vol. 24, no. 9, pp. 2874–2877, Sep. 2016.

[67] S. L. Vohralik, A. R. Bowen, J. Burns, C. E. Hiller, and E. J. Nightingale, "Reliability and validity of a smartphone app to measure joint range," *Am. J. Phys. Med. Rehabil.*, vol. 94, no. 4, pp. 325–330, Apr. 2015.

[68] S. Milanese *et al.*, "Reliability and concurrent validity of knee angle measurement: Smart phone app versus universal goniometer used by experienced and novice clinicians," *Man. Ther.*, vol. 19, no. 6, pp. 569–574, Dec. 2014.

[69] L. B. Johnson *et al.*, "Validity and reliability of smartphone magnetometer-based goniometer evaluation of shoulder abduction - A pilot study," *Man. Ther.*, vol. 20, no. 6, pp. 777–782, 2015.

[70] S. B. Sudin, "Wireless knee joint angle measurement system using gyroscope," University Tun Hussein Onn Malaysia, 2012.

[71] N. Friedman, J. B. Rowe, D. J. Reinkensmeyer, and M. Bachman, "The manumeter: a wearable device for monitoring daily use of the wrist and fingers," *IEEE J. Biomed. Heal. Informatics*, vol. 18, no. 6, pp. 1804–1812, Nov. 2014.

[72] A. Babchenko and J. Maryles, "A sensing element based on 3D imperfected polymer optical fibre," *J. Opt. A Pure Appl. Opt.*, vol. 9, no. 1, pp. 1–5, Jan. 2007.

[73] T. Seel, J. Raisch, and T. Schauer, "IMU-based joint angle measurement for gait analysis," *Sensors*, vol. 14, no. 4, pp. 6891–6909, Apr. 2014.

[74] S. Bakhshi, M. H. Mahoor, and B. S. Davidson, "Development of a body joint angle measurement system using IMU sensors," in *2011 Annual International Conference of the IEEE Engineering in Medicine and Biology Society*, 2011, vol. 2011, pp. 6923–6926.

[75] J. Favre, B. M. M. Jolles, R. Aissaoui, and K. Aminian, "Ambulatory measurement of 3D knee joint angle," *J. Biomech.*, vol. 41, no. 5, pp. 1029–1035, 2008.

[76] D. J. Crews, "Real-time estimation of knee angle, heel-strike, and toe-off events for gait rehabilitation devices," California State University, Long Beach, 2017.

[77] J. J. Castañeda, A. F. Ruiz-Olaya, C. N. Lara-Herrera, and F. Z. Roldán, "Knee joint angle monitoring system based on inertial measurement units for human gait analysis," in *IFMBE Proceedings*, vol. 60, I. Torres, J. Bustamante, and D. A. Sierra, Eds. Singapore: Springer Singapore, 2017, pp. 690–693.

[78] L. Vargas-Valencia, A. Elias, E. Rocon, T. Bastos-Filho, and A. Frizera, "An IMU-to-body alignment method applied to human gait analysis," *Sensors*, vol. 16, no. 12, p. 2090, Dec. 2016.

[79] J. Favre, R. Aissaoui, B. M. Jolles, J. A. de Guise, and K. Aminian, "Functional calibration procedure for 3D knee joint angle description using inertial sensors," *J. Biomech.*, vol. 42, no. 14, pp. 2330–2335, Oct. 2009.

[80] T. Seel and T. Schauer, "IMU-based joint angle measurement made practical," in *4th European Conference on Technically Assisted Rehabilitation - TAR*, 2013, p. 6.

[81] M. El-Gohary *et al.*, "Joint angle tracking with inertial sensors," in *2008 30th Annual International Conference of the IEEE Engineering in Medicine and Biology Society*, 2008, pp. 1068–1071.

[82] S. Salehi, G. Bleser, A. Reiss, and D. Stricker, "Body-IMU autocalibration for inertial hip and knee joint tracking," in *Proceedings of the 10th EAI International Conference on Body Area Networks*, 2015.

[83] V. Bonnet *et al.*, "Monitoring of hip and knee joint angles using a single inertial measurement unit during lower limb rehabilitation," *IEEE Sens. J.*, vol. 16, no. 6, pp. 1557–1564, Mar. 2016.

[84] N. F. Ribeiro *et al.*, "Validation of a knee angle measurement system based on IMUs," in *Human-Centric Robotics, Proceedings of the 20th International Conference on CLAWAR 2017*, 2017, pp. 645–652.

[85] Y. Labs, "Yost - calculating angles between two yost labs 3-space sensor™ devices on a human body," Portsmouth, Ohio, 2013.

[86] Aizan Masdar, B.S.K.K. Ibrahim, Dirman Hanafi, M. Mahadi Abdul Jamil, and K.A.A. Rahman, "Knee joint angle measurement system using gyroscop and flex-sensors for rehabilitation," *Biomed. Eng. Int. Conf.*, pp. 5–8, 2013.

[87] P. N. Pathirana, M. S. Karunarathne, G. L. Williams, P. T. Nam, and H. Durrant-Whyte, "Robust and accurate capture of human joint pose using an inertial sensor," *IEEE J. Transl. Eng. Heal. Med.*, vol. 6, pp. 1–11, 2018.

[88] É. Pinet, C. Hamel, B. Glišić, D. Inaudi, and N. Miron, "Health monitoring with optical fiber sensors: from human body to civil structures," in *Proceedings of SPIE*,

2007, vol. 6532, no. 418, p. 653219.

[89] L. Bilro, J. G. Oliveira, J. L. Pinto, and R. N. Nogueira, "A reliable low-cost wireless and wearable gait monitoring system based on a plastic optical fibre sensor," *Meas. Sci. Technol.*, vol. 22, no. 4, p. 045801, Apr. 2011.

[90] D. Z. Stupar, J. S. Bajic, L. M. Manojlovic, M. P. Slankamenac, A. V. Joza, and M. B. Zivanov, "Wearable low-cost system for human joint movements monitoring based on fiber-optic curvature sensor," *IEEE Sens. J.*, vol. 12, no. 12, pp. 3424–3431, Dec. 2012.

[91] Z. Wang, G. Liu, and G. Tian, "Human skeleton tracking using information weighted consensus filter in distributed camera networks," in *2017 Chinese Automation Congress (CAC)*, 2017, vol. 2017-Janua, pp. 4640–4644.

[92] A. Karatsidis *et al.*, "Predicting kinetics using musculoskeletal modeling and inertial motion capture," p. 19, Jan. 2018.

[93] S. Majumder *et al.*, "Smart homes for elderly healthcare—recent advances and research challenges," *Sensors*, vol. 17, no. 11, p. 2496, Oct. 2017.

[94] N. Agoulmine, M. Deen, J.-S. Lee, and M. Meyyappan, "U-health smart home," *IEEE Nanotechnol. Mag.*, vol. 5, no. 3, pp. 6–11, Sep. 2011.

[95] J. Kim, H. Choi, H. Wang, N. Agoulmine, M. J. Deen, and J. W.-K. Hong, "POSTECH's U-health smart home for elderly monitoring and support," in *2010 IEEE International Symposium on "A World of Wireless, Mobile and Multimedia Networks" (WoWMoM)*, 2010, pp. 1–6.

[96] M. J. Deen, "Information and communications technologies for elderly ubiquitous healthcare in a smart home," *Pers. Ubiquitous Comput.*, vol. 19, no. 3–4, pp. 573–599, Jul. 2015.

[97] G.-H. Feng and W.-M. Chen, "Piezoelectric-film-based acoustic emission sensor array with thermoactuator for monitoring knee joint conditions," *Sensors Actuators A Phys.*, vol. 246, pp. 180–191, Aug. 2016.

[98] O. Kröning and H. Rothe, "Gait motion analysis using optical and inertial sensor fusion to design human kinetic energy harvesting systems," in *Novel Optical Systems Design and Optimization XX*, 2017, p. 16.

[99] M. I. Mokhlespour Esfahani *et al.*, "Trunk motion system (TMS) using printed body worn sensor (BWS) via data fusion approach," *Sensors (Switzerland)*, vol. 17, no. 1, 2017.

[100] Kyoobin Lee and Dong-Soo Kwon, "Wearable master device using optical fiber curvature sensors for the disabled," in *Proceedings 2001 ICRA. IEEE International Conference on Robotics and Automation (Cat. No.01CH37164)*, 2001, vol. 1, pp. 892–896.

[101] J. Rantala, J. Hännikäinen, and J. Vanhala, "Fiber optic sensors for wearable applications," *Pers. Ubiquitous Comput.*, vol. 15, no. 1, pp. 85–96, Jan. 2011.

[102] A. K. Vimal, S. Bhasin, S. Sharma, S. Anand, and P. Swami, "Brace design for knee-angle measurement in human gait using infrared sensor," in *2015 International Conference on Signal Processing and Communication (ICSC)*, 2015, pp. 201–203.

[103] E. Udd and W. B. Spillman, *Fiber optic sensors*. Hoboken, NJ, USA: John Wiley & Sons, Inc., 2011.

[104] K. Wood, T. Brown, R. Rogowski, and B. Jensen, "Fiber optic sensors for health monitoring of morphing airframes: II. Chemical sensing using optical fibers with Bragg gratings," *Smart Mater. Struct.*, vol. 9, no. 2, pp. 170–174, Apr. 2000.

[105] S. S. Yin and P. Ruffin, "Fiber optic sensors," in *Wiley Encyclopedia of Biomedical Engineering*, Hoboken, NJ, USA: John Wiley & Sons, Inc., 2006.

[106] K. S. C. Kuang, W. J. Cantwell, and P. J. Scully, "An evaluation of a novel plastic optical fibre sensor for axial strain and bend measurements," *Meas. Sci. Technol.*, vol. 13, no. 10, pp. 1523–1534, 2002.

[107] L. Dunne, P. Walsh, B. Smyth, and B. Caulfield, "Design and evaluation of a wearable optical sensor for monitoring seated spinal posture," in *2006 10th IEEE International Symposium on Wearable Computers*, 2006, pp. 65–68.

[108] Y. Fu and H. Di, "Fiber-optic curvature sensor with optimized sensitive zone," *Opt. Laser Technol.*, vol. 43, no. 3, pp. 586–591, Apr. 2011.

[109] F. Pedersoli, S. Benini, N. Adami, and R. Leonardi, "XKin: an open source framework for hand pose and gesture recognition using kinect," *Vis. Comput.*, vol. 30, no. 10, pp. 1107–1122, Oct. 2014.

[110] J. Charles and M. Everingham, "Learning shape models for monocular human pose estimation from the Microsoft Xbox Kinect," in *Proceedings of the IEEE International Conference on Computer Vision*, 2011, pp. 1202–1208.

[111] Z. Zhang, Y. Liu, A. Li, and M. Wang, "A novel method for user-defined human posture recognition using Kinect," in *Proceedings - 2014 7th International Congress on Image and Signal Processing, CISP 2014*, 2014, pp. 736–740.

[112] T. L. Le, M. Q. Nguyen, and T. T. M. Nguyen, "Human posture recognition using human skeleton provided by Kinect," in *2013 International Conference on Computing, Management and Telecommunications, ComManTel 2013*, 2013, pp. 340–345.

[113] K. Rector, C. L. Bennett, and J. a. Kientz, "Eyes-free yoga: an exergame using depth cameras for blind & low vision exercise," in *Proceedings of the 15th International ACM SIGACCESS Conference on Computers and Accessibility*, 2013, pp. 1–8.

[114] Š. Obdržálek, G. Kurillo, J. Han, T. Abresch, and R. Bajcsy, "Real-time human pose detection and tracking for tele-rehabilitation in virtual reality," in *Studies in Health Technology and Informatics*, 2012, vol. 173, pp. 320–324.

[115] O. Patsadu, C. Nukoolkit, and B. Watanapa, "Human gesture recognition using Kinect camera," in *2012 Ninth International Conference on Computer Science and Software Engineering (JCSSE)*, 2012, pp. 28–32.

[116] A. Behrad and N. Roodsarabi, "3D human motion tracking and reconstruction using dct matrix descriptor," *ISRN Mach. Vis.*, vol. 2012, pp. 1–11, 2012.

[117] C. Wang, K. Xia, M. Jian, H. Wang, M. Zhang, and Y. Zhang, "Carbonized silk georgette as an ultrasensitive wearable strain sensor for full-range human activity monitoring," *J. Mater. Chem. C*, vol. 5, no. 30, pp. 7604–7611, 2017.

[118] Y. Zheng *et al.*, "A highly stretchable and stable strain sensor based on hybrid carbon nanofillers/polydimethylsiloxane conductive composites for large human motions monitoring," *Compos. Sci. Technol.*, vol. 156, pp. 276–286, Mar. 2018.

[119] S. Ryu *et al.*, "Extremely elastic wearable carbon nanotube fiber strain sensor for monitoring of human motion," *ACS Nano*, vol. 9, no. 6, pp. 5929–5936, Jun. 2015.

[120] "MTw Awinda - products - Xsens 3D motion tracking." [Online]. Available: https://www.xsens.com/products/mtw-awinda/. [Accessed: 28-Nov-2018].

[121] A. Muro-de-la-Herran, B. Garcia-Zapirain, and A. Mendez-Zorrilla, "Gait analysis methods: an overview of wearable and non-wearable systems, highlighting clinical applications," *Sensors*, vol. 14, no. 2, pp. 3362–3394, Feb. 2014.

[122] S. Majumder, T. Mondal, and M. J. Deen, "A simple, low-cost and efficient gait analyzer for wearable healthcare applications," *IEEE Sens. J.*, vol. 19, no. 6, pp. 2320–2329, Mar. 2019.

[123] Bo Jin *et al.*, "Walking-age analyzer for healthcare applications," *IEEE J. Biomed. Heal. Informatics*, vol. 18, no. 3, pp. 1034–1042, May 2014.

[124] P. Mandal, K. Tank, T. Mondal, C.-H. Chen, and M. J. Deen, "Predictive walking-age health analyzer," *IEEE J. Biomed. Heal. Informatics*, vol. 22, no. 2, pp. 363–374, Mar. 2018.

[125] A. Ahmadi *et al.*, "3D human gait reconstruction and monitoring using body-worn inertial sensors and kinematic modeling," *IEEE Sens. J.*, vol. 16, no. 24, pp. 8823–8831, Dec. 2016.

[126] X. Wang, M. Kyrarini, D. Ristic-Durrant, M. Spranger, and A. Graser, "Monitoring of gait performance using dynamic time warping on IMU-sensor data," in *2016 IEEE International Symposium on Medical Measurements and Applications (MeMeA)*, 2016, pp. 1–6.

[127] X. S. Ji, S. Wang, Y. Xu, Q. Shi, and D. Xia, "Application of the digital signal procession in the MEMS gyroscope de-drift," in *Proceedings of 1st IEEE International Conference on Nano Micro Engineered and Molecular Systems, 1st IEEE-NEMS*, 2006, pp. 218–221.

[128] C.-S. Fahn and H. Sun, "Development of a fingertip glove equipped with magnetic tracking sensors," *Sensors*, vol. 10, no. 2, pp. 1119–1140, Jan. 2010.

[129] S. Micera *et al.*, "Functional assessment of hand orthopedic disorders using a sensorised glove: preliminary results," in *2003 IEEE International Conference on Robotics and Automation (Cat. No.03CH37422)*, 2003, pp. 2212–2217.

[130] M. Browne, D. Barrett, A. Balabanis, and C. Rowland, "Passive monitoring of knee joint condition using acoustic emission," *Orthop. Proc.*, vol. 98, no. B:SUPP_1, pp. 54–54, 2016.

[131] H. Toreyin, S. Hersek, C. N. Teague, and O. T. Inan, "A proof-of-concept system to analyze joint sounds in real time for knee health assessment in uncontrolled settings," *IEEE Sens. J.*, vol. 16, no. 9, pp. 2892–2893, May 2016.

[132] C. N. Teague *et al.*, "Novel methods for sensing acoustical emissions from the knee for wearable Joint Health Assessment," *IEEE Trans. Biomed. Eng.*, vol. 63, no. 8,

pp. 1581–1590, Aug. 2016.

[133] C. N. Teague, S. Hersek, J. L. Conant, S. M. Gilliland, and O. T. Inan, "Wearable knee health rehabilitation assessment using acoustical emissions," in *AIP Conference Proceedings*, 2017, vol. 1806, p. 070008.

[134] S. Majumder and M. J. Deen, "Smartphone sensors for health monitoring and diagnosis," *Sensors*, vol. 19, no. 9, p. 2164, May 2019.

[135] W. Elmenreich, *An introduction to sensor fusion*. Vienna, 2002, pp. 1–28.

[136] Y. Li, X. Zhang, Y. Gong, Y. Cheng, X. Gao, and X. Chen, "Motor function evaluation of hemiplegic upper-extremities using data fusion from wearable inertial and surface EMG sensors," *Sensors*, vol. 17, no. 3, p. 582, Mar. 2017.

[137] "MetaWear-sample app-Android." [Online]. Available: https://github.com/mbientlab/MetaWear-SampleApp-Android. [Accessed: 29-Jul-2019].

[138] "Developers – MbientLab." [Online]. Available: https://mbientlab.com/developers. [Accessed: 29-Jul-2019].

[139] M. El-Gohary and J. McNames, "Human joint angle estimation with inertial sensors and validation with a robot arm," *IEEE Trans. Biomed. Eng.*, vol. 62, no. 7, pp. 1759–1767, Jul. 2015.

[140] N. N. Kelagote, "Human motion modeling and evaluation using wearable sensor devices," University of Houston - Clear Lake, 2017.

[141] O. O. Akintade and L. O. Kehinde, "Comparison of data fusion techniques for human knee joint range-of-motion measurement using inertial sensors," *Int. J. Electron. Electr. Eng.*, pp. 127–134, 2017.

[142] Q. Li, M. Young, V. Naing, and J. M. Donelan, "Walking speed estimation using a shank-mounted inertial measurement unit," *J. Biomech.*, vol. 43, no. 8, pp. 1640–1643, May 2010.

[143] F. Dadashi, B. Mariani, S. Rochat, C. Büla, B. Santos-Eggimann, and K. Aminian, "Gait and foot clearance parameters obtained using shoe-worn inertial sensors in a large-population sample of older adults," *Sensors*, vol. 14, no. 1, pp. 443–457, Dec. 2013.

[144] Y. Wahab, A. Zayegh, R. K. Begg, and R. Veljanovski, "Analysis of foot-to-ground clearance measurement techniques for MEMS realization," in *2007 10th International Conference on Computer and Information Technology*, 2007, pp. 1–5.

[145] R. Begg, R. Best, L. Dell'Oro, and S. Taylor, "Minimum foot clearance during walking: Strategies for the minimisation of trip-related falls," *Gait Posture*, vol. 25, no. 2, pp. 191–198, Feb. 2007.

[146] "Step length, cadence, and the walk ratio » ProtoKinetics." [Online]. Available: https://www.protokinetics.com/2018/10/17/step-length-cadence-and-the-walk-ratio/. [Accessed: 20-Feb-2020].

[147] C. Chen, "Evaluation of resistance–temperature calibration equations for NTC thermistors," *Measurement*, vol. 42, no. 7, pp. 1103–1111, Aug. 2009.

[148] C. Damsted, R. O. Nielsen, and L. H. Larsen, "Reliability of video-based

quantification of the knee- and hip angle at foot strike during running.," *Int. J. Sports Phys. Ther.*, vol. 10, no. 2, pp. 147–154, Apr. 2015.

[149] L. I.-K. Lin, "A concordance correlation coefficient to evaluate reproducibility," *Biometrics*, 1989.

[150] G. McBride, J. M. Bland, D. G. Altman, and L. I. Lin, "A proposal for strength-of-agreement criteria for Lin's concordance correlation coefficient," *NIWA Client Rep.*, 2005.

[151] V. Krishnan and B. Anto, "Features of wavelet packet decomposition and discrete wavelet transform for malayalam speech recognition," *Int. J. Recent Trends Eng.*, vol. 1, no. 2, pp. 93–96, 2009.

[152] R. R. Coifman and M. V. Wickerhauser, "Entropy-based algorithms for best basis selection," *IEEE Trans. Inf. Theory*, vol. 38, no. 2, pp. 713–718, Mar. 1992.

[153] N. Mammone, F. La Foresta, and F. C. Morabito, "Automatic artifact rejection from multichannel scalp EEG by wavelet ICA," *IEEE Sens. J.*, vol. 12, no. 3, pp. 533–542, Mar. 2012.

[154] Z. Wu and N. E. Huang, "Ensemble empirical mode decomposition: a noise assisted data analysis method," *Adv. Adapt. Data Anal.*, vol. 01, no. 01, pp. 1–41, Jan. 2009.

[155] Z. Zhao, R. Anand, and M. Wang, "Maximum relevance and minimum redundancy feature selection methods for a marketing machine learning platform," *Proc. - 2019 IEEE Int. Conf. Data Sci. Adv. Anal. DSAA 2019*, pp. 442–452, Aug. 2019.

[156] G. Roffo, "Feature selection library (MATLAB toolbox)," *Rank. to Learn Learn. to Rank Role Rank. Pattern Recognit. Appl.*, pp. 1–8, Jul. 2016.

[157] C. Goodall and I. T. Jolliffe, "Principal component analysis," *Technometrics*, vol. 30, no. 3, p. 351, Aug. 1988.

[158] L. I. Smith, "A tutorial on principal components analysis introduction," 2002.

[159] "Osteoporosis: what you need to know as you age | Johns Hopkins Medicine." [Online]. Available: https://www.hopkinsmedicine.org/health/conditions-and-diseases/osteoporosis/osteoporosis-what-you-need-to-know-as-you-age. [Accessed: 20-Feb-2020].

[160] "How to feed your bones and increase bone density - UBMD orthopaedics & sports medicine doctors – Buffalo, Niagara Falls, New York." [Online]. Available: https://ubortho.com/news/feed-bones-increase-bone-density/. [Accessed: 20-Feb-2020].

[161] D. A. Winter, "Biomechanical motor patterns in normal walking," *J. Mot. Behav.*, vol. 15, no. 4, pp. 302–330, Dec. 1983.

[162] D. A. Winter, "Energy generation and absorption at the ankle and knee during fast, natural, and slow cadences," *Clin. Orthop. Relat. Res.*, vol. NA;, no. 175, pp. 147–154, May 1983.

[163] S. Mulroy, J. Gronley, W. Weiss, C. Newsam, and J. Perry, "Use of cluster analysis for gait pattern classification of patients in the early and late recovery phases following stroke," *Gait Posture*, vol. 18, no. 1, pp. 114–125, Aug. 2003.

[164] K. M. T. Goutier, S. L. Jansen, C. G. C. Horlings, U. M. Kung, and J. H. J. Allum,

"The influence of walking speed and gender on trunk sway for the healthy young and older adults," *Age Ageing*, vol. 39, no. 5, pp. 647–650, Sep. 2010.

[165] "Ageing - muscles bones and joints - better health channel." [Online]. Available: https://www.betterhealth.vic.gov.au/health/conditionsandtreatments/ageing-muscles-bones-and-joints. [Accessed: 02-Jan-2020].

[166] L. Lee and W. E. L. Grimson, "Gait analysis for recognition and classification," in *Proceedings of Fifth IEEE International Conference on Automatic Face Gesture Recognition*, 2002, pp. 155–162.

[167] H. Shimokata and F. Kuzuya, "Aging, basal metabolic rate, and nutrition.," *Nippon Ronen Igakkai Zasshi. Japanese J. Geriatr.*, vol. 30, no. 7, pp. 572–576, 1993.

[168] S. Nuell *et al.*, "Sex differences in thigh muscle volumes, sprint performance and mechanical properties in national-level sprinters," *PLoS One*, vol. 14, no. 11, p. e0224862, Nov. 2019.

[169] G. G. Handsfield, K. R. Knaus, N. M. Fiorentino, C. H. Meyer, J. M. Hart, and S. S. Blemker, "Adding muscle where you need it: non-uniform hypertrophy patterns in elite sprinters," *Scand. J. Med. Sci. Sports*, vol. 27, no. 10, pp. 1050–1060, Oct. 2017.

[170] R. McCormick and A. Vasilaki, "Age-related changes in skeletal muscle: changes to life-style as a therapy," *Biogerontology*, vol. 19, no. 6, pp. 519–536, Dec. 2018.

[171] S. G. Haidar, R. M. Charity, R. S. Bassi, P. Nicolai, and B. K. Singh, "Knee skin temperature following uncomplicated total knee replacement," *Knee*, vol. 13, no. 6, pp. 422–426, Dec. 2006.

[172] K. Ammer, "Temperature of the human knee - a review," *Thermol. Int.*, vol. 12, pp. 137–151, 2012.

[173] R. K. Begg, M. Palaniswami, and B. Owen, "Support vector machines for automated gait classification," *IEEE Trans. Biomed. Eng.*, vol. 52, no. 5, pp. 828–838, May 2005.

[174] "Diseases and conditions osteoarthritis." [Online]. Available: https://www.rheumatology.org/I-Am-A/Patient-Caregiver/Diseases-Conditions/Osteoarthritis. [Accessed: 06-Apr-2020].

Appendix A

Supporting Information for Chapter 1

Movements of key human body joints

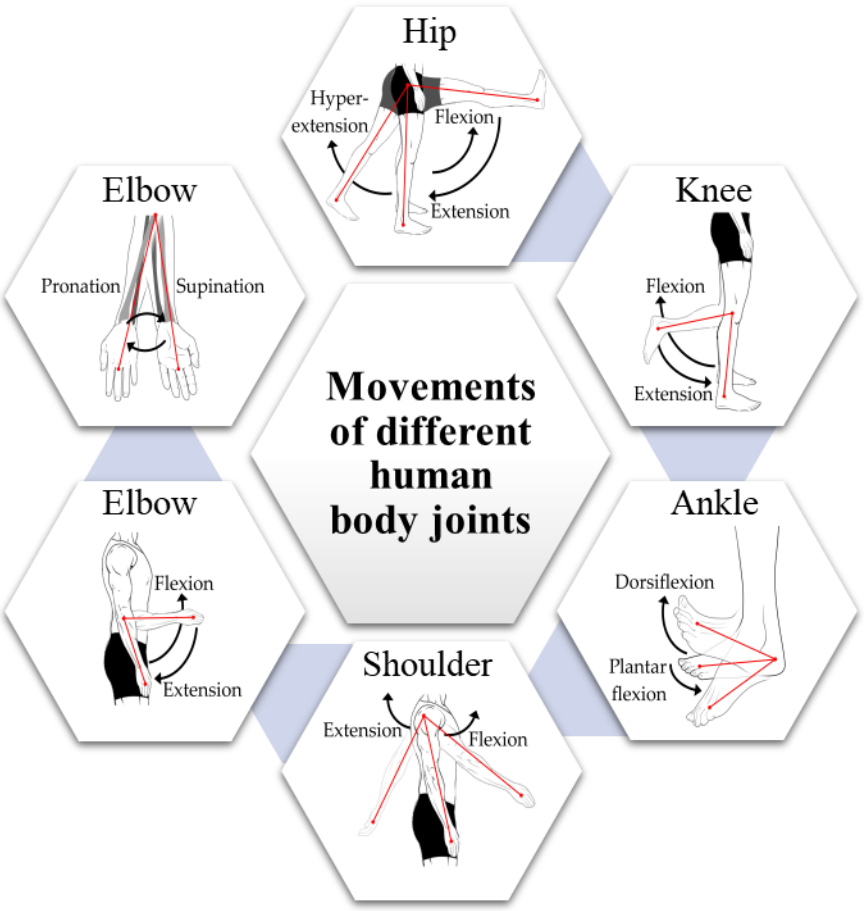

Figure A-1: Different types of human body joints' movements.

Normative values of different body joint range of motion (ROM)

Table A-1: Active range of motion (ROM) (°) for human joints by gender and age [19].

Age		2-8 years		9-19 years		20-44 years		45-69 years	
		Females (39)	**Males (55)**	**Females (56)**	**Males (48)**	**Females (143)**	**Males (114)**	**Females (123)**	**Males (96)**
Joint Motion	**1. Hip extension**	26.2 (23.9–28.5)	28.3 (27.2 – 29.4)	20.5 (18.6 – 22.4)	18.2 (16.6 – 19.8)	18.1 (17.0 – 19.2)	17.4 (16.3 – 18.5)	16.7 (15.5 – 17.9)	13.5 (12.5 – 14.5)
	2. Hip flexion	140.8 (139.2 – 142.4)	131.1 (129.4 – 132.8)	134.9 (133.0 – 136.8)	135.2 (133.0 – 137.4)	133.8 (132.5 – 135.1)	130.4 (129.0 – 131.8)	130.8 (129.2 – 132.4)	127.2 (125.7 – 128.7)
	3. Knee flexion	152.6 (151.2 – 154.0)	147.8 (146.6 – 149.0)	142.3 (140.8 – 143.8)	142.2 (140.4 – 144.0)	141.9 (140.9 – 142.9)	137.7 (136.5 – 138.9)	137.8 (136.5 – 139.1)	132.9 (131.6 – 134.2)
	4. Knee extension	5.4 (3.9 – 6.9)	1.6 (0.9 – 2.3)	2.4 (1.5 – 3.3)	1.8 (0.9 – 2.7)	1.6 (1.1 – 2.1)	1.0 (0.6 – 1.4)	1.2 (0.7 – 1.7)	0.5 (0.1 – 0.9)
	5. Ankle dorsiflexion	24.8 (22.5 – 27.1)	22.8 (21.3 – 24.3)	17.3 (15.6 – 19.0)	16.3 (14.9 – 17.7)	13.8 (12.9 – 14.7)	12.7 (11.6 – 13.8)	11.6 (10.6 – 12.6)	11.9 (10.9 – 12.9)
	6. Ankle plantar flexion	67.1 (64.8 – 69.4)	55.8 (54.4 – 57.2)	57.3 (54.8 – 59.8)	52.8 (50.8 – 54.8)	62.1 (60.6 – 63.6)	54.6 (53.2 – 56.0)	56.5 (55.0 – 58.0)	49.4 (47.7 – 51.1)
	7. Shoulder flexion	178.6 (176.9 – 180.3)	177.8 (176.7 – 178.9)	171.8 (169.8 – 173.8)	170.9 (169.1 – 172.7)	172.0 (170.9 – 173.1)	168.8 (167.3 – 170.3)	168.1 (166.7 – 169.5)	164.0 (162.3 – 165.7)
	8. Elbow flexion	152.9 (151.5 – 154.3)	151.4 (150.8 – 152.0)	149.7 (148.5 – 150.9)	148.3 (146.8 – 149.8)	150.0 (149.1 – 150.9)	144.6 (143.6 – 145.6)	148.3 (147.3 – 149.3)	143.5 (142.3 – 144.7)
	9. Elbow extension	6.8 (5.2 – 8.4)	2.2 (0.9 – 3.5)	6.4 (4.7 – 8.1)	5.3 (3.6 – 7.0)	4.7 (3.9 – 5.5)	0.8 (0.1 – 1.5)	3.6 (2.6 – 4.6)	-0.7 (-1.5 – 0.1)
	10. Elbow pronation	84.6 (82.8 – 86.4)	79.6 (78.8 – 80.4)	81.2 (79.6 – 82.8)	79.8 (77.8 – 81.8)	82.0 (81.0 – 83.0)	76.9 (75.6 – 78.2)	80.8 (79.7 – 81.9)	77.7 (76.5 – 78.9)
	11. Elbow supination	93.7 (91.4 – 96.0)	86.4 (85.3 – 87.5)	90.0 (88.0 – 92.0)	87.8 (85.7 – 89.9)	90.6 (89.2 – 92.0)	85.0 (83.8 – 86.2)	87.2 (86.0 – 88.4)	82.4 (80.9 – 83.9)

Appendix B

Supporting Information for Chapter 3

MetaWear CPro IMU board pin assignments and their functions

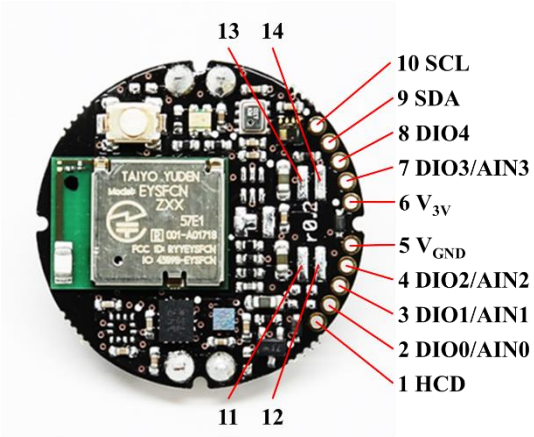

Figure B-2: MetaWear CPro IMU Board Pin Assignments.

Table B-2: MetaWear CPro Board Pin Functions.

	Pin	Pin Name	Function	Description
Power Supply	5	VGND	Power	Ground connection
	6	V3V	Power	+3V battery connection
Peripherals	1	HCD	High Current Driver	Switch for sinking high current peripherals
	2	DIO0 AIN0	Digital I/O Analog I/O	General purpose I/O and analog input
	3	DIO1 AIN1	Digital I/O Analog I/O	General purpose I/O and analog input
	4	DIO2 AIN2	Digital I/O Analog I/O	General purpose I/O and analog input
	7	DIO3 AIN3	Digital I/O Analog I/O	General purpose I/O and analog input
	8	DIO4	Digital I/O	General purpose I/O
	9	SDA	I2C Data	I2C data line
	10	SCL	I2C Clock	I2C clock line
SWD Debug Header	11	V3V	Power	System supply for debugger
	12	VGND	Power	System ground for debugger
	13	SWDIO/nRESET	Debug	SWD debugger I/O line and system reset
	14	SWDCLK	Debug	SWD debugger clock line

Letter of Information/Consent

Smart Knee Brace

Local Principal Investigator:

Dr. Tapas Mondal
Associate Professor,
Department of Pediatrics,
Division of Cardiology
McMaster University
Hamilton, Ontario, Canada
(905) 525-9140 ext. 75259
E-mail: mondalt@mcmaster.ca

Co-investigator(s):

1. *Dr. Jamal Deen. Distinguished University Professor, Department of Electrical and Computer Engineering, McMaster University.*
2. *Dr. David Cowan. Associate Professor, Division of Geriatric Medicine, Department of Medicine, St. Joseph's Healthcare Hamilton*

Research Sponsor: This research is supported by a Grant from the AGE-WELL Catalyst Funding Program of the McMaster Institute for Research on Aging (MIRA).

What are we trying to discover?

The project's objective is to analyze and identify mobility related problems among older adults and other joint related problems of different individuals (age: 18 and above) by monitoring knee joint. From this study, we aim to extract a complete set of data related to mobility including walking parameters, knee joint range of motion and the state of walking muscles in order to detect risk of certain musculoskeletal disorders that may not be noticeable at early stages.

What will happen during the study?

You will be recruited by the Local Principal Investigators or an undergraduate health sciences student. This project requires testing of individuals (both male and female) of all age groups (children, adults and elders). As a volunteer, you will be required to strap on the sensor tag (which will be attached on a knee brace and a Velcro strap) on their knee and then walk approximately 200 meter forward (including at least two turns - 90° and 180°), with one step consisting of the movement of right foot and the second step consisting of the movement of left foot forward and so on. You will also be required to climb and descend stairs for about 10 steps each. The entire procedure can be completed in 30 minutes including the gathering of informed consent and explaining the procedure to study subjects.

Potential Harms, Risks or Discomforts:

There is no anticipated risk, harm or injury during this session. We do not believe there will be any discomfort either as you will simply be walking. Regardless, if there is any discomfort or any concern please let me know immediately and we will stop the activity. If you have any symptoms (which is very unlikely) we will address these and take appropriate care.

Benefits:

The proposed research will have a direct benefit to the quality of healthcare provided in Canada. The proposed research will advance screening tests for individuals who may have diseases and illnesses that they are unaware of. The availability of wireless communication, coupled with minimally invasive systems that are customized to the specific personalized requirements for patients would encourage healthier individuals. Furthermore, the application of technological knowhow via knowledge transfer in providing better treatment would help address the rising costs for health-care.

The research will not benefit you directly. We hope that what is learned as a result of this study will help individuals across Canada be aware of their physical conditions and be able to approach any complications at early stages.

Who will know what I said or did in the study?

The data will be anonymized and will be maintained for further studies and for publication.

As you are participating in this study confidentially I will not use your name or any information that would allow you to be identified. No one but me (or other members of the research team such as the research assistant) will know whether you participated unless you choose to tell them.

We will collect the general health information about you that would not identify yourself at any time in the future (please refer to data collection sheet).

There is no Legally Required Disclosure in this study.

What if I change my mind about being in the study?

Your participation in this study is voluntary. It is your choice to be part of the study or not. If you decide not to be part of the study, you can stop (withdraw), from the knee monitoring study for whatever reason, even after signing the consent form or part-way through the study. If you decide to withdraw, there will be no consequences to you. In cases of withdrawal, please indicate whether you want us to use the data collected previously or to destroy it.

Your decision whether or not to be part of the study will not affect your continuing to be a part of the research team.

How do I find out what was learned in this study?

We will discuss the results of the study together.

Questions about the Study

If you have questions or need more information about the study itself, please contact Dr. Tapas Mondal at mondalt@mcmaster.ca or x 75259 and Dr. David Cowan at cowand@mcmaster.ca .

This study has been reviewed by the Hamilton Integrated Research Ethics Board and received ethics clearance. If you have concerns or questions about your rights as a participant or about the way the study is conducted, please contact:

Hamilton Integrated Research Ethics Board

Telephone: (905) 521-2100, Ext. 42013

CONSENT

1. *[Note to Researcher: Keep the Letter of Information and this consent portion together as one document. When obtaining written consent, make certain that you bring two copies: one for your records and one for the participant to keep.]*
    - I have read the information presented in the information letter about a study being conducted by Dr. Tapas Mondal/ Dr. David Cowan of McMaster University.
    - I have had the opportunity to ask questions about my involvement in this study and to receive additional details I requested.
    - I understand that if I agree to participate in this study, I may withdraw from the study at any time.
    - I will be given a signed copy of this form.
    - I agree to participate in the study.

Name of Participant (Printed) _____

Signature: _____ Date: _____

Person Obtaining Consent:

Name (Printed) _____

Signature: _____ Date: _____

2. I will receive a summary of the study's results.

   Please send them to this email address _____

   Or to this mailing address: _____

   _____

   _____

3. I agree to be contacted about a follow-up interview, and understand that I can always decline the request.
   … Yes. Please contact me at: _____
   … No.

Data Collection/Case Report

Date:

Time:

Personal information	**Sex**	
	Age	
	Weight	
	Height	
	BMI	
	Leg length	
	Measurement of the knee	
Clinical history	**Surgery (Hip, Knee, Ankle)**	
	Neurological problem	
	Diabetes	
	Stroke	
	COPD (Chronic obstructive pulmonary disease)	
	Poorly controlled CHF (Congestive heart failure)	
	High blood pressure	
Sensors will be used:	**1. Accelerometer & Gyroscope: To measure the joint movement** **2. Temperature: To measure knee skin temperature** **3. GSR (Galvanic Skin Response): To measure skin stress and perspiration** **4. Pressure sensor: To measure external muscle pressure around the knee** **5. Portable ECG: To take the ECG data before and after the activity for 30 sec with the heart rate to check the variability of cardiac function.**	

*** I would recommend to wear shoes which are comfortable for walking.**

**** As we need the knee braces to be put on bare skin, so it is advisable to wear shorts under your pants or wear loose pants.**

Screenshots of Data Collection from Two IMU Boards Using MetaBase Android application

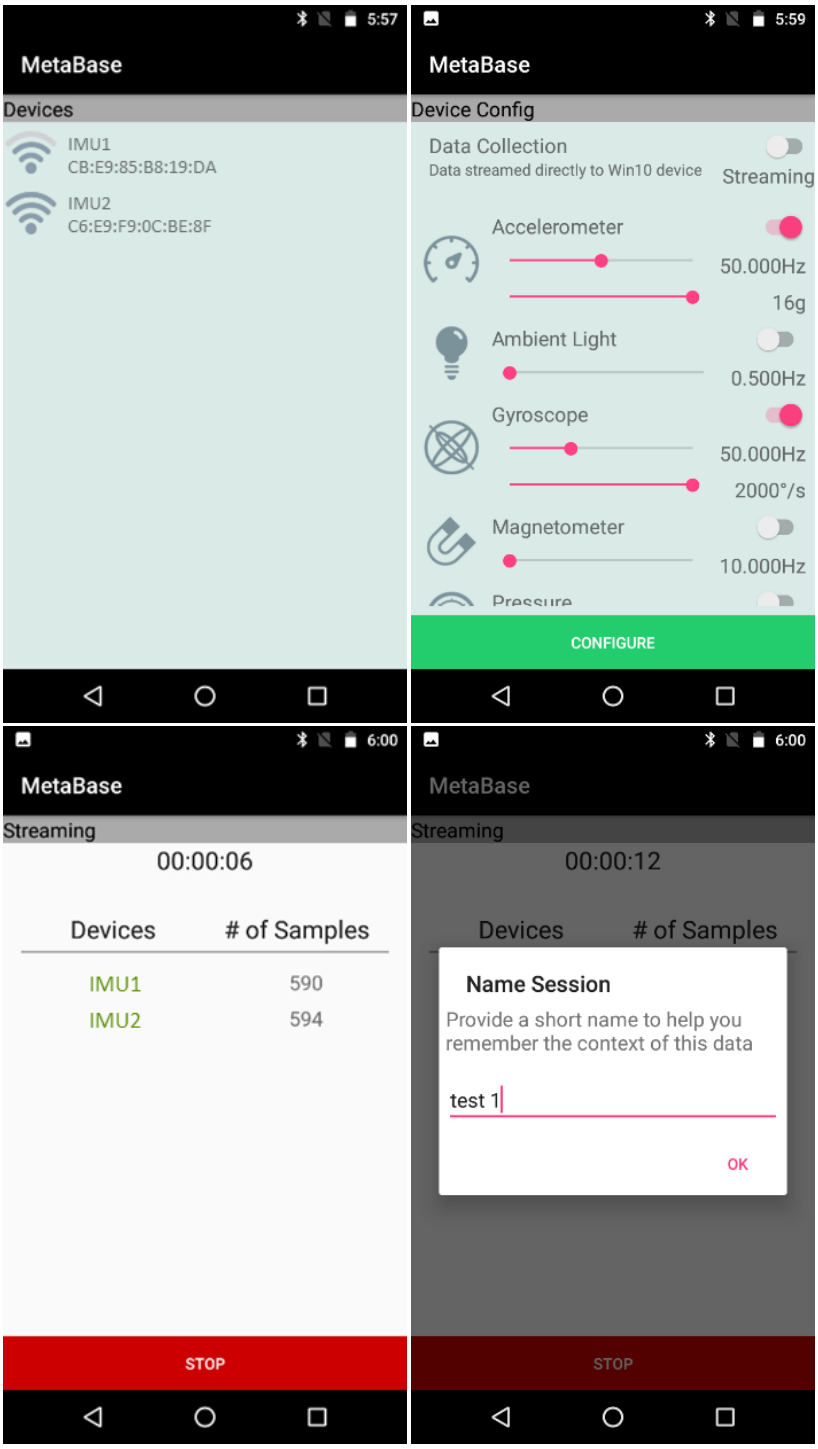

Screenshots of Data Collection from Temperature, Pressure and GSR Sensors Using MetaWear Android application

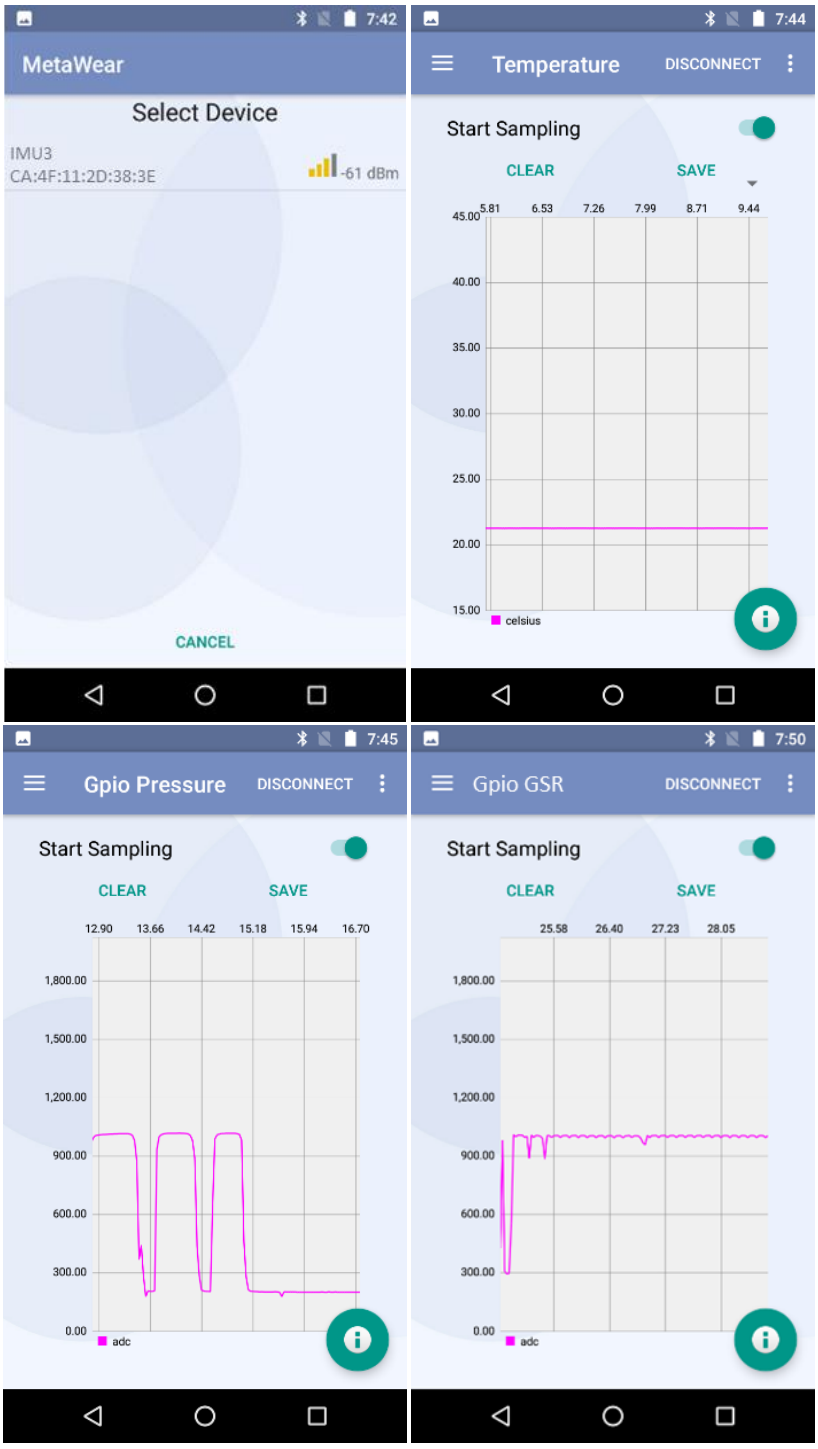

Appendix C

Copyright permissions*

MDPI Open Access Information and Policy

All articles published by MDPI are made immediately available worldwide under an open access license. This means:

- everyone has free and unlimited access to the full-text of *all* articles published in MDPI journals;
- everyone is free to re-use the published material if proper accreditation/citation of the original publication is given;
- open access publication is supported by the authors' institutes or research funding agencies by payment of a comparatively low **Article Processing Charge (APC)** for accepted articles.

Permissions

No special permission is required to reuse all or part of article published by MDPI, including figures and tables. For articles published under an open access Creative Common CC BY license, any part of the article may be reused without permission provided that the original article is clearly cited. Reuse of an article does not imply endorsement by the authors or MDPI.

* https://www.mdpi.com/openaccess